Multi-channel Bio-signal-based Human Movement Estimation for Assistive Robot Control

A dissertation presented

by

Jun-ichiro Furukawa

Student Number: 32A11044

Graduate School of Frontier Biosciences

Osaka University

March 2016

Abstract

Robot technologies have been widely introduced in industrial fields so far, and improved work efficiency. The robot research in the industrial have mainly focused on the autonomous of robot under the environment where humans do not intervene. However, thanks to recent highly-developed control and sensor technologies, the robot has become possible to assist human movement and work with human. For example, exoskeleton robot to assist human movement and general-purpose type humanoid robot are actively investigated. A major feature of these robots is to physically interact with human. In particular, since the assistive robot is controlled by the user wearing it, the human state changing dynamically has to be considered. Bio-signals have been extensively used to control assistive robot by estimating human movement intentions. For these applications, using multiple sensor channels is effective means to estimate user's movement intentions in detail. However, multi-channel bio-signal-based control has yet to be feasible technology in real world applications due to the difficulty of signal processing for the control. A robust estimation of human motor intention will be a promising approach for the high affinity robot control. In this study, I propose robust estimation methods of human motor intention from multi-channel Electromyography (EMG) or Electroencephalogram (EEG) to control assistive devices, and develop hardware and software to realize the systems.

In the EMG-based assistive robot control, estimating human joint torques robustly from muscle activities is the basic challenge. Most of conventional studies estimated joint torques from small number of electrodes based on a model calibrated by a data set corresponding to static load, and controlled the assistive robots with small degree of freedom. However, since the muscle activities are different between the static and dynamic motion, conventional data acquisition method can not describe the relations between joint torques and EMG during motion. Second, since assistive exoskeleton robots can make physical contact with environments or the limbs of human user, sensor electrodes and human motor intention might be affected. For example, the sensor electrodes can be dislodged from the users or damaged by collisions in the physical interaction. In addition, the probability of sensor electrode misplacement by human error increases as well as the sensor fault occurrence with multiple sensor electrodes. Such sensor anomalies as the disconnection, detaching of electrodes, and electrode misplacement cause significant errors in the estimation of user movement and cause large unwanted interaction between the user and robot. It seems difficult to use many sensor channels to control assistive robots, although using multiple sensor electrodes is useful to estimate user movement intentions. In addition, if the exoskeleton robot assist human joint movement as the consequence of interaction, the human intentional joint torques are affected, and the original estimation cannot be used. In this study, I propose methods to deal with above problems. For the model calibration, torque-EMG data set during dynamic motion are acquired by introducing inverse dynamics and bioengineering knowledge. Based on the data set acquisition, I propose robust estimation model using redundancy of the multi-channel bio-signals to control assistive robot with multi-degree of freedom by applying machine learning technologies. In addition, I

also propose a controller considering human-robot interaction. Moreover, I try to control the assistive robots by the human brain activities. In general, EEG which measure brain signals in non-invasive is noisier than EMG, and it is difficult to capture the information of motor intention and control the assistive robot. For the EEG-based assistive robot control, real-time EEG-decoding and autonomous robot technologies are combined.

In this paper, I also show a developed force control systems composed of pneumatic artificial muscles (PAM) and a hybrid PAM-electric motor driven system which were used in this study to realize safe human movement assist by my proposed robot control methods. The proposed method was evaluated by experiments with subjects.

In the EMG-based robot control experiment, the proposed dynamic joint torque estimation method was evaluated by my developed biosignal-based vertical weight support system simulating that the subjects have paralysis on one side of the body. The subjects performed a one-leg squat with his left leg while his right leg was assisted by my proposed system driven by vertical forces converted from estimated joint torques. In addition, in order to validate the robustness of my proposed estimation framework, I artificially disconnect an EMG electrodes, detach one side of an EMG probe from the skin surface, and intentionally misplace the two EMG electrodes during joint movement estimations and control the exoskeleton robots. The results show that my proposed method can estimate human movements based on EMG signals while conventional method was unable to deal with these fault situations. Moreover, the stability of estimated joint torque feedback in assistive interaction is evaluated with one-DOF exoskeleton robot assist experiment, and I show that the proposed method is more stable compared to conventional method. Finally, I implemented these proposed method to four-DOF assistive upper limb exoskeleton robot, and the results show that the robot assist human drinking motion with fault tolerability and stability. In the EEG-based robot control experiment, I implemented EEG-based squat support exoskeleton system driven by motor imagery, and discuss the way of feedback.

These results are promising to improve the affinity of human and machine in our society where the sensor and information processing technologies are developing. In addition, these my studies can not only be used for movement support applications in daily life and industrial but devices of neuro-rehabilitation, and are expected to develop for further worthy causes.

Contents

Correspondence of contents and research achievement

Contents 3.1, 3.2, 5.1 $\Longleftrightarrow$ Research Achievement 1.3, 3.1

Contents 3.3, 5.2.1, 5.2.2 $\Longleftrightarrow$ Research Achievement 1.2

Contents 3.3, 5.2.3, 5.2.4 $\Longleftrightarrow$ Research Achievement 2.1

Contents 3.4, 5.3 $\Longleftrightarrow$ Research Achievement 2.2, 3.2

Contents 3.3, 5.4 $\Longleftrightarrow$ Research Achievement 1.1

Contents 6 $\Longleftrightarrow$ Research Achievement 2.3

Chapter 1

Introduction

Life holds many mysteries and have yet to be unveiled. A lot of researchers investigate the complex life system and the knowledge helps us develop technologies in human society. Bio-inspired system is not only learning from nature but also applying them to design of real world engineered system [1] [2] [3] [4] [5]. In particular, robotics has began to focus on integration between human and robot [6] [7] [8]. In order to realize them, robots have to control its own body with same intelligence of human.

Human body has many joints and each joint is driven by a lot of muscles and can be independently controlled. Thus, when a human moves his/her limbs to some target point, all related muscles must be controlled simultaneously. The number of related muscles is larger than that of the joints, and this cause redundancy. Moreover, humans can control their limbs robustly even if some signal path to transmit the control command is damaged [9]. Why humans can precisely control their own redundant musculoskeletal system by robustly extracting the desired information? The redundancy problem of human body and dexterous motor control has been investigated in several approaches [10], e.g., reduction of degree of freedom, optimization, and synergy hypothesis. However, the discussion has been divided. In addition, although the robustness of information transmission was also confirmed in cellular signaling pathway [11], the mechanism has not been elucidated. From the control point of view, the redundancy make the problem more difficult. On the other hand, the redundancy contributes the robustness. Life system including humans take advantage of the redundancy.

In this study, I aim to approach the intelligence through a development of robot control strategy based on robust information extraction from redundant high-dimensional sensor signals for human-robot integration.

1.1 Bio-signal based Assistive Robot Control

In resent years, developed countries are expected rapid increase in the aging population ratio. Therefore, robots are now expected to good solution. Robotics have mainly focused on autonomy of robots or manipulating for industry so far. However, thanks to recent large-scale integrated circuit, sensor and control technologies, robot has become possible to physically interact with humans and support human activities in industry and in daily life. As a concrete application, using robotics technologies for the development of exoskeleton robots [12] or prosthesis devices [13] is becoming an important research direction. In a more recent years, the research for application of rehabilitation to recover the stroke and spinal cord injury patients has also been carried out [12] [14] [15] [16] [17] [18], and bio-signal based assistive control has been widely worked on. In the rehabilitation, the assisitve

control corresponding to the spontaneous brain and nerve activities that comes from when the patients tries to exercise their own paralyzed part of the body has been considered to be important to recover. For example, a training system for paralyzed hands exercise based on the muscle activities from healthy side of his/her hand were developed [19]. However, the bio-signal based assistive robot has yet to have low feasibility despite the high efficiency. One of the reason is instability and vulnerability of bio-signal for the control. Most of conventional bio-signal based robot control studies have been done under small number of channels and degree of freedom (DoF). In this study, I propose assistive control methods based on human motor intention estimated robustly from Electromyography (EMG) or Electroencephalogram (EEG) aiming to alternate or compensate the human motor function with high affinity, and develop hardwares to realize the assisitve control.

1.2 Research Target

A part from the assistive devices specially designed for rehabilitation purpose, which simply repetitively generate pre-designed joint angle trajectories [20] [21] [22] [23] [24] [25] [26]. However, these position based assist control strategies force the user into the robot and to follow the trajectories. Some studies experimentally show that humans control their own limbs by calculating the inverse dynamics in the brain, and the muscles are activated to realize the joint torques as a solution. In order to support human movement, it is important to estimate forces from human and control assist devices. Therefore, force control would be better than the position control to support human movement related to their muscle forces. Developed devices in this study are force controllable based on estimated human motor intention from bio-signals.

To control assistive devices based on bio-signals, EMG has been widely used since it is closely related to muscle activities [27] [28] [29] [30] [31] [32] [33] [34] [35] [36] [37] [38]. For these applications, using multiple sensor channel is a promising approach to estimate the intentions of user limb movements in detail [39] [40]. However, the multi-channel make the assistive robot control more difficult. Physical interaction between human and robot is quite characteristic of assistive robot. This interaction affect bio-signal itself and human motor intention. For example, the state of sensor electrode might be changed, and the human motor intention might also be affected due to the assist forces from device. In addition, if we increase the number of sensor channels, the probability of sensor electrode misplacement by human error might also increase. These anomalies cause significant errors in the estimation of user movements and an unexpected assistive device motion. Since assistive devices such as exoskeleton robots always contact with the limbs of human users, these sensor anomalies can be dangerous for the user. It seems difficult to use many sensor channels to control assistive robots, although using multiple sensor electrodes is useful to estimate user's multiple movement intentions. Moreover, if the exoskeleton robot assist human movement as the results of physical interaction with estimated torque, the human intentional force output might be affected. This possibly cause system instability. In the bio-signal based assist robot control, conventional studies typically set small feedback gain to prevent system's instability.

On the other hand, EEG has also been used to control assistive devices since the user can control assistive devices without actually moving his/her limbs. In order to control the devices based on EEG signals, it is necessary to consider how to capture the feature of human motor intention from EEG and control the assist devices. Because the EEG which measure brain activities with multi-channel in non-invasive is more noisy than EMG, and it is more difficult to estimate the human motor intention in detail for the assistive control.

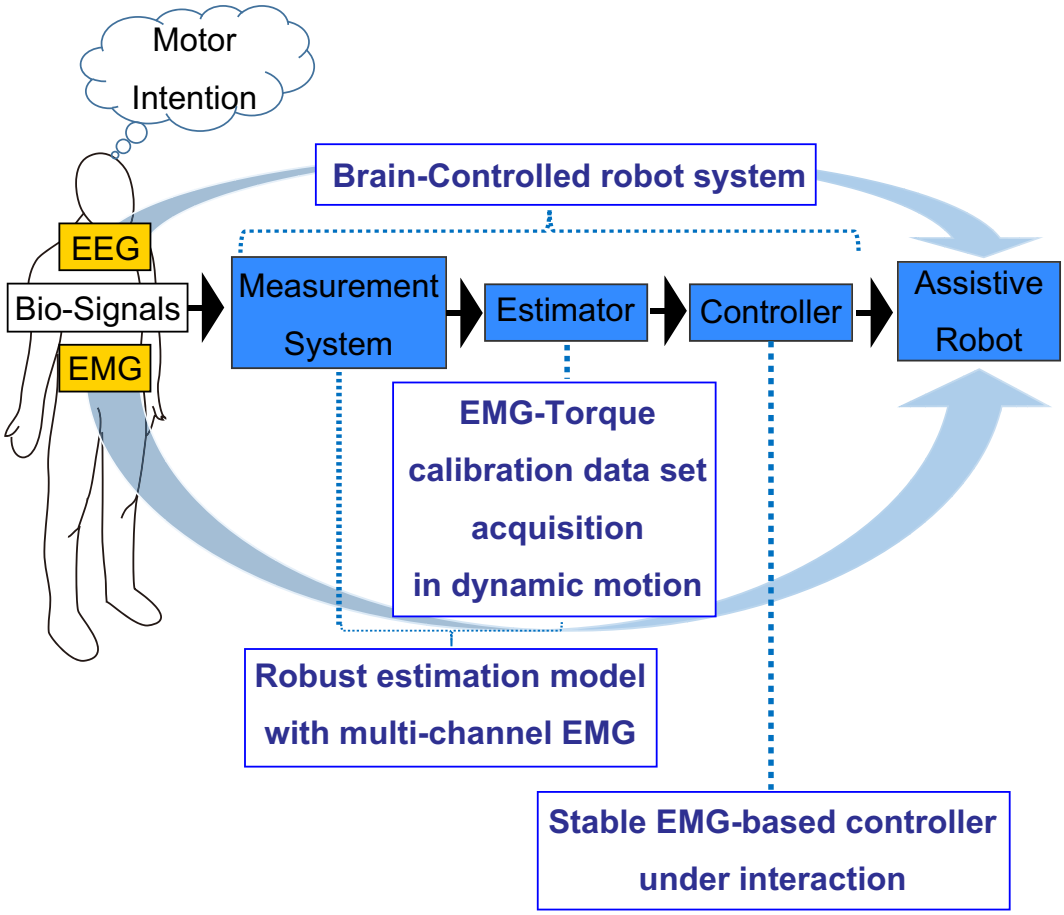

Figure 1.1: Challenges of this study. For the EMG-based control, I first propose EMG-torque data acquisition technique during dynamic motion for the estimator. Second, I propose a robust estimation model with multi-channel EMG sensors. Third, I propose controller under human-robot interaction. For the EEG-based control, I propose brain-controlled robot system that combining EEG-decoding and autonomous exoskeleton robot control technology.

Therefore, EEG-based assistive robot control faces big challenges, while it is expected to be useful for rehabilitation application of patients such as stroke and brain paralysis patients who can not move his/her limbs.

Based on these, I set the basic challenges as follows (see fig. 1.1);

- Robust torque estimation from reliable EMG sensors in dynamic motion for assistive devices control to make stable human-robot interaction.
  - To estimate joint torques during a user's dynamic movement, I first simultaneously measure the joint trajectories and the EMG profiles of a subject. Then, the torque sequences that corresponds to the measured joint angle trajectories are derived using inverse dynamics. Although previous studies also estimate joint torques from EMG, the torques and EMG profiles were measured when a subject generate the torques in a static situation, e.g., generate forces with constant angle and load. On the other hand, to find the relationship between the target dynamic torques and the measured EMG signals, I built a real-time

torque estimation model, which consider the non-linearity between the EMG and muscle forces.

  - Second, I consider using multi-sensor channel information to cope with sensor anomaly for bio-signal based robot control. Because the sensor anomaly is likely to occur for bio-signal based assistive device where the physical interaction among human, robot, and environment exists. In order to extract sensor anomaly, I focus on the muscle cooperativeness and the bio-signal redundancy in machine learning framework.
  - Third, I consider the way of feedback of estimated torques or forces to assistive devices. Because the human motor intentions are affected by the interactions from the assistive robots.

- EEG-based assistive robot system which can support human intended movement by user's brain activities.

  - I apply the autonomous control technologies of humanoid robot as a basic function for the assist devices and I also try to control them based on real-time EEG-decoding feedback system which can directly capture the human motor intention.

I discuss them in the next chapter in detail.

1.3 Configuration of the Thesis

The rest of this paper is organized as follows. In chapter 2, I show the related works and explain my study. In human motor control study, feed-forward control by calculating the inverse dynamics is considered to be as most likely in dynamic voluntary movement [41], and the muscle activities are transmitted as the motor commands from the brain [42]. Therefore, The electromyography (EMG) which can measure muscle activities has been widely used for assistive robot research because it is effective to estimate human movement and forces.

A lot of previous studies tried to control assistive robots based on EMG [27] [28] [29] [30] [31] [32] [33] [34] [35] [36] [37] [38]. These conventional studies capture the relationship between EMG and torques by static load situations e.g., gives the static load on his/her knee in the situation where the subject sit on the chair and measured the EMG related to the joint torque [32] [33] [38]. Then, feedback to the system based on the relations. However, the stiffness and impedances of human joints are different between static and dynamic motion [43] [44] [45] [46]. From them, It can be said that the control criteria are different in the static and dynamic motion, and the data set acquisition need to be done during the dynamic motion. In addition, there is a non-linearity between the muscle activities and muscle forces. Therefore, EMG-torque data set acquisition and non-linearity of EMG-muscle forces are the basic challenges. In addition, to control assistive devices, multi-channel EMG has been a promising approach. However, if the number of sensor channels increase, the probability of sensor anomaly occurrences might also increase. Since assistive devices such as exoskeleton robots can make physical interaction with environments or the limbs of human users, sensor electrodes can be dislodged from the users or damaged by collisions. In addition, sensor electrodes misplacement is likely to occur by human error with multiple sensor channels. Such sensor anomalies cause significant errors in the estimation of user movements. The large deviation of estimated from actual user movements can cause large unwanted interaction joint torques between the robot and the user, and damage the assisted user's limbs. It seems difficult to use many sensor channels to control assistive robots, although using multiple sensor electrodes is useful to estimate user's multi-degree of freedom movement intentions. Furthermore, the estimated torques have typically been fed back to assistive system by multiplying gain in most of conventional studies. However, the human intentional joint torque might be affected by the physical interaction with robot, and the feedback gain need to be carefully set not to cause system's instability. In this study, I cope with the effect of interaction explicitly for feedback to realize stability even in the case of the problem appears.

Chapter 3 describe my proposed method for EMG-based robot control considering that challenges. In order to evaluate the bio-signal based assist control strategy during dynamic motion, I first show my newly developed EMG-based weight support system driven by estimated joint torques. The joint torques are estimated from the model calibrated by using the floating base inverse dynamics and considering the non-linearity between EMG and muscle forces to describe the relations between EMG and torques during dynamic motion. In addition, to estimate joint torques robustly even when the sensor anomaly is occurred, I propose robust human movement estimation. When human moves his/her limbs, muscles related to driven joints are activated cooperatively. I assume that the relations among muscles can be measured by correlation structure of multi-channel EMG sensors and the structures do not collapse while all of the sensors are normal. From this assumption, the anomaly sensors are found by focusing on the muscle correlation structure. Then, estimate the target value using the redundancy of multi-channel bio-signals. Furthermore, I show the stability of EMG-based force feedback controller which explicitly considers human-robot interaction.

Chapter 4 describe the devices used in this study. The systems in my experiments are actuated by Pneumatic Artificial Muscles (PAM) and Electric Motors, and can precisely control the big forces to support human weight.

Chapter 5 shows the experiment and results of EMG-based control. The experiments were conducted with subjects and assistive robot. In the first experiment, to validate my system's control performance in dynamic motion, four healthy subjects performed a one-leg squat with his left leg while right leg was assisted by my proposed EMG-based weight support system. I used the vertical force estimated from the measured EMG signals as a control input to the system. I compared EMG magnitudes with four different experimental conditions. To validate the robustness of my proposed control framework using multi-channel EMG against sensor anomaly. In the experiment, I artificially disconnect and EMG electrodes or detach one side of an EMG probe from the skin surface during the joint movement estimation to control the robot. I show proper control of assistive robots based on the estimated joint torques using my proposed method even when EMG electrodes have sensor problems; a standard method with no fault tolerability against uncertain observations was unable to deal with these fault situations. From these, the robots could be controlled stably by multi-channel EMG to support human dynamic movement with fault tolerability. To assist human movement stably by exoskeleton robot based on estimated human joint torques, I apply human-robot interaction relationship to EMG-based force feedback controller. Conventional approaches have been only consider one-directional mapping from EMG to control input for assistive robot control. However, EMG and force generated by the assistive robot interfere each other, e.g., amplitude of EMG decreases if limb movements are assisted by the robot. On the other hand, in my proposed method, the feed forward interaction torque is feedback into torque controller to acquire the necessity loads. Finally, my proposed robust multi-channel EMG-based assistive robot control was implemented to four-DOF upper limb exoskeleton robot to support human drinking motion with subjects. In this experiment, we consider the two sensor simultaneous anomalies; sensor electrode disconnection and detaching. In addition, we also consider the two EMG electrodes misplacement. The results show that our proposed method can robustly estimate human joint movement even under the anomaly situations and the robot properly assist human drinking motion based on human motor intention with fault tolerability and stability.

In chapter 6, I discuss the EEG-based feedback systems and assist strategies. Recently, brain activity based assistive devices in rehabilitation has been getting useful to recover brain paralysis or stroke patients [47]. Namely, the brain activity which is the source of exercise based assistive system is important for neuro-rehabilitation. In this study, I also show my attempt to develop an EEG-based assistive robot system which can contribute to Brain-Machine-Interface (BMI) rehabilitation. For the BMI rehabilitation, I contribute to construct a Electroencephalogram (EEG)-Exoskeleton robot system, where the robot is connected to the EEG system so that the users can control the exoskeleton robot by using their brain activities. The decoded brain activities are used to control exoskeleton movements by binary classification. This study consider assisting the stand-up movement which is one of the most frequently appeared in daily life and also a standard movement as a rehabilitation. The results shows that the exoskeleton robot successfully assisted user's stand-up motion, where the assist system was actuated by the decoded brain activities.

I finally conclude and show future direction of this study in chapter 7.

Chapter 2

Related Works

Estimating human motor intention from multi-channel bio-signal is expected way to assist human movement with assistive devices according to the user's state. On the other hand, conventional studies have often used small number of bio-signals and control assistive robot with simple controller. In order to realize high affinity physical interaction between human and robot, we need to estimate target value of motor intention robustly from multi sensor channels and control the devices safely. In addition, force controllability of hardware is important, because the assist ratio of the robot can be adjusted. In this chapter, I show some related works from these point of view, and propose my approach with the problems of conventional studies.

2.1 Position based assist control

Most conventional studies tried to assist human movement by position based control [24] [25]. For example, feedback the estimated human joint angles or walking cycle to the assistive robot [48], the robot track the human joint angles [23] [21] [22], assist human by controlling the robot with pre-defined joint trajectories [20] [26]. However, these position based controller can not adjust the assist ratio. In addition, the position based control might forces the user to move his/her limbs by the robot and can give restraint feeling to the user. In order to assist human movement, force control is more effective because it can fit the forces according to human state. In this study, I developed soft and hard ware for assist system which can control forces.

2.2 Human motor control model

It has been shown experimentally that human movement (which means voluntary movement in this paper) is performed by not only feedback but feed-forward control [49]. In order to explain the feed-forward control, some conventional studies mainly proposed a hypothesis of virtual trajectory theory that human activates his/her muscles following the pre-defined equilibrium point to attain some task in stead of calculating the inverse dynamics in the brain [50] [51] [52] [53]. However, D.Bannett et al., [43] [44], Gomi and Koike et al., [45] [46] showed that impedance and stiffness of human in dynamic motion is lower, and Katayama et al., also showed that the virtual trajectory became complex with that low impedance and stiffness value in human kinetic model which has two links and six muscles although the simple task [54] [55]. Since this complexity is mathematically equal to calculating the inverse dynamics, the hypothesis that human being compute inverse dynamics

based on internal model has become a leading [41]. On the other hand, P.Cheney et and E.Fetz et al., reported that motor cortex transmit muscle activations as a control command to realize movement [42]. From these studies, since the EMG signals during dynamic motion can be regarded as a control command to perform the target motion, estimating driven joint torques from EMG is useful for healthy people and patients who have residual function. Dealing with the data set during dynamic motion is important because the control criteria between static and dynamic motion is different. The method of estimating joint torques and muscle forces from EMG is shown in the following section.

2.3 Calibration of joint torque and EMG

EMG has been investigated in a lot of studies because it contains motor control information [37] [38] [36], and recently used in rehabilitation application [19]. In order to describe the non-linearity between muscle activities and forces, Hill proposed a muscle model [56]. Some studies implemented the Hill model to estimate muscle forces finding parameters of that non-linear function [57] [58]. Others estimated human movement from EMG considering the non-linearity by machine learning techniques (e.g.,neural networks), and controlled upper limb exoskeleton robot [29] [28] [30] [31]. However, these neural network algorithm require a lot of cost to learn parameters (after it called calibration) with increase the number of sensor channels and hidden layer. In addition, some reported that although the consideration of non-linearity using machine learning techniques like neural network, a significant improvement of the muscle force estimation is not seen compared to Hill's muscle model [27] [28].

C. Fleischer et al., controlled one-leg exoskeleton robot based on estimated human joint torques from EMG using Hill type muscle model [35]. However, the calibration was conducted in the static situation and they could not describe the relationship between EMG and joint torques during dynamic movement as shown in 2.2. Namely, estimating joint torques from EMG using data set related to dynamic motion is the basic challenge.

2.4 Joint torque estimation from multi-channel EMG for assistive robot control

EMG has been widely used to control assistive devices for detecting human movement intentions. For example, the following types of EMG-based robot control devices or robots have been investigated: hand prostheses [59], upper prostheses [60] [61] [62], lower prostheses [63] [64], hand exoskeletons [65] [66] [67], upper limb exoskeletons [68] [69], and lower exoskeletons [70] [71] [33] [72] [35]. For these applications, using multiple sensor channels is a promising approach to estimate user movement intentions [73] [39] [74] [40].

However, increasing the number of sensor channels also raises the probability of sensor fault occurrences such as sensor electrode disconnection, and misplacement. In addition, since prostheses or exoskeleton robots can make physically interaction with environments or the limbs of human users, the sensor electrodes can be detached from the users or be damaged by the physical contact. In particular, since such sensor anomalies cause unexpected motions of the assistive devices, these sensor anomalies can be dangerous. Therefore, perhaps using many sensor channels is not a suitable approach to control assistive robots, but using multiple sensor electrodes is useful to estimate user movement intentions.

Previous studies proposed EMG sensor fault detection methods to cope with sensor electrode disconnection and detaching failure situations. Most focused on independently

monitoring the information of each EMG channel to find a fault sensor [75] [76] [77] [78] [79] [80] [81]. For example, Variance Weighted Average (VWA) copes with sensor disconnection [77]. In this approach, two EMG signals are fused into one signal based on the signal variance to determine the weight parameter and to monitor increases of the sensor signal variance. However, since the variance of the sensor signal might not always increase when sensor fault occurs, this method can only be used for limited fault situations. Using such higher order statistics as skewness and kurtosis to capture the changes of probability distribution for sensor fault detection has also been proposed [78]. However, since this approach requires batch calculation to derive higher order statistics, it might not be suitable for online robot control. Extracting sensor fault by monitoring the deviation from the mean values of each EMG sensor channel output is a simple and useful approach since it can be easily implemented. The cumulative sum (CUSUM)-based fault detection method, which uses the deviation from the mean value, controls an assistive device [79] [80]. However, this simple approach needs careful threshold tuning to define the fault state and an observation period to monitor the deviation from the mean.

2.5 EMG-based controller of assistive robot

EMG-based controller for assistive robot movement has been the long term research field addressed in several studies, and EMG signal was considered as control command source related to human intention. time-varying estimated joint torque, $\hat{\tau}_{emg}$ as intentional torque, was estimated and feed-backed into the controller. Typically, feedback torque τ_{robot} was

$$\tau_{robot} \leftarrow \alpha_1 \hat{\tau}_{emg}, \tag{2.1}$$

where the α_1 is the feedback gain; provided that estimating human intentional torque (τ_{human}) is equivalent to torque estimated from EMG (e.g., $\tau_{human} = \hat{\tau}_{emg}$). However, if the exoskeleton robot assists human intentional torque τ_{human} should be affected and can not use the original estimation. Additionally, if the exoskeleton completely assist human movement, in ideal case $\alpha_a = 1$, the next moment gives human joint torque $\tau_{human} = 0$, resulting in $\tau_{robot} = 0$. This actually doesn't occur in practical application because there are dynamics of muscle activity and EMG decreases with time delay. More practically, interaction is rather complex that the constraint between human and robot is incomplete, and that the joint rotation axis is different. At least, increasing α_1 reduces τ_{human}, and rises the system's instability.

2.6 Brain controlled assistive robot

In recent years, BMI (Brain Machine Interface) systems to control lower-body and upper-body exoskeleton robot became a focus of bio-signal based assistive robot control research as well as the EMG. Since the BMI system can control the devices and assist user's motion by brain activities without the actual movement of user's limbs, the systems have attracted attention mainly in neurological rehabilitation applications. Some conventional studies tried to control assistive devices using invasive methods [82]. However, since invasive methods have the risks associated with surgery and degradation in signal quality, non-invasive methods to measure brain activities are generally preferred. There are several non-invasive techniques acquiring brain activities: functional magnetic resonance imaging (fMRI) [83], near-infrared spectroscopy (NIRS) [84], magnetoencephalography (MEG) [85], electroencephalography (EEG) [86] and so on. Among them, the EEG has

been widely using for brain-controlled robot, because it has high time resolution, less environmental limits (portability).

Controlling assistive devices based on human motor intention decoded from EEG is challenging problem, because it is difficult to extract enough information to completely and safely control the robot. In addition, the non-invasive EEG has difficulty in decoding brain states under physical interaction which is generated by actuating the robot, because the EEG is easy to pick up noises. In order to control assistive devices using such a rough information, robust estimation of human motor intention and high performance controllable robot systems are needed.

2.7 Device development

I introduce practical device to support human movement. Some studies developed exoskeleton robot for military purpose [21] [22] [23], improvement the working efficiency in factory [16], and farming [17]. Others developed power suits as a welfare device [14] [32] [33] [34], walking support device [18] [15] for rehabilitation, and also have proposed brain activities based robotic assist device to support recovering brain function for brain paralysis. The exoskeleton robot has been developed in many studies and the purpose is wide-ranging.

Most of these exoskeleton robots target to be used for healthy user, and there is few devices for un-healthy user (e.g., spinal cord injury and brain paralysis patients). Therefore, they (device for healthy subject) don't need to have high spec to support full weight of user and most of them don't deal with high forces. In addition, as noted in section 2.1, most of conventional controllers of exoskeleton robot are based on position or angles, and does not have force, balance, and self-control. From the point of rehabilitation view, it is necessary to develop new system because there is a limitation of existing devices.

2.8 The problems of conventional studies and the solution

Fig. 2.1 shows the research target of my EMG-based robot control study. For achieving the purpose, I show the problems of conventional studies and the solution shortly in this section. In addition, I briefly explain the EEG-based robot control which have challenging problems.

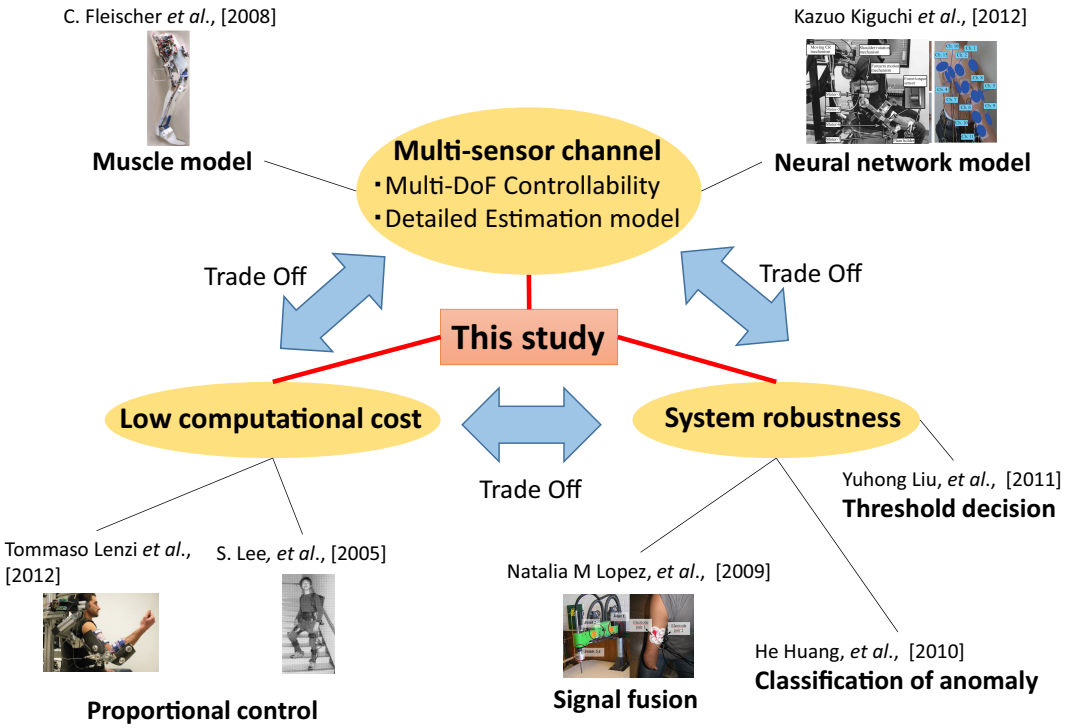

Figure 2.1: Positioning of this study

2.8.1 Torque-EMG data set acquisition during dynamic motion

Some conventional studies aimed at practical application used linear model to estimate joint torques from EMG [14] [36]. However, since the approximate range of estimation is limited, the non-linearity of muscle activities and forces can not be described. On the one hand, Fleischer et al.,[35] as shown in section 2.3 estimated lower limb joint torques by the function calibrated in static motion (e.g., measure the EMG and joint torque data set when subject are loaded in sitting state.) while they used muscle model. However, they also can not match the correspondence relation during the dynamic motion because the non-linearity of velocity is excluded. In addition, they did not consider the change of lower limb joint torques based on ground reaction force.

In order to assist human movement, the joint torques are need to be estimated by control command of voluntary motion and feedback to assistive devices. However, it is impossible to measure the joint torques in the dynamic motion directly, and technically difficult to acquire the EMG-torque data set related to the dynamic motion. In this study, I propose to acquire the EMG-torque data set in the dynamic motion by introducing floating base inverse dynamics which can consider the ground reaction force especially for lower limb movement. Then, the muscle activities are converted to non-linearity based on the biomechanical knowledge [57] and estimate the joint torques by the linear model calibration

which can be expected to high generalization in spite of the low calibration cost.

2.8.2 Robust joint torque estimation with multi-channel EMG for assistive robot control

In order to detect anomaly EMG sensor channels, the previous approaches need to monitor the long period of the EMG signal sequence because they only rely on the temporal profiles of the data and do not consider such spatial information as the relationships between the different EMG signals measured by different sensor electrodes. Consequently, these methods aren't useful to extract immediate changes in sensor conditions and are not preferable for real-time robot control. Indeed, most conventional studies tend to end up only showing the fault detection performance without presenting the results of robot control [78] [79] [81]. Moreover, a threshold that is used to define the fault situation needs to be carefully determined because appropriate thresholds can vary among participants or for different EMG electrode placements.

In this study, I propose using multi-sensor channel information to extract sensor faults to cope with sudden sensor failure for biosignal-based robot control. I focus on developing a measurement system with multi-sensor channels to have fault tolerability. For such the system, I propose that the tolerability is realized by focusing on the muscle cooperativeness and the redundancy of bio-signals. Concretely, correlation structure of EMG is used so that I can use not only the temporal profiles but also the spatial information to quickly extract sensor anomaly. In this study, I assume two types of situation. One situation is that assistive system with multi-sensor channels but not too many, and the fault state can be predictable. Supervised learning such as classification method can be used in this situation. The other is that the assistive system with multi-channels and the sensor fault state can not be predictable. In such case, I address the problems in unsupervised learning framework.

2.8.3 EMG-based robot control under interaction

The problem that eq3.30 is not closed form, because τ_{emg} is dependent to the τ_{robot}. During the assist, the human torque controller should decrease joint torque to achieve τ_{human}. In this study, I consider the following hypothesis based on torque coordination controller as follows,

$$\hat{\tau}_{emg} = \tau_{human} - \tau_{rh}, \tag{2.2}$$

where τ_{rh} is interaction assistive torque applied from robot to human, and $\hat{\tau}_{emg}$ is the simplified human muscle activity as desired joint torque to achieve τ_{human}.

2.8.4 Real-time EEG-based assistive robot control

Brain computer interface (BCI) is developed for people who is hard to control their own body spontaneously to improve their quality of life in several studies [87] [88]. In more recent study, the BCI technologies have been investigating to decode brain states from non-invasive EEG signals into commands to control assistive robot for rehabilitation application [89] [90]. However, most of conventional studies investigated the performance of EEG-based feature extraction in off-line and few studies proposed real-time EEG-based assistive robot system.

Although the EEG can be used portably and safely, small signal-to-noise ration cause the difficulty in robustly decoding enough information to control external devices. EEG-based exoskeleton robot is challenging problems. Shared control system consisted of brain

control and autonomous robot control (e.g., self balancing, walking and so on) is one key to make a breakthrough the difficulty [91]. In this study, I contributed to develop an shared controlled real-time EEG-exoskeleton robot systems which can support user's movement by his/her own motor imagery (the mental execution of a movement without any overt movement or without any muscle activation).

Chapter 3

Robust Hman Motor Estimation using Multi-channel EMG to Control Assistive Robot

3.1 Joint torque acquisition with Floating Base Inverse Dynamics for dynamic motion

To derive joint torques during dynamic motion from joint angle trajectories, an inverse dynamics model of an approximated subject body is used. If we consider lower limb motion such as squat which is involved in daily behaviors different from previous studies that worked on estimating knee movements from EMG signals when a subject was siting on a chair [72] [92], it is need to explicitly take the ground reaction forces $\mathbf{f}_{grf}$ into account. For this purpose, we use floating base inverse dynamics:

$$\mathbf{M}(\theta)\ddot{\theta} + \mathbf{h}(\theta, \dot{\theta}) + \mathbf{g}(\theta) = \mathbf{S}^\top \tau + \mathbf{J}_c^\top(\theta)\mathbf{f}_{grf}, \tag{3.1}$$

where θ represents the general coordinate system of the joint angles, $M(\theta)$ is the floating base inertia matrix, $h(\theta, \dot{\theta})$ is the floating base centripetal Coriolis, $\mathbf{g}(\theta)$ is the gravity force, $\mathbf{S}$ is the actuated joint selection matrix, and $\mathbf{J}_c$ is the Jacobian matrix which represents relationships between joint angle movements and deviations of contact points. If the $\mathbf{f}_{grf}$ can be measured by force sensor, the inverse dynamics torques can be computed from (3.1). However, this approach is undesirable because the force sensors must be located at all contact points. Therefore, we calculate the torques and the ground reaction forces that correspond to the joint angles, the velocity, and the acceleration by computing the QR decomposition of $\mathbf{J}_c$ [93]:

$$\mathbf{J}_c^\top = \mathbf{Q}\begin{bmatrix} \mathbf{R} \\ 0 \end{bmatrix} \tag{3.2}$$

where $\mathbf{Q}$ is orthogonal, and $\mathbf{R}$ is an upper triangle matrix of rank k if given $rank(J_c) = k$. We can decompose the dynamics (3.1) into two independent equations from (3.2).

$$\mathbf{S}_c\mathbf{Q}^\top(\mathbf{M}\ddot{\theta} + \mathbf{h} + \mathbf{g}) = \mathbf{S}_c\mathbf{Q}^\top\mathbf{S}^\top\tau + \mathbf{R}\mathbf{f}_{grf} \tag{3.3}$$

$$\mathbf{S}_u\mathbf{Q}^\top(\mathbf{M}\ddot{\theta} + \mathbf{h} + \mathbf{g}) = \mathbf{S}_u\mathbf{Q}^\top\mathbf{S}^\top\tau \tag{3.4}$$

Though the equations (3.3) and (3.4) are independent, the full dynamics is represented with either equation. The equation (3.4) describes the full dynamics without ground reaction

forces, and the ground reaction forces are computed from (3.3), where $\mathbf{S} = [\mathbf{I}_{n\times n}\ \mathbf{0}_{n\times 6}]$, $\mathbf{S}_c = \left[\mathbf{I}_{k\times k}\ \mathbf{0}_{k\times(n+6-k)}\right]$, and $\mathbf{S}_u = \left[\mathbf{0}_{(n+6-k)\times k}\ \mathbf{I}_{(n+6-k)\times(n+6-k)}\right]$. $\mathbf{I}_{n\times n}$ is a unit matrix of the n rows and n columns.

3.2 Estimating muscle force

The muscle force is derived by using the Hill-Stroeve model [56] [58] from EMG signals. The model takes the nonlinearities of the muscle length-tension relationship and force-velocity relationship:

$$u_t^i = k(\xi_t^i)h(\eta_t^i, \xi_t^i)q_t^i, \tag{3.5}$$

where each non-linear function $k(\cdot)$ and $h(\cdot)$ cites Hatze's parameterized fitting function [57] with two parameters a_1 and a_2. q_k^i is full-wave rectified and a low-pass filtered signal of raw EMG signal e_k^i. I use the second order Butterworth filter. the Hill-Strove model used in (3.5). The $h(\eta^i, \xi^i)$ and $k(\xi^i)$ are computed as follows:

$$\begin{aligned} h(\eta^i, \xi^i) &= \frac{1+\tanh(a_1\dot{\eta}^i - a_2)}{b_2} - b_1 e^{-2.6(\xi^i-1)} && (3.6)\\ k(\xi^i) &= 0.32 + 0.71e^{-1.112(\xi^i-1)} \\ &\quad \times \sin(3.722(\xi^i - 0.656)) && (3.7) \end{aligned}$$

where $\xi^i = \frac{l^i(\theta)}{l^{i,n}}$, $\eta^i = \frac{\dot{\xi^i}(\theta)}{v^{i,max}}$, $v^{i,max} = 3.0$, $l^i(\theta)$ is the current length of muscle i, $l^{i,n}$ is its natural length, and $v^{i,max}$ is its maximum contraction rate. In this study, the natural muscle length is approximately set as the same to the link length. The current muscle length is computed by adding partial periphery length of the joint pulley to the natural muscle length with considering the current joint angle. $b_1 = [1-\tanh\{a_1(1+a_2)\}]/b_2$ and $b_2 = \tanh\{a_1(1+a_2)\}$. The parameters, a_1 and a_2, depend on the muscle type, and the approximate range of values for a_1 and a_2 are $a_1 = 1.6$ to 2.7 and 2.9 to 3.8, and $a_2 = -0.05$ to 0.1 and -0.01 to 0.1 for fast and slow fibres, respectively. In this paper, we defined these parameter for each muscles experimentally by repeating the cross-validation to minimize the error of torque estimation.

We consider tendon-pulley linear model between joint torques from inverse dynamics and muscle forces to estimate joint torque from EMG. The parameters to estimate joint torques are determined by the least square estimation method to minimize the error between them.

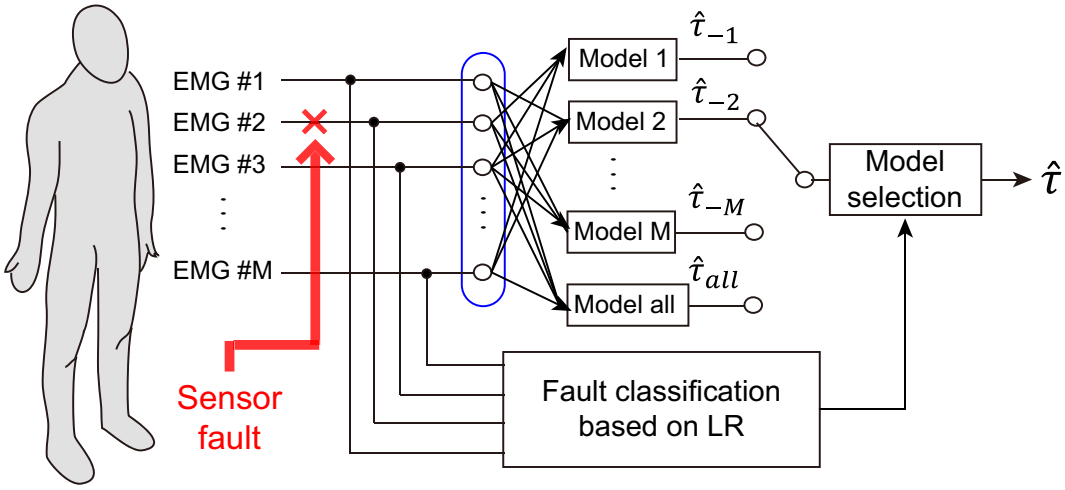

Figure 3.1: Schematic diagram of our proposed fault tolerant biosignal-based control architecture. It selects a proper torque estimation model based on classifier output. Fault channel is identified by logistic regression where input to the classifier is the correlation among EMG signals.

3.3 Robust joint torque estimation model with multi channel EMG

In this study, I propose to use correlation structure to find EMG sensor anomaly assuming that human move his/her own limb by activating muscle cooperatively related to joint, and this relations acquired by multi-channel EMG do not collapse while all sensors are normal.

3.3.1 Supervised learning framework

To evaluate my proposed method using multi-sensor channel information (correlation structure of EMG) for extract sensor faults. I first focus on developing a measurement system with multi-channels but not too many channels. For such a measurement system, I consider a classification method to extract a fault situation for which we do not need to explicitly design a threshold. Figure 3.1 shows a schematic diagram of my proposed fault tolerant architecture in classification framework.

To find sensor faults, we classify the fault channel by logistic regression using the correlation among the EMG sensor channels. Since muscles are synergetically activated to generate target movements as pointed out in previous studies [94] [95] [96] [97], the correlation among muscle activities can be a useful feature to classify sensor fault situations. The correlation of the i-th and j-th EMG channels is given as:

$$r_{ij} = \frac{c_{ij}}{\sqrt{c_{ii}}\sqrt{c_{jj}}}, \tag{3.8}$$

where r_{ij} represents the i-th row and the j-th column element of the correlation matrix and c_{ij} is the i-th row and the j-th column element of the covariance of the EMG signals. The covariance can be derived as $c_{ij} = \frac{1}{N}\sum_k^N (e_k^i - \bar{e^i})(e_k^j - \bar{e^j})$, where e^i denotes the i-th EMG signal and $\bar{e^i}$ is the mean. Then we use the off-diagonal elements of the lower triangle part

of the correlation matrix as the classifier input. Assuming that we simultaneously measure M EMG channels, the input vector is represented as $\mathbf{z}^\top = \left[z_1, z_2, z_3, \ldots, z_{\frac{M(M-1)}{2}}\right]^\top = [r_{12}, r_{13}, r_{23}, \ldots, r_{M-1,M}]^\top$. In the experiments, the correlation matrix is computed every time step with a 100-msec sliding window, where the window size is determined by cross validation.

Here we label the normal state of the EMG channel as class S_1 and the fault state as class S_2. A linear discriminant function that separates classes S_1 and S_2 is represented by the weighted sum of each input value:

$$f(\mathbf{z}; v) = \sum_{i=1}^{D} v_i z_i + v_0, \tag{3.9}$$

where $\mathbf{z} = [z_1, ..., z_D, 1]^\top$ is the augmented input feature vector in $D = \frac{M(M-1)}{2}$ dimensional space and $v = [v_1, ..., v_D, v_0]^\top$ is a parameter vector including bias v_0. Hyperplane $f(\mathbf{z}; v) = 0$ determines the boundary between two classes. In logistic regression, the log odds of the probabilities of P($S_1|\mathbf{z}$) and P($S_2|\mathbf{z}$) called *logit* are represented as a linear function of input vector $\mathbf{z}$:

$$\ln\left(\frac{P}{1-P}\right) = f(\mathbf{z}; v). \tag{3.10}$$

Probability P can be derived:

$$P = \frac{1}{1+\exp(-f(\mathbf{z}; v))} = P(S_1|\mathbf{z}). \tag{3.11}$$

It ranges from 0 to 1 and equals 0.5 when $f(\mathbf{z}; v) = 0$. As output of the logistic regression, binary random variable y is introduced. The input data in class S_1 are paired with output $y = 1$, while the input data in class S_2 are paired with output $y = 0$. Given a data set of N paired samples $(e_1, y_1), (e_2, y_2), ..., (e_N, y_N)$, the likelihood is given as:

$$\begin{aligned} P(y_1, ..., y_N|\mathbf{z}_1, ..., \mathbf{z}_N; v) &= \prod_{n=1}^{N} P(y_n|\mathbf{z}_n; v) \\ &= \prod_{n=1}^{N} P_n^{y_n}(1-P_n)^{1-y_n}. \end{aligned} \tag{3.12}$$

Next we optimize parameter vector v so that the likelihood function is maximized. If probability $P > 0.5$, the measured EMG sensor signal is classified as S_1; otherwise it is classified as S_2.

I robustly estimate human joint torque from EMG signals for the torque control of an assistive device even when sensor faults suddenly occur. In my fault tolerant EMG-based robot control strategy with classification, I selected a reliable torque estimation model based on the output of the sensor fault classifiers so that information from the failure channel is not utilized in the torque estimation:

$$\hat{\tau} \leftarrow \begin{cases} \hat{\tau}_{all} & (\prod_{n=1}^{M} y_i = 1) \\ \hat{\tau}_{-i} & (y_i = 0), \end{cases} \tag{3.13}$$

where estimated torque $\hat{\tau}$ is given by model $\hat{\tau}_{all}$, which uses all the channels to estimate the joint torque, or by model $\hat{\tau}_{-i}$, which does not use the detected i-th fault channel. In other words, if one of the sensor channels has a problem, one of the torque estimation models, $\hat{\tau}_{-i}$, is used. Otherwise we use estimation model $\hat{\tau}_{all}$.

Since EMG nonlinearity was considered in a previously introduced model, here I assume the simple linear tendon-pulley model [98] and estimate the joint torques from the EMG signals:

$$\begin{cases} \hat{\tau}_{all} = w_{all}^{\top} \mathbf{u}_{all} \\ \hat{\tau}_{-i} = w_{-i}^{\top} \mathbf{u}_{-i}. \end{cases} \tag{3.14}$$

Considering the non-linearity of EMG [99], input variables $\mathbf{u}_{all}$ and $\mathbf{u}_{-i}$ for the linear tendon-pulley models are represented as follows:

$$\begin{aligned} \mathbf{u}_{all} &= \left[u^1, u^2, \ldots u^M, u^0\right]^{\top}, \\ \mathbf{u}_{-i} &= \left[u^1, u^2, \ldots, u^{i-1}, u^{i+1}, \ldots, u^M, u^0\right]^{\top}, \end{aligned} \tag{3.15}$$

where M is the number of sensor channels and element u^i is the preprocessed EMG signal related to muscle forces as shown in section3.2.

Parameter vectors w_{all} and w_{-i} in Eq. (3.14) are derived using the least square method to minimize the error between target torque τ, as in previous studies [72] [100] [98], computed from the inverse dynamics shown in section3.1 of a subject's movement and estimated torque $\hat{\tau}$:

In my proposed approach, the joint torque estimation model is switched when a sensor fault is detected. Therefore, the torque command profile can contain the discontinuity. To cope with this problem, we introduce first order dynamics for torque output $\hat{\tau}$ in Eq. (3.14):

$$\gamma \dot{\overline{\tau}} = -\overline{\tau} + \hat{\tau}, \tag{3.16}$$

where γ represents the time constant of the dynamics. We set the time constant to $\gamma = 100$ msec, which is close to the time difference between the EMG signal observation and the corresponding muscle force generation [100]. Then smoothed torque output $\overline{\tau}$ is used as the final torque command to the robot.

3.3.2 Unsupervised learning framework

In the supervised learning method with logistic regression for sensor fault detection, the threshold is determined by the learning method. This method is useful in limited situations because the anomaly detection problem can be treated with classification. However, scalability is limited since I need to prepare all possible sensor failure situations to train the supervised learning method. In order to estimate human movement from EMG with fault tolerability in unsupervised learning framework, I propose a novel approach. Most previous EMG-based control studies consider EMG signals to be user control commands, and the user commands of EMG signals are converted to the joint movements of the robot by linear conversion model [68] [72] or a nonlinear neural network model [69] [100]. In this study, I consider EMG signals to be observation variables and estimate user intended movements from observations (Fig.3.2). By treating the EMG-based control problem as an estimation problem of user movement intentions from observed EMG signals, we can properly handle noise problems and sensor failure situations. We propose a state estimation model that can cope with uncertain observations, where the uncertainty is determined by an anomaly detection method. Sensor channel anomalies are found by checking the current covariance of the EMG signals measured by multiple EMG electrodes against the normal condition.

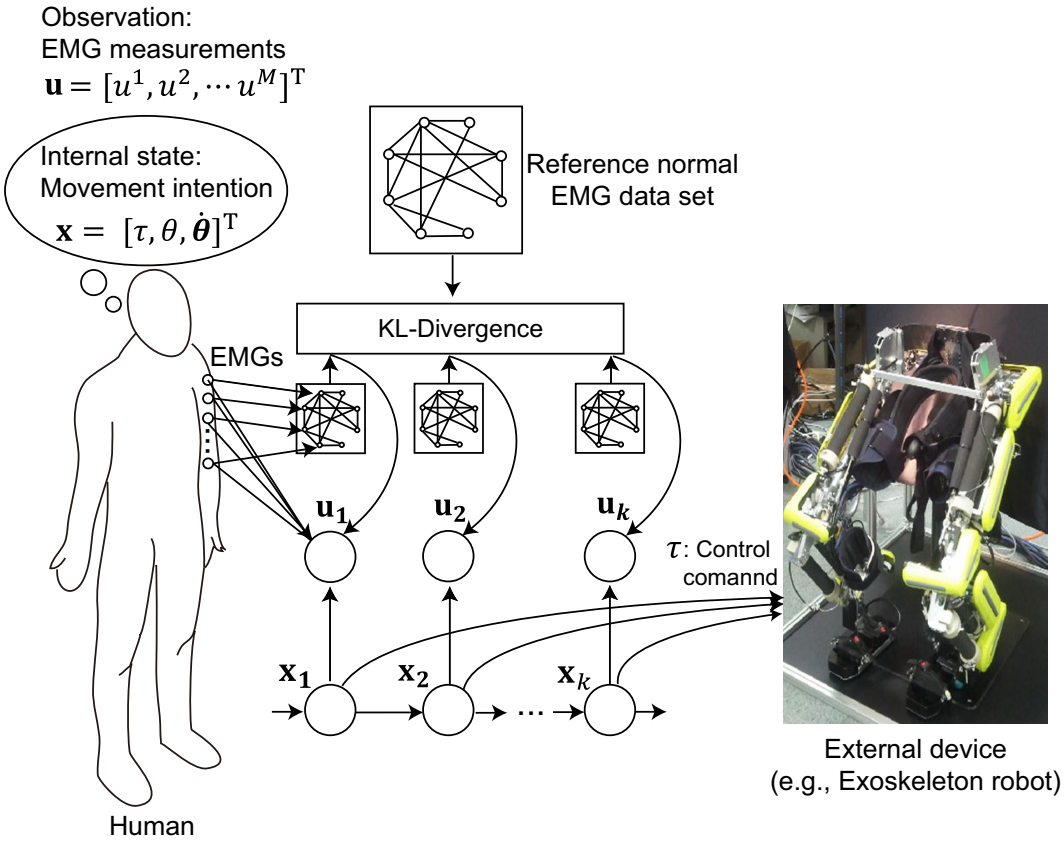

Figure 3.2: Schematic diagram of our proposed estimation method of human joint movements from observed EMG-signals for assistive robot control even under sensor failure situations with using multiple EMG electrodes.

Body dynamics and movement pattern generation models

In our movement estimation approach, we use a movement model composed of forward body dynamics, movement pattern generation model, and EMG-signal observation model. We assume that the joint movement intention is represented as a sequence of the joint torques. Below we introduce how we combine these three models to estimate user movement intention.

Forward body dynamics

As presented in Fig.3.2, we consider joint angle θ, angular velocity $\dot{\theta}$, and joint torque τ as internal state of the human movement model: $\mathbf{x}(k) = [\theta^{\top}(k), \dot{\theta}^{\top}(k), \tau^{\top}(k)]^{\top}$. As a part of the human movement model, we consider forward body dynamics:

$$\begin{bmatrix} \theta(k+1) \\ \dot{\theta}(k+1) \end{bmatrix} = \mathbf{F}\left(\theta(k), \dot{\theta}(k)\right) + \mathbf{G}\left(\theta(k), \dot{\theta}(k)\right)\tau(k) + \begin{bmatrix} \mathbf{w}_{\theta}(k) \\ \mathbf{w}_{\dot{\theta}}(k) \end{bmatrix}, \tag{3.17}$$

where $\mathbf{F}$ and $\mathbf{G}$ can be derived from identified exoskeleton robot parameters and from knowledge of human body parameters. $\mathbf{w}_{\theta}$ and $\mathbf{w}_{\dot{\theta}}$ represent system noise that can be also used to cope with modeling errors.

Pattern generation model

As the pattern generation model, we use a linear dynamics:

$$\tau(k+1) = \mathbf{A}\begin{bmatrix}\theta(k)\\ \dot{\theta}(k)\end{bmatrix} + \mathbf{B}\tau(k) + \mathbf{w}_\tau(k), \tag{3.18}$$

so that overfitting problem can be better avoided while the model can represent movement trajectories better than the constant model which was frequently used for estimating parameters in a state estimation model. However, the model complexity can be selected according to purpose of a target task. The model parameters **A** and **B** can be derived from the measured motion profiles for finding the model parameters. Joint torques profiles to identify these parameters are derived from the inverse dynamics of a subject and a robot.

Observation model

As presented in Fig.3.2, we consider processed EMG signals u in (3.5) as observation variables of the human movement model:

$$\mathbf{u}(k) = \mathbf{C}\mathbf{x}(k) + \mathbf{v}(k). \tag{3.19}$$

We used a linear observation model since previous studies have been find that the processed EMG signals can have linear relationship with joint torque [35] [68] [101]. Processed EMG signals $\mathbf{u}(k) = \left[u^1(k), u^2(k), \cdots, u^i(k), \cdots, u^M(k)\right]^\top$ are observed by using M EMG channels. Element u^i is calculated from i-th EMG signal q^i by considering non-linearity as shown in 3.2. where q^i is the full-wave rectified and low-pass filtered signals of the raw EMG signal e^i.

Observation matrix **C** in Eq. (3.19) and nonlinear shape factor in Eq. (3.5) are optimized using the MATLAB Optimization Toolbox to minimize the following cost function: $\sum_k (\mathbf{u}(k) - \mathbf{C}\mathbf{x}_{target}(k))^2$, where $\mathbf{x}_{target} = [\theta_{target}^\top, \dot{\theta}_{target}^\top, \tau_{target}^\top]^\top$ is the measured motion profiles for finding the model parameters and τ_{target}, as in previous studies [72] [100] [98], which were computed from the inverse dynamics of a subject's and robot's arms.

In this study, we design covariance $\mathbf{R}(k)$ of observation noise $\mathbf{v}(k) \sim \mathcal{N}(0, \mathbf{R}(k))$ in Eq. (3.19) so that the observation model can take the sensor failure situations into account. The covariance is represented as:

$$\mathbf{R}(k) = \begin{pmatrix} \sigma_{e^1} + a_k^1\sigma_a & & & \cdots & 0 \\ & \ddots & & & \vdots \\ & & \sigma_{e^i} + a_k^i\sigma_a & & \\ \vdots & & & \ddots & \\ 0 & \cdots & & & \sigma_{e^M} + a_k^M\sigma_a \end{pmatrix}. \tag{3.20}$$

Here σ_a indicates basis noise variance which is used to represent uncertainty comes from sensor failure. The size of the uncertainty is scaled with the anomaly score a^i of the i-th channel, where the anomaly score is calculated by monitoring the muscular coordination as we introduce in the next subsection. In this study, we simply set $\sigma_a = 1$ while this parameter could be optimized. σ_{e^i} is the observation noise variance of each EMG sensor channel without sensor failure situations.

Anomaly score calculation

Here we introduce how we calculate the anomaly score a_i in (3.20). Given EMG sensor data set $\mathscr{D}$,

$$\mathscr{D} = \left\{ \mathbf{e}_n | \mathbf{e}_n \in \mathbb{R}^M, n = 1, 2, ..., N \right\}, \tag{3.21}$$

where N denotes the number of samples and M denotes the number of sensor channels, i.e., $\mathbf{e} = [e^1, e^2, ..., e^M]^\top$. e^i is the raw EMG signal measured by i-th channel. The probability of the sample can be represented by M-dimensional Gaussian distribution:

$$\mathscr{N}(\mathbf{e}|0, \Lambda^{-1}) = \frac{\det(\Lambda)^{1/2}}{(2\pi)^{M/2}} \exp\left(-\frac{1}{2} \mathbf{e}^\top \Lambda \mathbf{e} \right), \tag{3.22}$$

where $\Lambda \in \mathbb{R}^{M \times M}$ represents a precision matrix which is the inverse matrix of a covariance.

Sparse inverse covariance learning

Here, we assume that the data sets $\mathscr{D}$ has been standardized to have zero mean and unit variance. Then, the empirical covariance matrix $\mathbf{S}$ of the EMG data sets is given by

$$\mathbf{S} = \frac{1}{N} \sum_{n=1}^{N} \mathbf{e}_n \mathbf{e}_n^\top. \tag{3.23}$$

Here we derive a precision matrix Λ of the multivariate Gaussian in (3.22). However, since the sample covariance matrix is often rank deficient and the inverse does not exist, using a regularization method is necessary. In this study, as suggested in [102] [103], we consider L_1-norm regularization to find the sparse precision matrix by maximizing the objective function:

$$\Lambda^* = \arg\max_{\Lambda} \left[\ln \det \Lambda - \mathrm{tr}(\mathbf{S}\Lambda) - \rho ||\Lambda||_1 \right]. \tag{3.24}$$

When block coordinate descent algorithm is used for the objective function in (3.24) [102] [103], we focus on a particular single channel e_i and set partition for the precision matrix Λ and its inverse as

$$\Lambda = \begin{pmatrix} L & l \\ l^\top & \lambda \end{pmatrix}, \ \mathbf{S} \equiv \Lambda^{-1} = \begin{pmatrix} S & s \\ s^\top & \sigma \end{pmatrix}, \tag{3.25}$$

where the rows and columns are always arranged so that the z_i-related entries are set in the last row and column. Therefore, $L, S \in \mathbb{R}^{(M-1)\times(M-1)}$, $\lambda, \sigma \in \mathbb{R}$, and $l, s \in \mathbb{R}^{M-1}$.

Anomaly score

The difference between the two data sets $\bar{\mathscr{D}}$ and $\mathscr{D}$ in terms of i-th sensor channel is measured by Kullback-Leibler (KL) divergence of the probabilistic models:

$$d^{i,\bar{\mathscr{D}}\mathscr{D}} \equiv \int d\mathbf{h}^i p_{\bar{\mathscr{D}}}(\mathbf{h}^i) \int de^i p_{\bar{\mathscr{D}}}(e^i|\mathbf{h}^i) \ln \frac{p_{\bar{\mathscr{D}}}(e^i|\mathbf{h}^i)}{p_{\mathscr{D}}(e^i|\mathbf{h}^i)}, \tag{3.26}$$

where, $\mathbf{h}^i = [e^1, \cdots, e^{i-1}, e^{i+1}, \cdots, e^M]^\top$. Since we assume a Gaussian distribution, the expected KL divergence d_i can be computed as follows [104]:

$$\begin{aligned} d^{i,\bar{\mathscr{D}}\mathscr{D}} &= \bar{s}^\top (l - \bar{l}) \\ &+ \frac{1}{2}\left\{ \frac{l^\top \bar{S} l}{\lambda} - \frac{\bar{l}^\top \bar{S} \bar{l}}{\bar{\lambda}} \right\} \\ &+ \frac{1}{2}\left\{ \ln \frac{\bar{\lambda}}{\lambda} + \bar{\sigma}\left(\lambda - \bar{\lambda}\right) \right\}. \end{aligned} \tag{3.27}$$

The d^i measures the change in the neighborhood graph of the i-th node.

The other measure $d^{i,\mathscr{D}\bar{\mathscr{D}}}$ also exists and is obtained by replacing $\mathscr{D}$ with $\bar{\mathscr{D}}$ in the above. Then, the anomaly score of the i-th variable is defined as follows:

$$a^i \equiv \max(d^{i,\mathscr{D}\bar{\mathscr{D}}}, d^{i,\bar{\mathscr{D}}\mathscr{D}}). \tag{3.28}$$

Using above calculations, we derive the anomaly score which is used in (3.20).

Internal state estimation

By combining the forward body dynamics model (3.17) and torque pattern generation model (3.18), we can represent the movement model as an autonomous system, i.e., dynamics without explicit control input:

$$\mathbf{x}(k+1) = \mathbf{H}(\mathbf{x}(k)) + \mathbf{w}(k), \tag{3.29}$$

where $\mathbf{x}(k) = [\theta^\top(k), \dot{\theta}^\top(k), \tau^\top(k)]^\top$ and $\mathbf{w} = \left[\mathbf{w}_\theta^\top, \mathbf{w}_{\dot{\theta}}^\top, \mathbf{w}_\tau^\top\right]^\top$. $\mathbf{w}(k) \sim \mathscr{N}(0, Q(k))$ is the zero mean Gaussian system noise with Q as its covariance. $\mathbf{H}(\mathbf{x})$ represents the internal state dynamics composed of the functions (3.17) and (3.18).

Then, with considering the observation model introduced in (3.19), we can estimate the internal state by using a state estimation method. For example, the Kalman filter has been used to extract the user's motion intention from brain activities [105]. In this study, we use the extended Kalman filter [106].

3.4 Estimated joint torque feedback controller considering interaction

EMG has been widely used to estimate joint torques to control assistive devices such as exoskeleton robot. Typically, feedback torque τ_{robot} was

$$\tau_{robot} \leftarrow \alpha_1 \hat{\tau}_{emg}, \tag{3.30}$$

where the α_1 is the feedback gain. However, if the exoskeleton robot assists human intentional torque τ_{human} should be affected and can not use the original estimation. Additionally, if the exoskeleton completely assist human movement, in ideal case $\alpha_a = 1$, the next moment gives human joint torque $\tau_{human} = 0$, resulting in $\tau_{robot} = 0$. This actually doesn't occur in practical application because there are dynamics of muscle activity and EMG decreases with time delay. More practically, interaction is rather complex that the constraint between human and robot is incomplete, and that the joint rotation axis is different. At least, increasing α_1 reduces τ_{human}, and rises the system's instability. The problem is that eq3.30 is not closed form, because τ_{emg} is dependent to the τ_{robot}. During the assist, the human torque controller should decrease joint torque to achieve τ_{human}. In this study, I consider the following hypothesis based on torque coordination controller as follows,

$$\hat{\tau}_{emg} = \tau_{human} - \tau_{rh}, \tag{3.31}$$

where τ_{rh} is interaction assistive torque applied from robot to human, and $\hat{\tau}_{emg}$ is the simplified human muscle activity as desired joint torque to achieve τ_{human}. Here I propose the coordinated torque feedback τ_{robot} as follows.

$$\tau_{robot} \leftarrow \alpha_1 \hat{\tau}_{emg} + \alpha_2 \tau_{rh}. \tag{3.32}$$

The first term is same as eq.(3.30), and the second is the coordination term for discounted EMG by assistive intentional based on eq.(3.31). As described, I installed coordinating term for discounted EMG signal in eq.(3.32). This term is conceptual because direct measurement of this term τ_{rh} is very difficult (consider where to insert the torque/force sensor). It is equivalent to the evaluation of assistive torque in each joint that human received as the results of human-robot interaction.

Here I design the interaction estimated effect using human-robot kinematics.

$$\tau_{rh} = \mathbf{J}_h^{\top} \mathbf{J}_r \tau_{robot}, \tag{3.33}$$

where $\mathbf{J}_r$ is the forward kinematic of the robot from generated torque to the force at the interaction point, and $\mathbf{J}_r^{\top}$ is the static kinematic model from the interaction force to assistive joint torque, e.g., the $\mathbf{J}_h$ denotes the Jacobian relating human joint angle rates with interaction point (considered as end effector). τ_{robot} is desired torque to be generated in the joint. Note that, in this design, the interaction is modeled as the feed-forward (no feedback from sensors), and the effect of $\alpha 2$ depending on the controller frequency. Eq.(3.33) is provided with the following simplified human-robot interaction;

- Simplifying interaction at static related point (as contact is usually on plane such as robot's belt bounding human body)
- Ignorable moment transferred (similar kinematic skeleton/structure)

Chapter 4

Assistive Devices

4.1 Pneumatic-Electric Hybrid Actuator (PEHA-system)

In this chapter, I introduce exoskeleton system used in this study. While many exoskeleton robots are controlled by position based controller, the torque based control is suitable to support human movement because the exoskeleton eventually control the interaction force to assist human user movements. In order to control forces, Pneumatic Artificial Muscles (PAM) and electric motor are used as the actuator.

While the PAM is very light-weight, it can generate large force by converting pressured gas energy into the contraction force through its rubber tubes. The force generation principal is the path contraction of the spiral expansion embedded by the pneumatic bladder.

However, in the large force operation, PAM torque control is difficult because the wire extension cases large error of PAM force generation. On the other hand, the motor consequently cannot generate large torque to cover it. In order to address this problem, previous study developed Micro-Mini Actuation system [107]. But this system could be actuated in limited range. Our previous study improved PAM force model and developed better the Pneumatic-Electric Hybrid Actuator (PEHA) torque controller. The motor torque can be transmitted in parallel, e.g., small torque is transferred through a mechanical belt. The PAMs excel at generating DC or low frequency torque, and additionally small electric motor covers error of τ_{PAMs} as quick and high frequent torque but can be small.

$$\tau = \tau_{PAM} + \tau_{motor}. \tag{4.1}$$

Where, the τ_{motor} is motor torque and the τ_{PAM} is PAM torque. The PAM torque is generated by converting the PAM force f to the torque through the wires and the pulley as follows,

$$\tau_{PAM} = \frac{f_{PAM1} - f_{PAM2}}{r_0}, \tag{4.2}$$

where r_0 is the pulley radius and is constant setup in this system. In order to make PAM force controller better, the tendon-spring equilibrium model of PAM was proposed in our previous study. The PEHA-system and PAM model are explained in next section.

4.2 One-DOF exoskeleton robot

Fig.4.1 shows One-DOF exoskeleton robot developed in our study to evaluate PEHA-system and tendon-spring model. I explain the PEHA-system using this One-DOF exoskeleton in detail. The PAM force f_{PAM} is generated by path contraction of spiral fibers

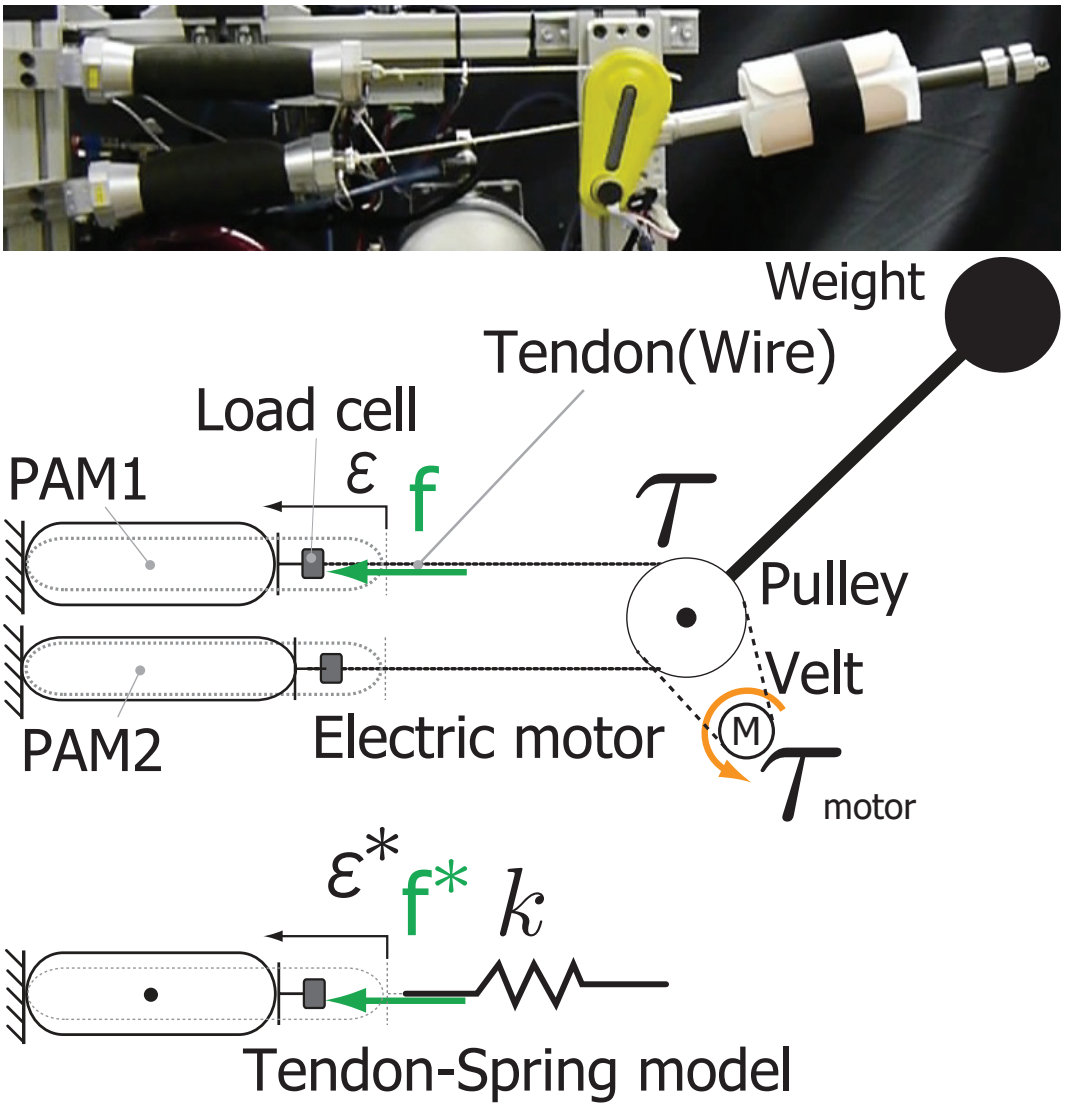

Figure 4.1: PAM-Electric Hybrid system. the upper PAM is the flexor muscle and the lower is the extensor muscle. Two PAMs antagonistically generate large force transmitted to a joint through the wires. The small electric motor additionally generates torque to the joint

embedded in a pneumatic bladder. PAM pressure p can be controlled by a proportional pressure valve. The PAM force model [108] [109] which depends on the PAM pressure and the contraction rate is represented as:

$$f_{PAM} = \frac{\pi D_0^2}{4}\frac{3}{\tan^2\psi_0}(1-\varepsilon)^2 p - \frac{1}{\sin^2\psi_0}, \tag{4.3}$$

where ε is the contraction rate, D_0 is PAM diameter, and ψ_0 denotes angle of the embedded spiral fibers when the PAM pressure is equal to the atmosphere pressure. This can be reformulated as a quadratic function of the contraction:

$$f_{PAM} = g(\varepsilon, p) = p(a\varepsilon^2 + b\varepsilon + c), \tag{4.4}$$

where a, b and c are as follows:

$$a = \frac{3\pi D_0^2}{4\tan^2\psi_0}, \quad b = -\frac{3\pi D_0^2}{2\tan^2\psi_0},$$
$$c = \frac{\pi D_0^2}{4}\left(\frac{3}{\tan^2\psi_0} - \frac{1}{sin^2\psi_0}\right), \tag{4.5}$$

and these parameters are determined at calibration process from measured data by using the load cell, the valve pressure, and the encoder. To generate desired joint torque τ^*_{PAM} by the one-DOF robot, first, corresponding desired PAM force f^*_{PAM} is derived by the force-torque conversion model (4.2). Then, desired valve pressure p^* can be calculated from the inverse model $p^* = g^{-1}(f^*_{PAM}; \varepsilon)$ with considering the current contraction rate ε.

The major torque for movement is covered by PAM, and actual torque can be measured from Load Cell (LC). The high frequency torque is generated by motor. The desired motor torque is

$$\tau^*_{motor} = \tau^* - \tau_{PAMs}. \tag{4.6}$$

4.3 Lower limb exoskeleton robot

Fig.4.2 shows Lower limb exoskeleton robot (XoR) developing in Dept. of Brain Robot Interface, ATR, Computational Neuroscience Labs. This XoR has ten degree of freedom and six PEHA-system active joints.

In this study, the vertical assistive force for stand-up motion is generated as:

$$\tau = J^\top F, \tag{4.7}$$

where J is the COM Jacobian matrix, F is the desired virtual forces to assist stand-up motion, and τ is the desired torque at each joint of exoskeleton robot. Here we only consider the vertical force and assume that horizontal force applied to COM of user-robot system, and vertical force support is most important for daily life basic motion.

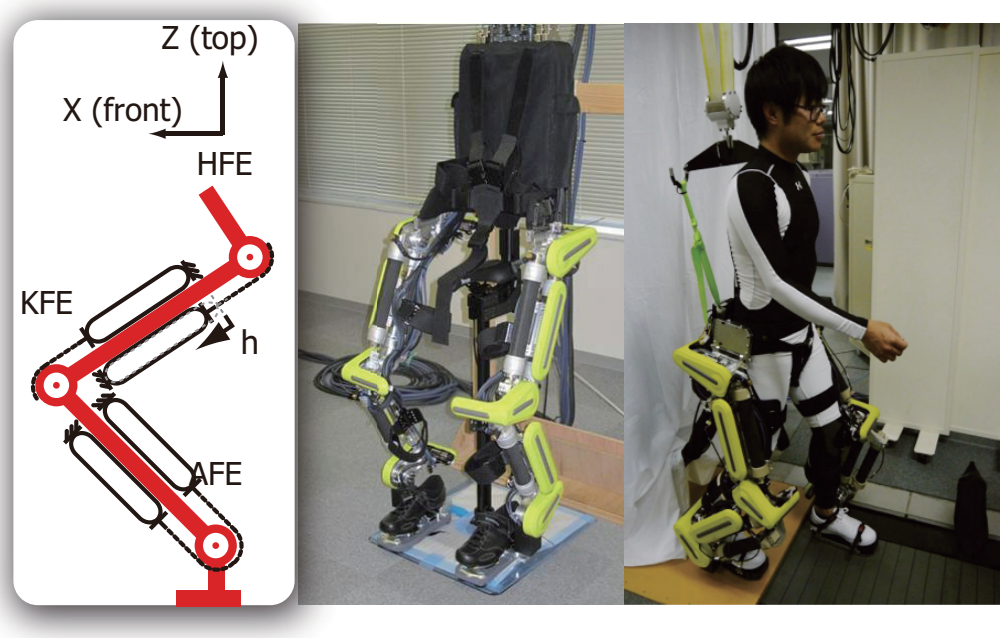

Figure 4.2: Lower limb exoskeleton robot (XoR) ; Height: 1.5m, weight: 24kg. XoR has ten degree of freedom and six active joints. Each active joint uses hybrid actuator composed of air muscle and an electric motor. XoR is designed to assist human lower-limb movements.

4.4 Upper limb exoskeleton robot

Fig. 4.3 shows the upper-limb exoskeleton robot developing in our study. This upper limb exoskeleton robot has four degrees of freedom: Shoulder Flexion/Extension (SFE), Shoulder Abduction/Adduction (SAA), Elbow Flexion/Extension (EFE), and Wrist Flexion/Extension (WFE) joints. Each joint torque τ_{PAM} is mainly generated by a Pneumatic Artificial Muscle (PAM), and the SFE and EFE joints are also actuated by electric motor output τ_{Motor}. Details of the mechanical design and the torque-based control method are presented in [110].

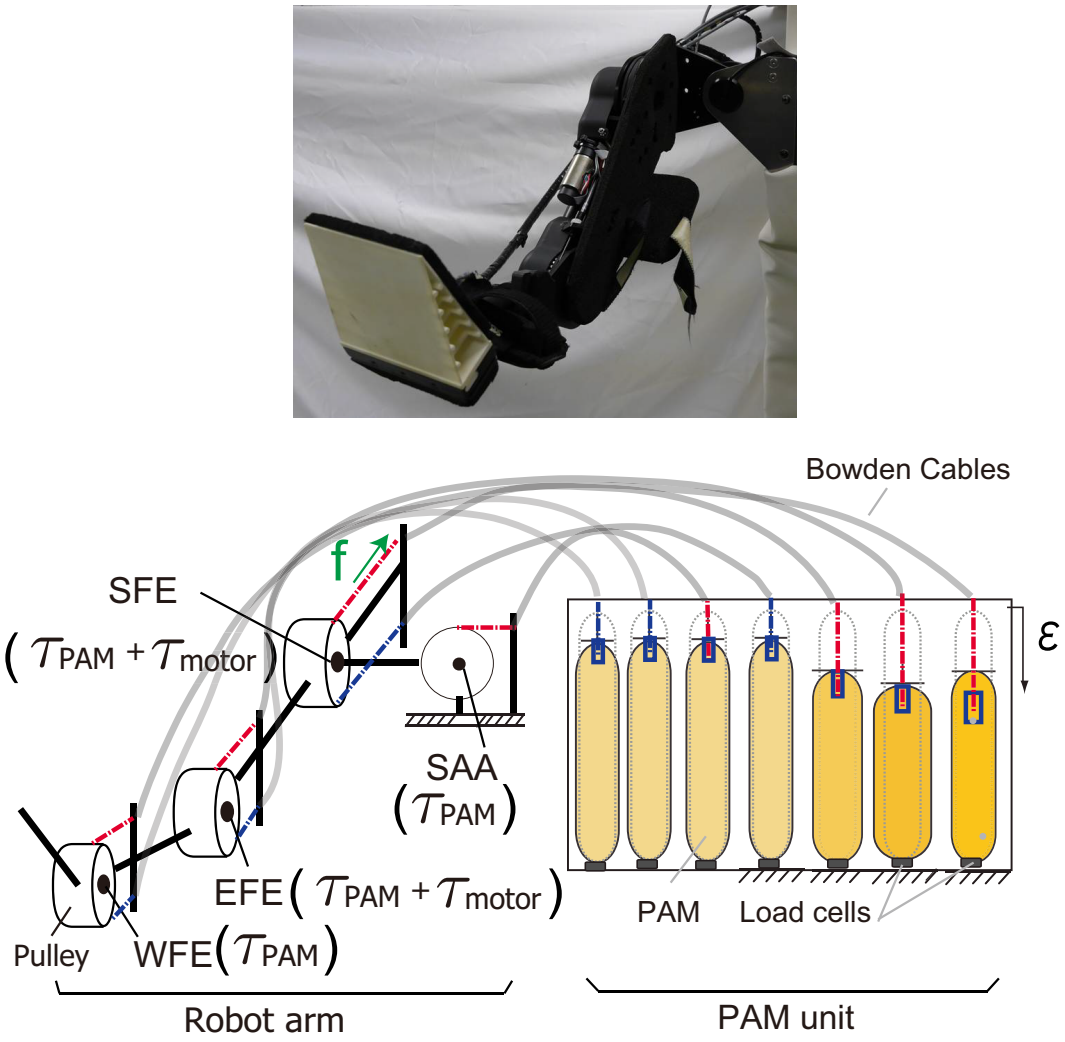

Figure 4.3: Upper limb exoskeleton robot with has four degrees of freedom: Shoulder Flexion/Extension (SFE), Shoulder Abduction/Adduction (SAA), Elbow Flexion/Extension (EFE), Wrist Flexion/Extension (WFE). SFE and EFE joints are actuated by the Pneumatic Artificial Muscle (PAM) and Motor. SAA and WFE joints are actuated by PAMs, which are located apart from the joint and robot link and generate forces. Each PAM force is transmitted to the joint through Bowden cables and the pulley. Motor torque is applied to the SFE and EFE joints.

4.5 PAM-Weight Support System

To support human squat motions, I develop a weight support system (Fig. 4.4), where the actuator is a paired pneumatic artificial muscles (PAMs).

I use 1.4 m length PAM (FESTO Inc.,) which has 10 mm diameter and 25% contraction rate from natural length. According to the specification provided by FESTO Inc., the PAM can generate 630 N maximum force. The system is about 0.8 kg without including air compressor and valve. In addition, the system can operate up to 0.5 Hz with the amplitude of 0.35 m. These specifications were experimentally validated as described later.

While PAM is lightweight, it can produce large force; converting pressured gas energy into contraction force through its rubber tubes. The force is generated by the path contrac-

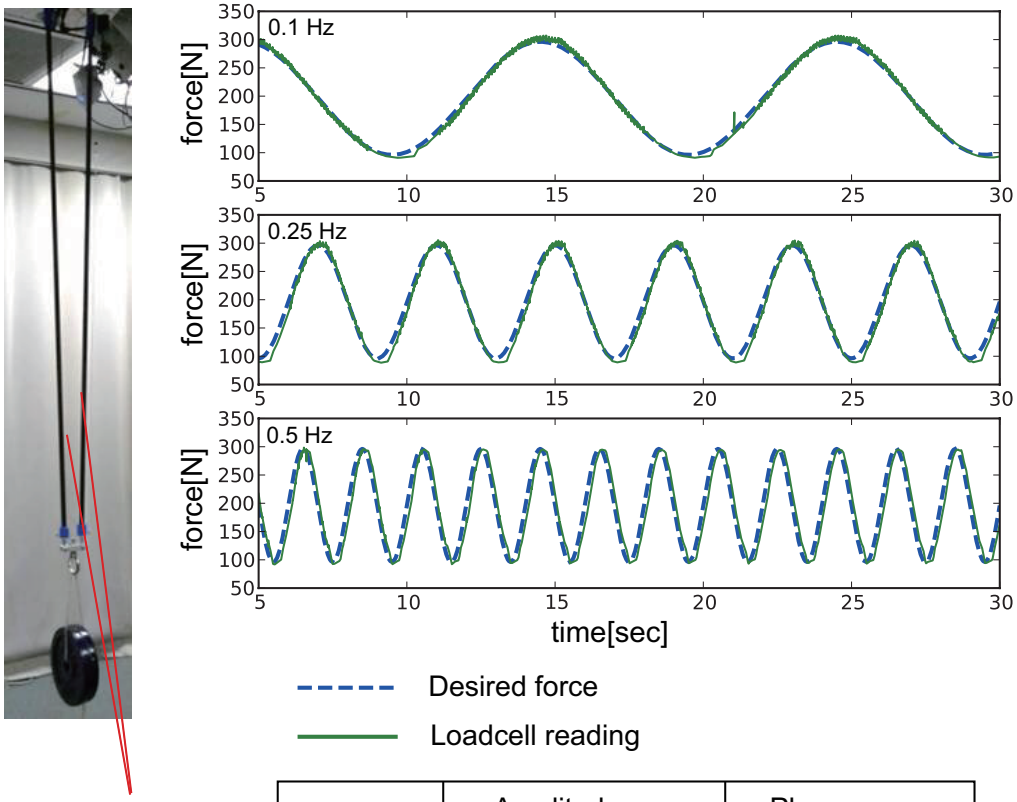

	Amplitude error	Phase error
0.1 Hz	1.22 [N]	0.123 [rad]
0.25 Hz	9.29 [N]	0.107 [rad]
0.5 Hz	2.24 [N]	0.0881 [rad]

Figure 4.4: Torque tracking performance of PAM-based weight support system with frequencies of 0.1 Hz, 0.25 Hz and 0.5 Hz. 30 kg weight was attached to the bottom of the support system.

tion of the spiral fiber expansion embedded by the pneumatic bladder. With proportional pressure valves, PAM pressure p can be controlled. The force generated by PAM depends on the pressure p and the contraction rate, the PAM force model [108], [109] is given in4.2.

At the calibration stage, we obtain load cell variables that measure the actual vertical PAM force, the valve pressure, and the contraction rate by periodically changing the loads. Using the least-square method, we estimate the PAM parameters in (4.4) with using the initial values in (4.5) and initialize encoder so that we can find an initial length of PAM to calculate PAM contraction rate. For the quadratic regression of (4.4), we consider forces and contraction rates as inputs and the valve pressure as output. Figure 4.4 shows the frequency responses of the PAM-based weight support system. We obtained the data by generating support force with a range from 100 N to 300 N. The amplitude error and the phase error are shown in Fig. 4.4. From these performance, this PAM-weight system is enough to support human squat motion.

Chapter 5

Experiment of EMG-based Assistive Robot Control

5.1 EMG-Driven Weight Support System in dynamic squat motion

In order to evaluate estimated torque performance in dynamic motion, I use Weight Support System shown in 4.5.

Weight support is essential in rehabilitation for lower limbs, where standing up, stepping, walking, or balancing movements can be involved. In conventional weight support systems, assist force is typically constant and operational height ranges are limited. Therefore, weight support devices have only been used for safety or fault tolerance instead of actively changing amount of weight support. On the other hand, for active weight and movement support, research attention on the development of an exoskeleton robot is increasing [14] [15] [18] [35] [111] [112]. However, it remains difficult for therapists to work with such systems since exoskeleton robots generally require complicated setups. In this study, I propose EMG-driven weight support system that has a wider operational range and can adaptively change the amount of support rather than simply generating constant force. To satisfy above specifications, I used Pneumatic Artificial Muscles (PAMs) with force sensors and a device to measure the PAM length. PAMs are used for robotics applications [112] [113] [114] [115] [116]. Fig. 5.1 shows a schematic diagram of our proposed weight support system.

In this experiment, I estimate knee and ankle joint torque from measured EMGs. I first simultaneously measure the joint angle trajectories and the EMG profiles of a subject. Then the torque sequence that corresponds to the measured joint angle trajectories is derived using inverse dynamics . Although previous studies also used inverse dynamics to estimate knee-joint torque from EMG signals, the knee movements were generated when a subject was sitting [72] [92]. To deal with such daily-life related behaviors as squat movements, I must explicitly consider the ground reaction force in inverse dynamics. Therefore, I use floating base inverse dynamics as explained in 3.1.

5.1.1 Experimental setup

Figure 5.2 shows the control strategy of the proposed weight support system. First, I measure the EMG signals and the joint angles simultaneously from the left leg during the normal squat motion and the parameters of the tendon-pulley model in (5.1) are estimated from the acquired EMG and joint angle data. Then the online operation of the weight

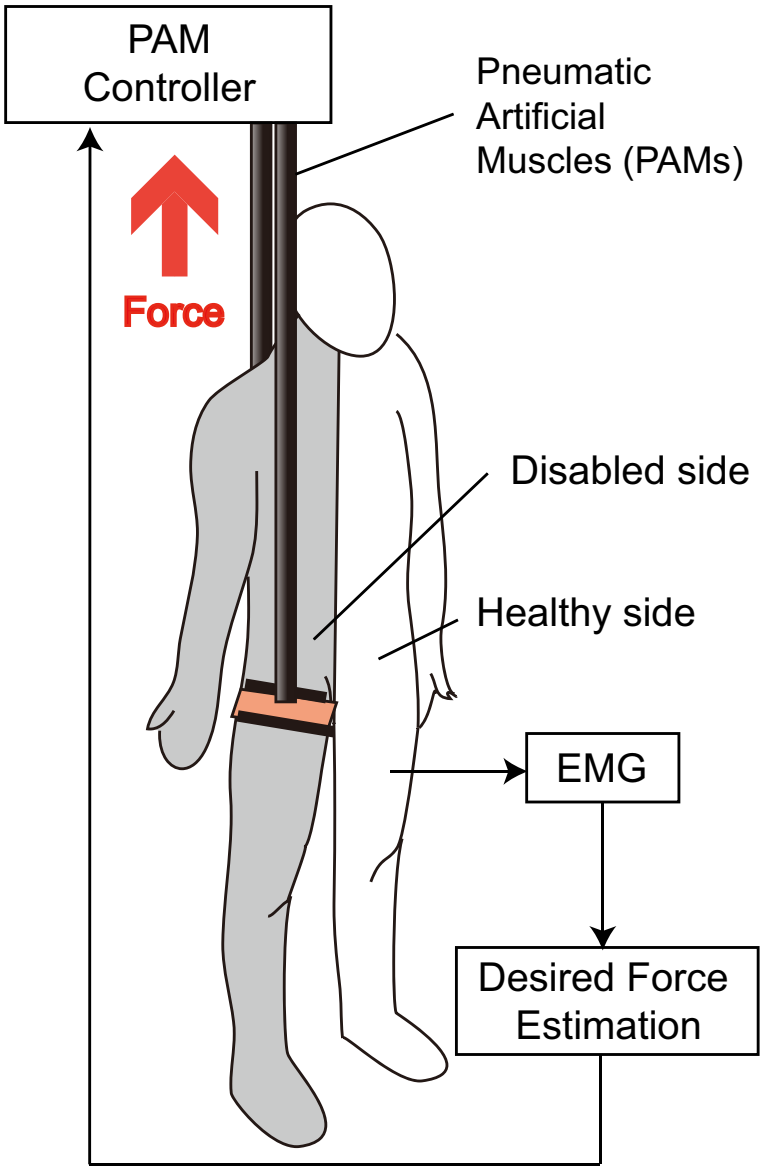

Figure 5.1: Schematic diagram of our proposed weight support system: up-and-downward movements are assisted with the force estimated from measured EMG.

support system is as follows:

1. Online EMG and joint angle measurements during the motion.

2. Derive the muscle force from the Hill-Strove model as shown in 3.2.

3. Estimation of the knee and ankle joint torques by using the tendon-pulley model with the identified parameters.

4. Calculate the vertical assist force from the estimated knee and ankle joint torques by using the Jacobian matrix which represents the relationship between the joint movements and a hip position movement.

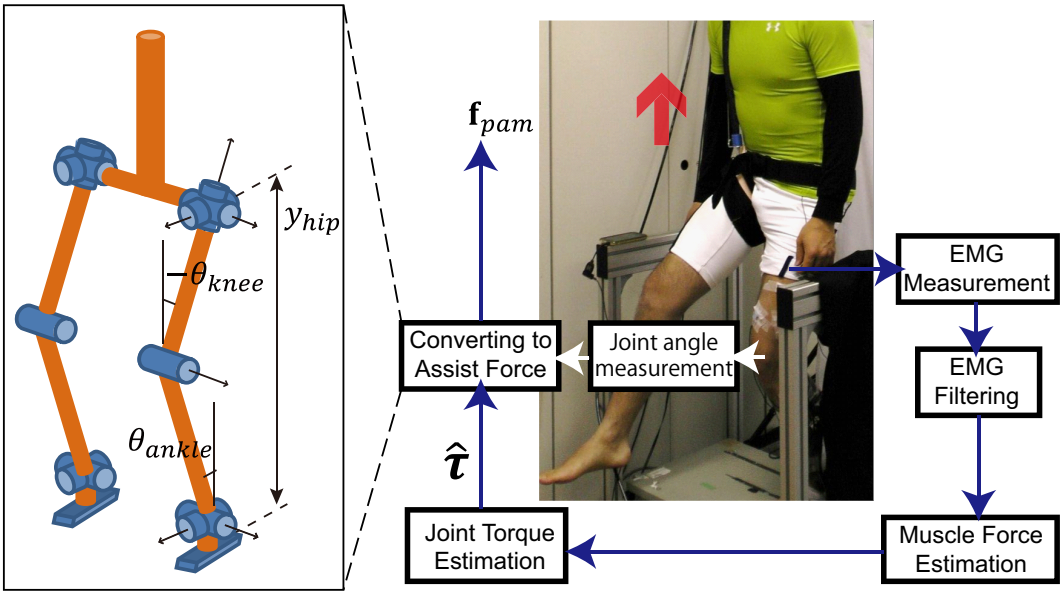

Figure 5.2: Control strategy of weight support system. Muscle forces are estimated from full wave rectified and bandpass filtered EMG signals. Joint torque $\hat{\tau}$ is derived from the estimated muscle force by using tendon-pulley model. Then, the derived torque is converted to desired assist force f_{pam} for PAM by taking measured joint angles into account.

5.1.2 EMG to Joint Torque estimation Model

I consider knee and ankle joint estimation torques $\hat{\tau}_t$ and muscle forces $\mathbf{u}_t$ using the following standard simple linear model:

$$\hat{\tau}_t = \mathbf{w}^\top \mathbf{u}_t, \tag{5.1}$$

where $\mathbf{u}_t = \left(u^1, \ldots, u^m, 1\right)^\top$ is the muscle contraction force and $\mathbf{w} = \left(w^1, \ldots, w^n, w^0\right)$ is the model parameter vector of a constant pulley model at knee and ankle joints. These parameters are determined by the least square estimation method to minimize the torque estimation error:

$$E = \frac{1}{2}\sum_{t=0}^{N} (\tau_t - \hat{\tau}_t)^2, \tag{5.2}$$

where the target torque τ_t is derived from the inverse dynamics model as explained in the following section. N is the number of the training sampling.

Weight Support Force

Finally, the estimated joint torques are converted to the force inputs for the PAM with using joint angle information measured by the goniometers. The measured joint angles are used to derive the Jacobian matrix:

$$\mathbf{J} = \begin{bmatrix} \dfrac{\partial y_{hip}}{\partial \theta_{knee}} & \dfrac{\partial y_{hip}}{\partial \theta_{ankle}} \end{bmatrix}, \tag{5.3}$$

where y_{hip} denotes vertical hip position, θ_{knee} denotes left knee joint angle, and θ_{ankle} denotes left ankle joint angle (see also Fig. 5.2). By using the derived Jacobian, we convert

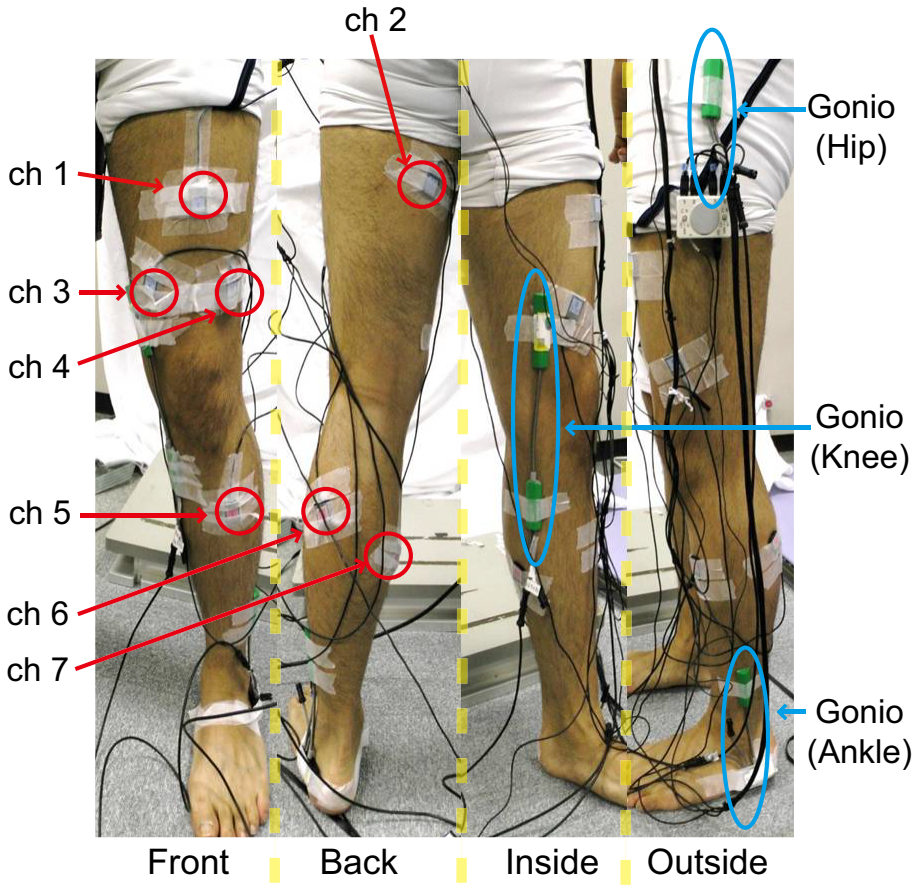

Figure 5.3: EMG electrode and goniometer placements.

the estimated knee and ankle joint torques to the vertical support forces:

$$f_{PAM} = (\mathbf{J}\mathbf{J}^{\top})^{-1}\mathbf{J}\begin{bmatrix} \hat{\tau}_{knee} \\ \hat{\tau}_{ankle} \end{bmatrix}, \tag{5.4}$$

where $\hat{\tau}_{knee}$ and $\hat{\tau}_{ankle}$ are estimated left knee and ankle torques respectively.

5.1.3 Calibration

PAM Pressure to Force Model

At the calibration stage, I obtain load cell variables that measure the actual vertical PAM force, the valve pressure, and the contraction rate by periodically changing the loads. Using the least-square method, I estimate the PAM parameters in (4.4) with using the initial values in (4.5) and initialize encoder so that we can find an initial length of PAM to calculate PAM contraction rate. For the quadratic regression of (4.4), I consider forces and contraction rates as inputs and the valve pressure as output. Figure 4.4 shows the frequency responses of the PAM-based weight support system. I obtained the data by generating support force with a range from 100 N to 300 N. The amplitude error and the phase error are shown in Fig. 4.4.

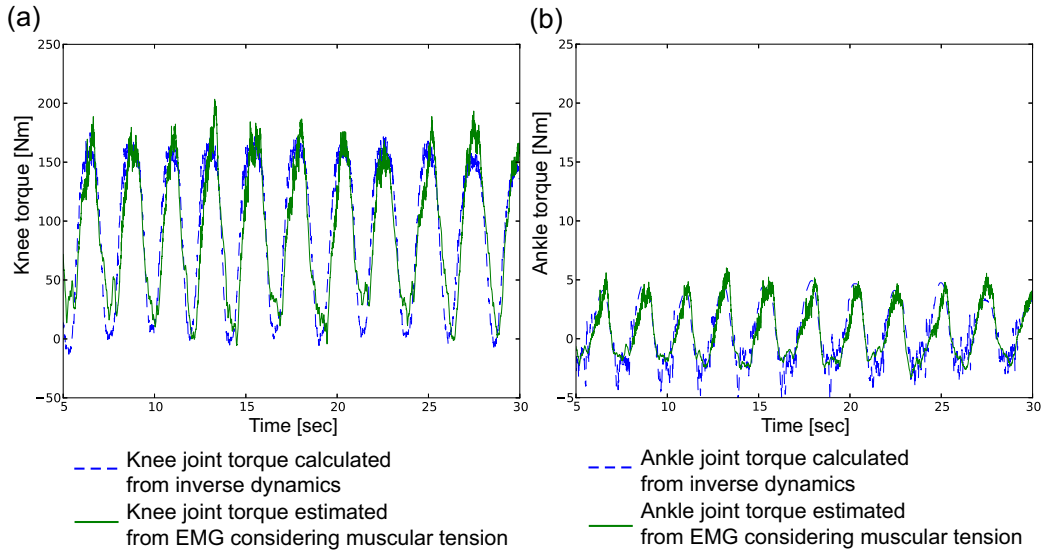

Figure 5.4: Torque estimation performance. The estimated knee and ankle joint torques from EMG signals is indicated by solid line. Target joint torque profile derived from joint angle trajectory with using floating base inverse dynamics model is plotted by dashed line. This estimation performance is evaluated with using a test dataset which is not used for finding parameters of tendon-pulley model in (5.1).

EMG to Joint torque model

The parameter of the tendon-pulley model in (5.1) was estimated from squat motion data for 30 seconds with different frequency and depth. In other words, the number of samples used to find the parameters was $N = 7500$. Figure 5.3 shows the placements of EMG electrode and goniometers. We measured EMG signals of the femoral muscle (Channel 1: e^1), the biceps muscle of the thigh (Channel 2: e^2), the vastus medialis muscle (Channel 3: e^3), the vastus lateralis muscle (Channel 4: e^4), the tibialis anterior muscle (Channel 5: e^5), the lateral head of the gastrocnemius muscle (Channel 6: e^6), and the medial head of the gastrocnemius muscle (Channel 7: e^7). The left leg pitch angles of hip, knee and ankle joints are measured by goniometers. Then the measured joint angles are used in the floating based inverse dynamics model. I sample the amplified EMG and goniometer signals with sampling rate of 250 Hz, i.e., sampling period is $\Delta t = 4$ ms.

To estimate the knee joint torque, I compute muscle forces with a augmented input for bias estimation: $\mathbf{u} = \left(u^1, \ldots, u^7, 1\right)^\top$ from the EMG signals measured by the seven sensor channels. Similarly, the ankle joint torque is estimated by three muscle forces $\mathbf{u} = \left(u^5, u^6, u^7, 1\right)^\top$. u^1 is derived from the femoral muscle activity, u^2 is from the biceps muscle of the thigh, u^3 is from the vastus medialis muscle, u^4 is from the vastus lateralis muscle, u^5 is from the tibialis anterior muscle, u^6 is from the lateral head of the gastrocnemius muscle, and u^7 is from the medial head of the gastrocnemius muscle.

Figure 5.4 shows torque estimation performances. This estimation performances are evaluated with using a test datasets which are not used for finding parameters of tendon-pulley model in (5.1). The correlation between the predicted knee torques from the EMG signals and target torque trajectories was 0.86 and the root mean squared error was 33.9 Nm. The correlation coefficient between the predicted ankle torques from the EMG signals and target torque trajectories was 0.86 and the root mean squared error was 8.62 Nm. These results indicate that our torque estimation method from the EMG signals is useful to control

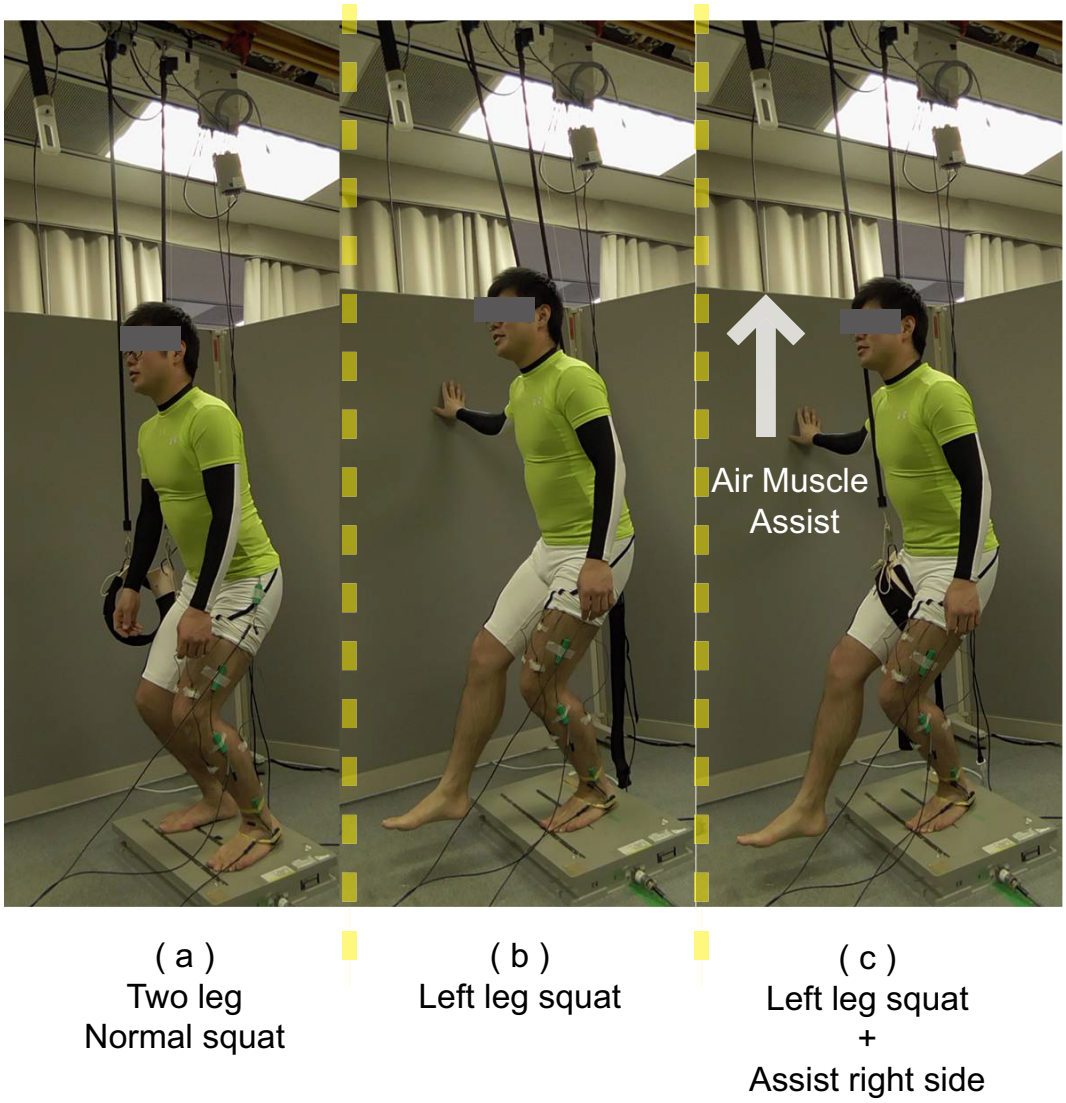

Figure 5.5: Experimental setups. (a) normal two-leg squat, (b) one-leg squat without using the assist system, and (c) one-leg squat with the weight support. In experimental setups (b) and (c), subjects are instructed to touch the wall to maintain the balance.

our PAM-based weight support system. Note that since the knee joint torque is dominant in the squat movement, we mainly analyze the EMG signals around knee joint in subsection 5.1.5.

5.1.4 Assisting Squat Movements

I compared EMG magnitudes with four different experimental conditions: (i) normal two-leg squat, (ii) one-leg squat without the assist system, and (iii) one-leg squat with EMG-based weight support, (iv) one-leg squat with constant force support, where the constant force is derived as the mean value of target assist force calculated from the floating base inverse dynamics. Fig. 5.5 shows the three squat experimental setups used for the four different experimental conditions.

I set two different frequencies as lower and upper limit for each squat in order to validate real-time assist performance of the weight support system: 0.2Hz for the slow dynamic

motion and 0.5Hz for fast dynamic motion. 0.2Hz was decided as the lower limit that the subject was able to squat continuously with using one leg without weight assist. 0.5Hz was the upper limit that was able to be controlled accurately with respect to the response of the valve from the result of PAM calibrations in Section 5.1.3. Four healthy subjects took part in the experiments (age 23-30, males). The subjects were instructed to match the timing of squat motion to metronome sound.

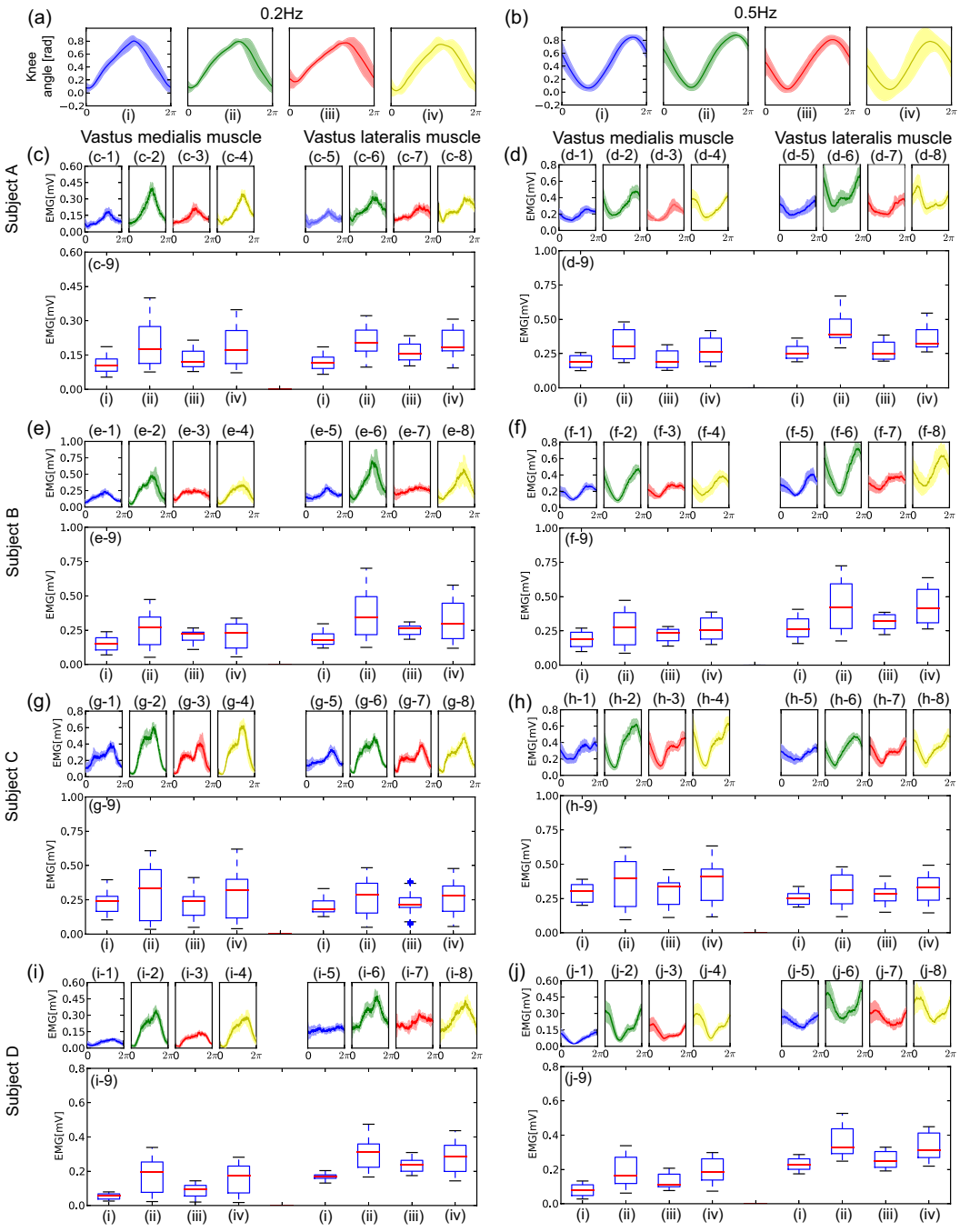

Figure 5.6: Squat movement profiles of each subject with frequencies of 0.2Hz and 0.5Hz among the four different experimental conditions with box plot. Blue line shows normal squat, green line shows one-leg squat without weight support, red line shows one-leg squat with EMG-based weight support and yellow line shows one-leg squat with constant force support. (a),(b): Mean and variance of knee joint angles of representative subject during one cycle 0.2Hz and 0.5Hz squat movements in the four different squat condition. (c)-(j): Squat movement profiles of the vastus medialis and the vastus lateralis muscle with frequencies of 0.2 Hz and 0.5Hz.

5.1.5 Results

In this subsection, I show the results of real-time assist performance of the squat movements by using the developed weight support system.

Individual data analysis

Figure 5.6 (a) and (b) show mean and variance of the knee joint angles of representative subject (subject A) during one cycle 0.2Hz and 0.5Hz squat movements in the four different squat conditions. Figure 5.6 (c-1)-(c-8) show the mean and variance of EMG signals measured from the vastus medialis muscle (e^3) and the vastus lateralis muscle (e^4) of subject A during one cycle 0.2Hz squat movements in the four different squat conditions, and (c-9) shows the box plot of the corresponding EMG magnitude. Figure 5.6 (d-1)-(d-8) show the mean and variance of EMG signals measured from the vastus medialis muscle (e^3) and the vastus lateralis muscle (e^4) of subject A during one cycle 0.5Hz squat movements in the four different squat conditions, and (d-9) shows the box plot of the corresponding EMG magnitude. Figure 5.6 (e) and (f) show the EMG data of subject B. Figure 5.6 (g) and (h) show the EMG data of subject C. Figure 5.6 (i) and (j) show the EMG data of subject D. We focused on monitoring these two muscles, i.e., vastus medialis and vastus lateralis muscle, because these knee-joint related muscles mainly contributed to generate the squat movements. All the EMG profiles in Fig. 5.6 are low-pass filtered with cut-off of 2 Hz and full wave rectified.

As presented in Figs. 5.6(a) and (b), the subject generated squat movements with the similar amplitude and frequency in the four different squat conditions. Figures 5.6 (c)-(j) show that the amplitudes of EMG signals in the four different squat condition. These results indicate that the magnitude of EMG signals in the normal and the EMG-based assist conditions are less than that in the one-leg condition and than that in the constant-force-based assist conditions are little less.

Table 5.15.2 shows the Root Mean Square (RMS: $\sqrt{\frac{1}{T}\int_0^T x(t)^2 dt}$ for 30 seconds, $T = 30$) of raw EMG signals from seven muscles ($e^1 \sim e^7$) with the two different movement frequencies of 0.2 Hz and 0.5 Hz in the four different squat conditions. Results in Table 5.15.2 show that the vastus medialis muscle activities (e^3) and vastus lateralis muscle activities (e^4) in (i) the normal squat conditions and (iii) the one-leg squat with EMG-based weight support are comparable in each subject while these muscle activities are much larger in (ii) the one-leg squat without weight support condition. These two muscles in (iv) the one-leg squat with constant force support are also assisted, but not as much as EMG-based weight support.

On the other hand, for other five muscles, we did not observe consistent differences in EMG signals in the four different experimental conditions among the four subjects (see also Table 5.15.2). For subject D, we found much larger muscle activities on the tibialis anterior muscle e^5. This is possibly due to the subject D intensively uses that muscle to maintain the balance during the squat movements.

Table 5.1: The Root Mean Square (RMS) of the raw EMG signals (Subject A and B)

Subject A					
Squat frequency	**EMG**	**RMS (** $\times 10^{-2}$ **)**			
		(i)	(ii)	(iii)	(iv)
0.2 Hz	e^1	5.50	9.61	7.29	8.78
	e^2	1.78	3.47	2.65	2.30
	e^3	**11.9**	22.5	**14.1**	20.5
	e^4	**12.6**	22.1	**16.7**	21.3
	e^5	26.7	8.13	15.9	7.18
	e^6	2.29	4.56	3.06	3.08
	e^7	2.67	5.95	2.65	2.24
0.5 Hz	e^1	11.6	23.2	11.9	16.8
	e^2	2.80	4.30	3.77	3.70
	e^3	**20.0**	33.4	**22.0**	29.3
	e^4	**27.2**	45.5	**28.2**	38.1
	e^5	34.8	16.9	10.1	8.52
	e^6	1.65	2.42	2.39	2.70
	e^7	1.62	1.73	2.68	2.13
Subject B					
Squat frequency	**EMG**	**RMS (** $\times 10^{-2}$ **)**			
		(i)	(ii)	(iii)	(iv)
0.2 Hz	e^1	7.29	12.5	8.03	10.0
	e^2	3.21	5.00	4.54	4.97
	e^3	**16.0**	29.7	**21.0**	23.5
	e^4	**19.8**	42.2	**25.6**	36.0
	e^5	8.57	11.4	9.71	4.47
	e^6	5.30	10.1	5.73	4.83
	e^7	4.94	12.4	12.9	9.10
0.5 Hz	e^1	10.6	13.3	9.84	13.7
	e^2	3.22	5.03	4.49	4.71
	e^3	**19.8**	30.5	**22.8**	28.7
	e^4	**28.8**	47.7	**32.3**	47.1
	e^5	8.08	4.68	8.42	5.08
	e^6	7.67	8.90	5.70	8.42
	e^7	6.28	12.8	12.7	10.7

Table 5.2: The Root Mean Square (RMS) of the raw EMG signals (Subject C and D)

Subject C					
Squat frequency	**EMG**	**RMS ($\times 10^{-2}$)**			
		(i)	(ii)	(iii)	(iv)
0.2 Hz	e^1	7.31	12.3	8.91	11.8
	e^2	3.87	4.22	4.13	4.82
	e^3	**25.1**	35.9	**25.5**	35.2
	e^4	**21.5**	30.0	**23.9**	29.2
	e^5	34.6	26.7	19.4	29.6
	e^6	2.70	5.45	5.74	4.43
	e^7	4.00	9.22	9.94	7.50
0.5 Hz	e^1	11.3	16.1	12.8	15.6
	e^2	4.00	5.51	4.37	5.40
	e^3	**30.6**	41.5	**32.5**	41.0
	e^4	**26.0**	33.7	**29.2**	34.2
	e^5	30.9	18.4	18.0	18.9
	e^6	2.62	7.38	7.29	6.05
	e^7	2.58	7.42	10.6	8.23
Subject D					
Squat frequency	**EMG**	**RMS ($\times 10^{-2}$)**			
		(i)	(ii)	(iii)	(iv)
0.2 Hz	e^1	7.43	14.6	10.1	14.0
	e^2	1.64	4.49	3.33	4.90
	e^3	**5.79**	20.3	**9.68**	18.1
	e^4	**17.1**	31.7	**24.0**	29.6
	e^5	85.4	102	102	90.2
	e^6	1.87	2.15	2.19	2.08
	e^7	7.59	5.55	6.29	7.85
0.5 Hz	e^1	9.81	16.8	12.5	15.9
	e^2	2.22	8.12	4.45	4.88
	e^3	**8.77**	21.1	**14.1**	21.3
	e^4	**23.4**	37.6	**26.5**	34.7
	e^5	111	124	102	102
	e^6	2.25	2.43	2.15	2.06
	e^7	10.1	8.86	5.65	7.38

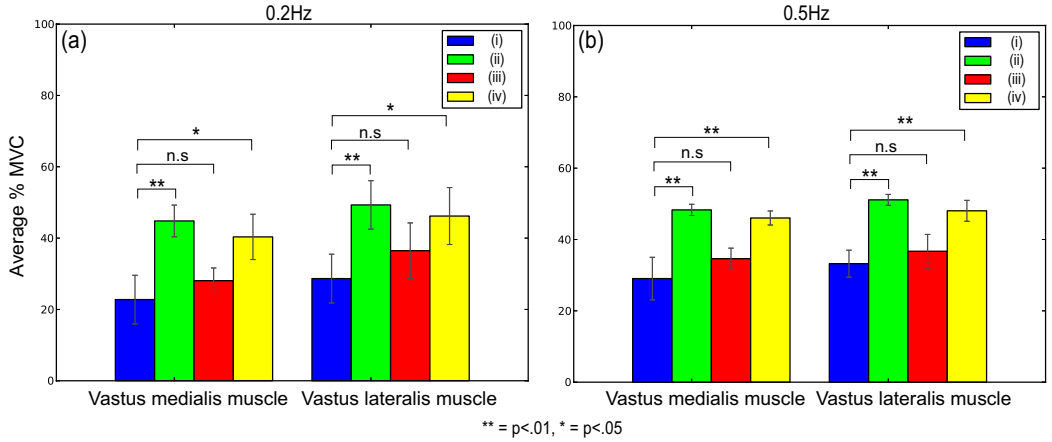

Figure 5.7: Statistical comparisons with bar plots of the vastus medialis muscle and the vastus lateralis muscle %MVC across all subjects. Blue bar shows normal squat movement, green bar shows the one-leg squat movement without weight support, red bar shows the one-leg squat movement with EMG-based weight support, and yellow bar shows the one-leg squat movement with constant force support. (a):0.2Hz squat movement. (b):0.5Hz squat movement.

Integrated data analysis

Figures 5.7 (a) and (b) show the average %MVC of the vastus medialis muscle activities (e^3) and vastus lateralis muscle activities (e^4) with the two different movement frequencies of 0.2 Hz and 0.5 Hz in the four different squat conditions across all subjects. The %MVC is normalized muscle activity (e) for each subject and each muscle separately, by using maximum value of rectified and low-pass filtered EMG signal (e_{max}): %MVC = e/e_{max}. This allows comparing among different subjects. Where, the e_{max} is the maximum value of the muscle activity e, which is calculated in each experiment and regarded as the muscle activity level of maximum voluntary contraction in this study. We applied a t-test to the average %MVC of (ii) one-leg squat without the weight support, (iii) one-leg squat with the EMG-based weight support, and (iv) one-leg squat with the constant force support with reference to (i) normal two-leg squat. I found a significant difference between (i) and (ii) ($p<0.01$) and between (i) and (iv) ($p<0.05$), but we found no significant difference between (i) and (iii) ($p>0.05$) in the 0.2Hz squat movements. And I also found a significant difference between (i) and (ii) ($p<0.01$) and between (i) and (iv) ($p<0.01$), but found no significant difference between (i) and (iii) ($p>0.05$) in the 0.5Hz squat movements. These results suggest that the developed weight support system can assist the left leg of the subjects with the similar force that the right leg supposed to generate using a PAM-based weight support system. My system is controlled by the force estimated from the EMG signals of the left leg, assuming that humans move both left and right legs with the same force while squatting. The constant force support also assisted, but the effectiveness was less than EMG-based weight support. Consequently, we showed that the usefulness of our proposed weight support system for actively assist subjects by using the measured EMG signals.

Discussion

In this experiment, I introduced our newly developed PAM-based weight support system which can be controlled by the estimated joint torques with the online EMG measurement. The parameters of the torque estimation model are calibrated with using an inverse dynamics model which represents physical property of a subject. In particular, I considered using floating base inverse dynamics to explicitly take the ground reaction force into account so that we can treat the movements with both feet on the ground such as squat behaviors. As a concrete example, I applied our developed system to assist squat movement. The results show that muscle activities measured from vastus medialis and vastus lateralis muscle EMG signals were not significantly different between one-leg squat with the EMG-based weight support and normal two-leg squat while the difference between normal two-leg squat and one-leg squat, and normal two-leg squat and one-leg squat with the constant force support were significant. As an application, this system can possibly be used for partial weight bearing therapies. Concretely, compensating the disabled side of the body for the early stage of therapies. Then, the vertical component force can be gradually decreased as the patient recovers lower body motor functions.

Since the PAM-based weight support system is lightweight, safe, high power-weight ratio, and easy to attach to the ceiling or a small gantry, the system can potentially be useful not only for rehabilitation but also for industrial applications.

Although I focused on assisting one particular movement, i.e., squatting, it would be possible to apply our weight support system to assist other kinds of movements such as stepping or walking by using the estimated torque from EMG signals with considering phase difference between the left leg and right leg movements. Moreover, I can possibly use our developed weight support system with constant assist force to simply compensate the gravity but with much wider movement range than existing devices so that the weight support system can help a therapist when the therapist is near by a patient. This gravity compensation strategy can also be useful for the industrial applications, such as the load carriage assistance.

To further improve the force control performance of the weight support, it can be beneficial to explicitly take hysteresis model of the PAM into account. In addition, in this experiment, I used load cells only for the calibration and did not use it for force feedback control since there is delay in the air-pressure-based control system. However, using the load cell feedback for on-line adaptation of the parameters of the weight support system would be one of the interesting directions as a part of future study.

5.2 Robust joint torque estimation using multi-channel bio-signal sensors against sensor faults

In this experiment, I evaluated my proposed fault tolerant estimation method with two different sensor fault situations: an EMG electrode Sensor is DisConnected from the amplifier and I named this failure situation as SDC, and one side of an EMG Sensor electrode is DeTached from skin surface and I named this failure situation as SDT (seed Fig. 5.8).

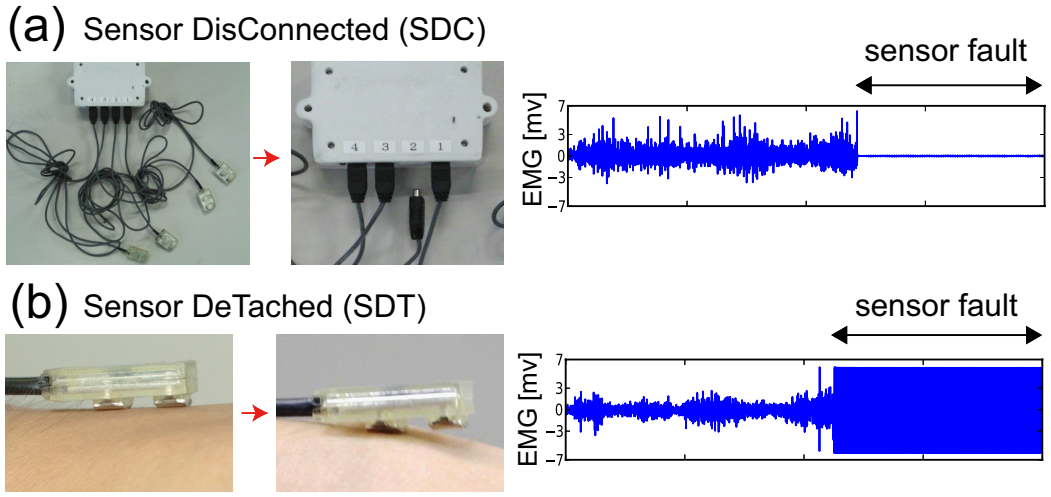

Figure 5.8: Three types of sensor failure situations and the raw EMG signals. (a) an EMG electrode sensor is disconnected from amplifier. (b) one side of an EMG electrode sensor is detached from skin surface.

5.2.1 Experiment with Supervised learning framework

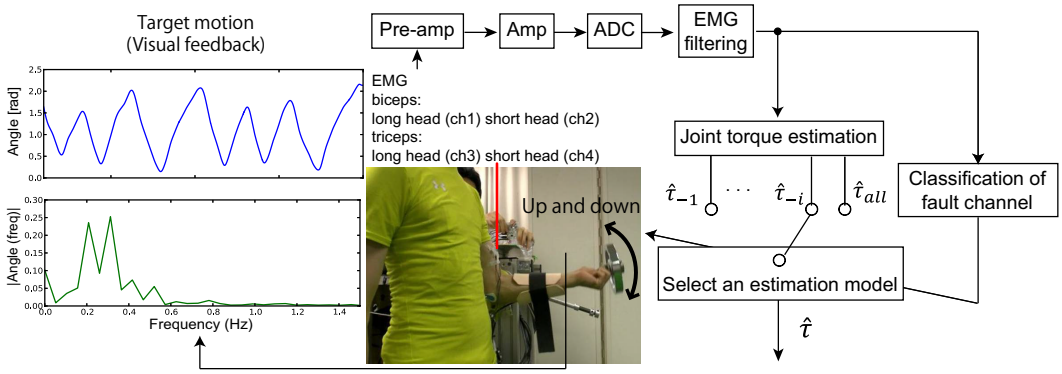

Figure 5.9: Experimental setup to evaluate our proposed fault tolerant framework. Participants generate elbow-joint movements to track the displayed target motion by wearing the one-DOF exoskeleton robot, and elbow-joint angle trajectories are recorded through the one-DOF system ' s encoder. Participants tracked the target motion by looking at their elbow angle displayed on a monitor. Experiments were conducted after several training trials to track the target trajectory. Target motion, which is plotted in figure ' s top-left, is acquired from actual elbow-joint movements of the experimenter. Power spectrum of the target motion is plotted in figure ' s bottom-left. This plot clearly shows that the target motion is not a simple sinusoidal trajectory that only includes one periodic basis. EMG signals are measured from the biceps brachii long head (Channel 1: e_k^1), biceps brachii short head (Channel 2: e_k^2), triceps brachii long head (Channel 3: e_k^3), and triceps brachii short head (Channel 4: e_k^4). 5.0 kg is attached to the tip of the one-DOF robot to acquire EMG data to find the parameters of the joint torque estimation models.

My proposed fault tolerant estimation method in supervised learning framework as shown in 3.3.1 was evaluated with five healthy male participants (ages ranged from 24-31) who gave informed consent. I also compare my approach with a conventional sensor fault detection approach [77].

Fig. 5.9 shows the experimental setup. The EMG signals were measured from the participant's left arms when their elbow-joint movements were generated to track the displayed target motions while they were wearing the one-DOF exoskeleton robot. I used four bipolar surface EMG electrodes and measured the EMG signals from the bicep brachii long head (Channel 1: e_k^1), the biceps brachii short head (Channel 2: e_k^2), the triceps brachii long head (Channel 3: e_k^3), and the triceps brachii short head (Channel 4: e_k^4). Simultaneously, the elbow-joint angle trajectories were recorded using the one-DOF system's encoder. The target motions were designed by an experimenter who actually moved his own arm so that the target joint trajectory also represents natural movements for the other human subjects. The experimenter also generated complex joint angle movements, which included various joint angle amplitudes and frequencies so that the target trajectories contain more than one periodic basis in terms of the Fourier series (bottom-left of Fig. 5.9). The participants were instructed to track the target motions. A subject's target and current joint angles were displayed on a monitor. For each subject, torque estimation experiments were conducted after several training trials to track the target motion.

I evaluated my supervised learning based-proposed method with two different sensor fault situations: 1) an EMG electrode was disconnected from the amplifier (SDC), and 2) an EMG electrode was detached from the skin surface (SDT). (see also Fig. 5.8). In fault

situation 1), the signal measured by disconnected channel 2 became zero. On the other hand, in fault situation 2), the signal measured by detached channel 2 burst. Note that as an example, I use channel 2 as a channel with problems. Since I use identical measurement systems for other channels, we will have the same results if we use other channels as the fault channel. The estimated torque profiles derived from the proposed fault detection method are then used to control the mannequin-arm-attached one-DOF robot. In these experiments, each participant conducted an elbow-joint movement trial every three minutes and completed twelve trials, where in one trial, the subject tracked the desired joint angle trajectory for twenty seconds. These twelve trials contained three different sensor fault situations, where the subject conducted four trials in each one. The first situation has no sensor failure. The second situation includes a sensor probe disconnection failure, and the third considers the case in which an EMG electrode is detached from the skin surface.

To estimate the parameters in Eq. (3.9), I used three out of four trials in each sensor fault situation. I used a total of nine trials in three different fault situations to acquire the parameters of our proposed method as training data. The remaining three trials, one for each fault situation, were used as test data to evaluate the trained parameters. To find the sliding-window size to derive the covariance in Eq. (3.8), I used all the training trials of the no sensor fault situation of the five participants for cross validation. Then for each participant, I used the three training trials of the no sensor fault situation to find the subject-dependent nonlinear shape factor in Eq. (3.5) and the linear tendon-pulley model parameter in Eq. (3.14) for cross validation.

5.2.2 Experimental Results with supervised learning framework

In this section, I first show that using multiple EMG electrodes improves the joint torque estimation performance even for the one-DOF system. Then I show the joint torque estimation performance with two different sensor fault situations and compare our proposed method with a joint torque estimation method without using sensor fault detection and a method that uses the conventional sensor fault detection algorithm. Finally, I show the control performance of the one-DOF robot system using the estimated joint torque sequences. I evaluated whether the measured data followed the normal distribution using the Anderson-Darling test [117] and found that the distribution of the measured data was not significantly different from the normal distribution with a 5% significance level ($p > 0.05$).

Joint torque estimation with different sets of electrodes

Figure 5.10 shows the estimated joint torque performance with two different sets of EMG electrodes: 1) locating only two EMG electrodes at the biceps brachii long head (Channel 1: e_k^1) and the triceps brachii long head (Channel 2: e_k^2)), and 2) locating four EMG electrodes at the biceps brachii long head (Channel 1: e_k^1), the biceps brachii short head (Channel 2: e_k^2), the triceps brachii long head (Channel 3: e_k^3), and the triceps brachii short head (Channel 4: e_k^4)). Figs. 5.10 (A)-(C) show a subject's elbow-joint movements and estimated elbow-joint torque profiles with two and four EMG electrodes. Fig. 5.10(D) shows the Root Mean Squared Error (RMSE) between the target and the estimated joint torques of the five participants. The RMSE with four EMG channels was less than with two EMG channels. I applied a t-test to the RMSE of the estimated torque with two EMG channels and four EMG channels and found a significant difference among the torque estimation performances ($p < 0.05$). These results show that using multiple EMG channels is useful to improve the joint torque estimation performance even for a one-DOF movement.

Joint torque estimation with sensor fault

Figures 5.11(A)-(E) show the joint torque estimation performances with three different sensor failure detection approaches. In this example, one EMG channel was disconnected from the amplifier at around 12 sec. The gray region represents the period after the sensor fault occurrence. As plotted in the figures, without any sensor fault detection, the estimated joint torque exceeded the range of the true torque profile. Even when we used the conventional method [77], the estimated joint torque profile became apart from the true value. One reason might be that the conventional method relies on the variance to detect sensor failures and resembles other previously proposed methods. Therefore, the conventional methods were unable to precisely detect sensor failures when the measured signal became zero, as plotted in Fig. 5.8 (a). On the other hand, with the proposed method, the sensor fault was accurately detected, as in Fig. 5.11 (A), and the joint torques were properly estimated, as in Fig. 5.11(D).

Figures 5.12(A)-(E) show, again, the joint torque estimation performances with three different sensor failure detection approaches. Here, we consider the sensor fault situation in which one side of an EMG channel, as shown in Fig. 5.8 (b), was detached from the skin surface at around 11 sec. The gray region represents the period after the sensor fault occurrence. As plotted in the figures, without any sensor fault detection, the estimated joint torque was unable to follow the true torque profile. Even with the conventional method, the estimated joint torque profile failed to capture the periodic pattern of the true value. On the other hand, when I used the proposed method, the sensor fault was accurately detected, as

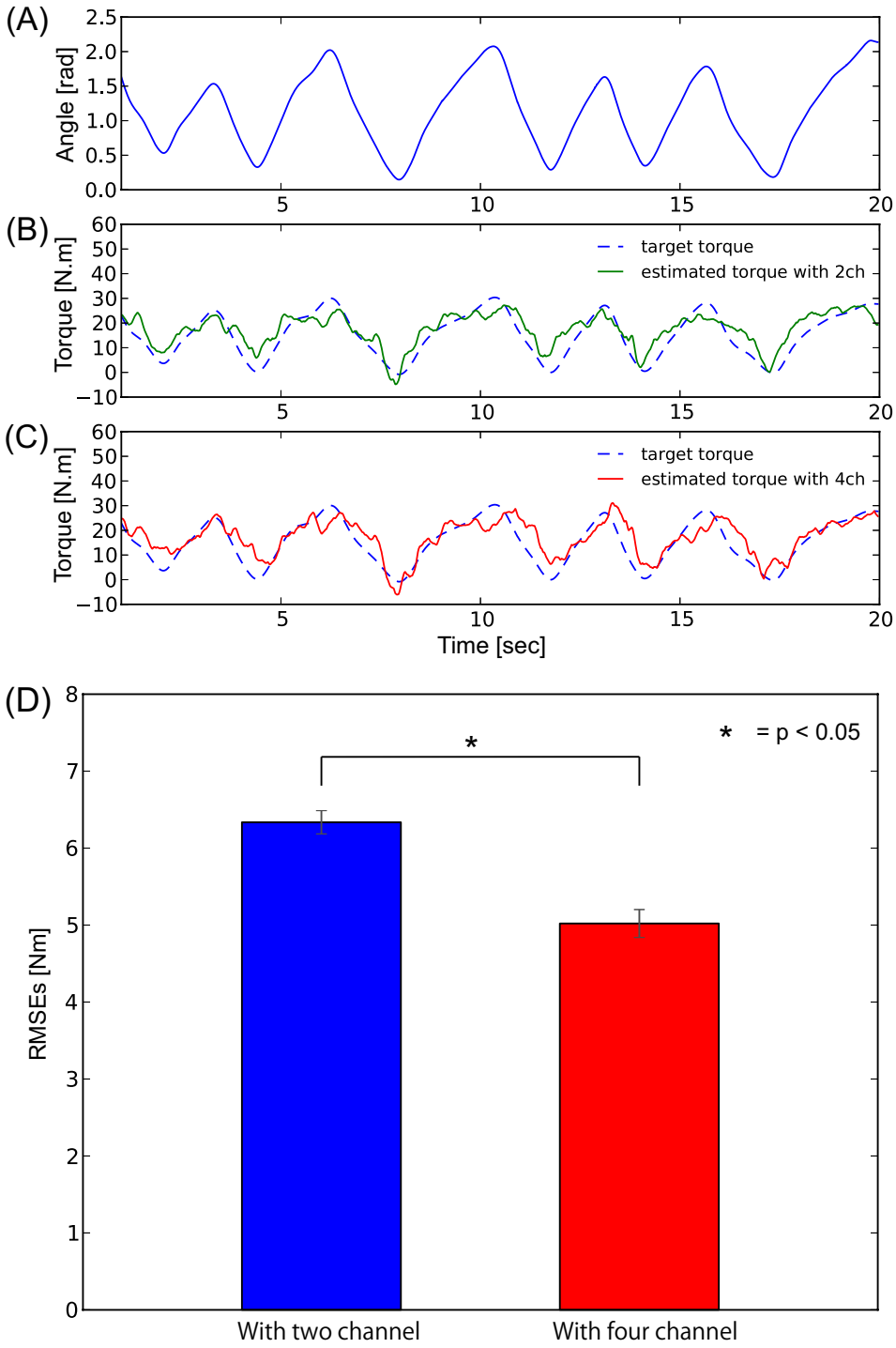

Figure 5.10: (A) Participant ' s elbow-joint angle. (B) Estimated elbow-joint torque performance using two EMG channels with no sensor fault. (C) Estimated elbow-joint torque performance using four EMG channels with no sensor fault. (D) Comparison of Root Mean Squared Error (RMSE) of estimated joint torque using two EMG channels (biceps brachii long head (Channel 1: e_k^1), triceps brachii long head (Channel 2: e_k^2)) and four EMG channels (biceps brachii long head (Channel 1: e_k^1, biceps brachii short head (Channel 2: e_k^2), triceps brachii long head (Channel 3: e_k^3), and triceps brachii short head (Channel 4: e_k^4)).

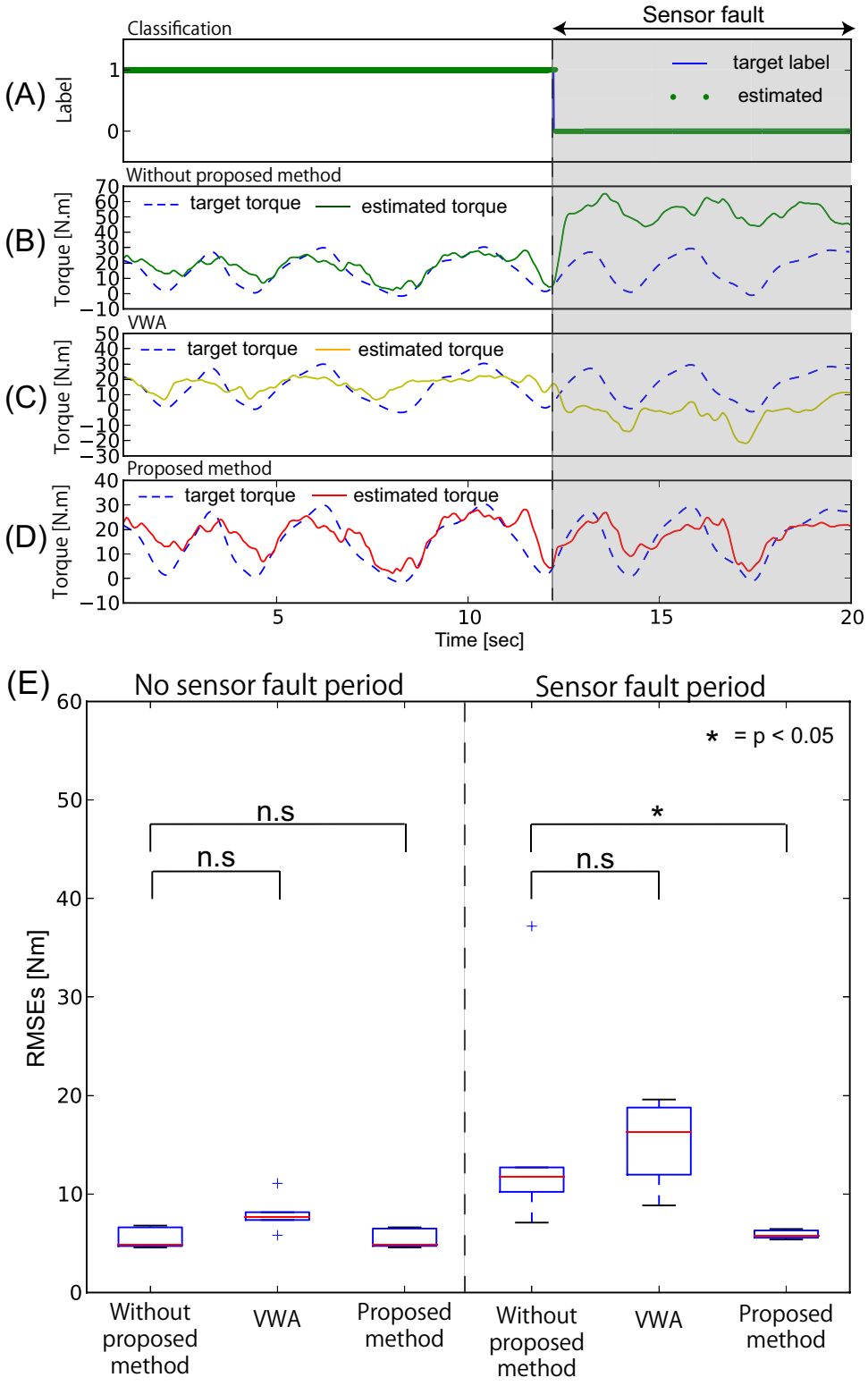

Figure 5.11: (Left-A) Classification results and estimated torque profiles without proposed method (Left-B), VWA (Left-C), and with it (Left-D) when sensor fault type (a) in Fig. 5.8 occurred in the middle of elbow movement duration. Dashed blue lines in Left-B to Left-D show the torques computed from approximated inverse dynamics of the participant's arm introduced in Eq. (3.1). Error between the estimated torque $\hat{\tau}$ from EMG signals and the target torque derived by the inverse dynamics is much larger without the proposed torque estimation method. (Right-E) Root Mean Squared Errors (RMSE) of estimated torques of each method with five participants at no sensor fault and sensor fault periods.

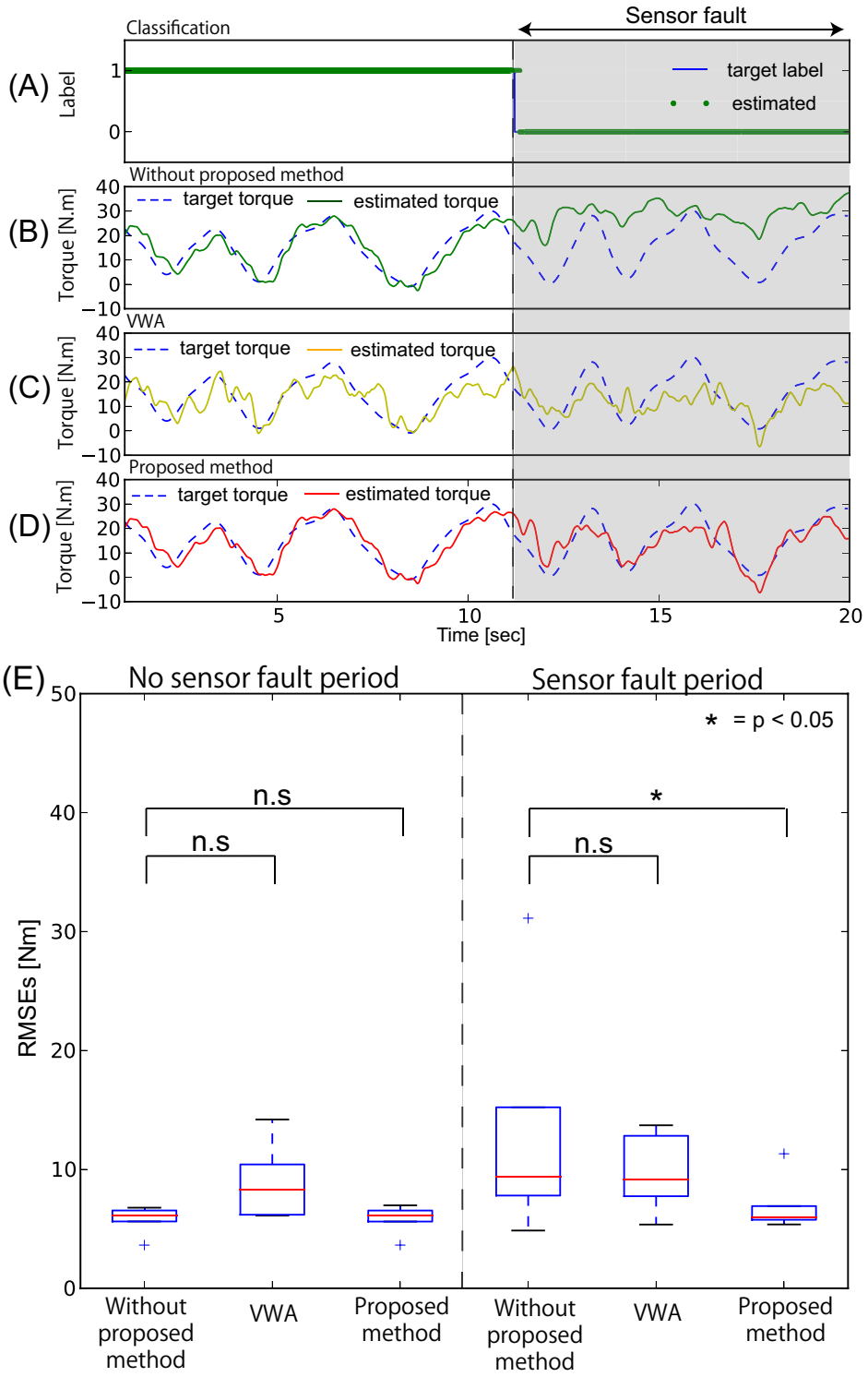

Figure 5.12: (Left-A) Classification results and estimated torque profiles without proposed method (Left-B), VWA (Left-C) and with it (Left-D) when sensor fault type (b) in Fig. 5.8 occurred in middle of elbow movement duration. Dashed blue lines in Left-B to Left-D show torques computed from approximated inverse dynamics of participant's arm introduced in Eq. (3.1). Error between estimated torque $\hat{\tau}$ from EMG signals and target torque derived by inverse dynamics is larger without proposed torque estimation method. (Right-E) Root Mean Squared Errors (RMSE) of estimated torques of each method with five participants at no sensor fault and sensor fault periods.

in Fig. 5.12(A), and the joint torques were correctly estimated, as depicted in Fig. 5.12(D).

Note that, in [77], the EMG signal estimated by VWA was linearly converted to a joint angle. However, estimating joint torque is easier than estimating joint angle since the muscle activities and the joint torque have closer relationship. Therefore, applying VWA to estimate joint torque can be reasonable.

To estimate the torques with our proposed method, I set the sliding-window size to 100 ms, which was decided by 3-fold cross validation among the three sets of training data to get high classification performance. The computation time for each sensor state classification was less than 1 ms. This result indicates that my proposed approach is potentially applicable to real-time robot control with the current number of EMG electrodes. Since the computational cost of the correlation increased at a rate proportional to $O(M^2)$, I need to verify the computational cost if the number of EMG electrodes increases.

Figures 5.11(E) and 5.12(E) show the RMSE between the target and estimated joint torques with five participants using each method: (B) without proposed method, (C) VWA, and (D) proposed method in the no sensor fault and sensor fault periods. I also applied Welch's t-test adjusted by Bonferroni correction to the RMSE of (C) and (D) with reference to (B). From Fig. 5.11(E), I found no significant difference between (B) and (C) or (B) and (D) ($p > 0.1$) in the no sensor fault period. On the other hand, in the sensor fault period, I found a significant difference between (B) and (D) ($p < 0.05$) but no significant difference between (B) and (C) ($p > 0.1$). From Fig. 5.12 (E), there is no significant difference between (B) and (C) or (B) and (D) ($p > 0.1$) in the no sensor fault period. On the other hand, in the sensor fault period, I found a significant difference between (B) and (D) ($p < 0.05$) but no significant difference between (B) and (C) ($p > 0.1$). The torque estimation performance of VWA looks slightly worse than without the proposed method in the no sensor fault period although I did not find statistically significant difference. This is because VWA fuses a pair of EMG channels into one signal so that the combined signal becomes robust against the sensor fault situation. On the other hand, since the two signals are fused based on the variance of each EMG signal, VWA possibly lose useful information that is included in the original two sensor channels for joint torque estimation. These results clearly show the advantage of my proposed method although the supervised learning framework.

Biosignal-based robot control

Here I show the control performances of our mannequin-arm-attached one-DOF robot with the derived torque profiles.

Figure 5.13 shows its joint angle trajectories with and without my proposed method. If I did not use the proposed joint torque estimation method, the one-DOF robot became stuck around a posture with a constant joint angle during the sensor fault period. On the other hand, when I did use the torque sequence derived by our proposed torque estimation method, it generated periodic movements both in the normal and sensor fault periods. As a consequence, the estimated torque trajectory derived using the proposed method robustly controlled the robot system to cope with sudden sensor failures (Fig. 5.14).

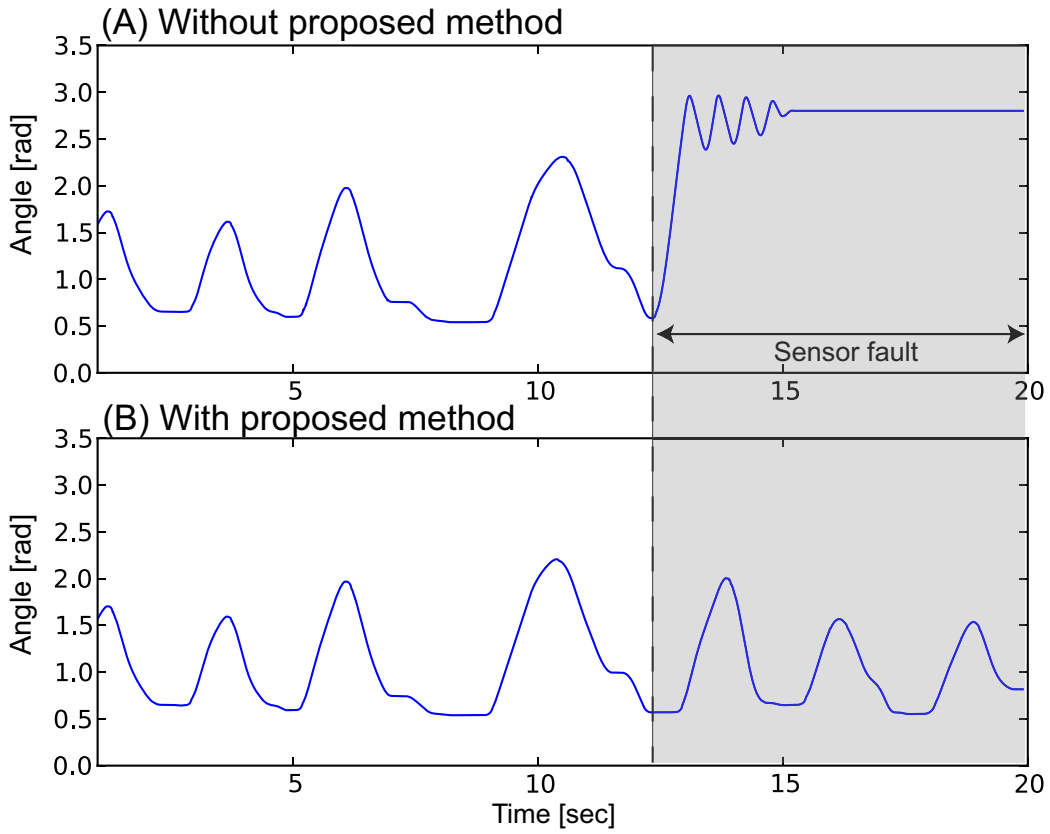

Figure 5.13: Joint angle trajectories of one-DOF exoskeleton robot (A) without and (B) with proposed method. If we did not use the proposed joint torque estimation method, the one-DOF robot became stuck around a posture with a constant joint angle during sensor fault period. When we used our proposed torque estimation method, it generated periodic movements both in the normal and sensor fault periods.

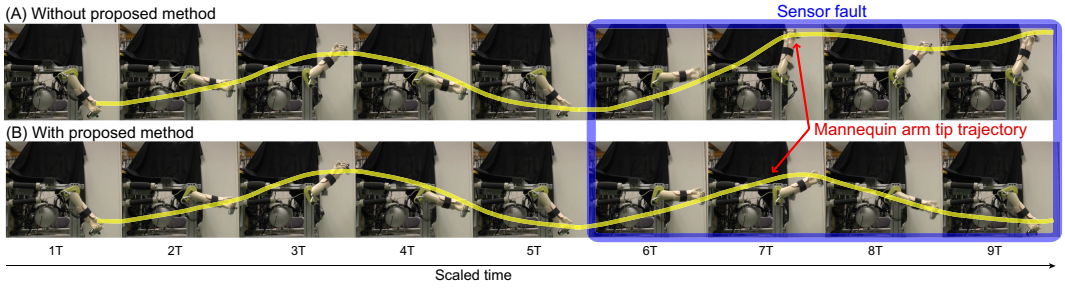

Figure 5.14: Control performances of one-DOF robot using estimated torque profiles: (A) without proposed method (B) with it.

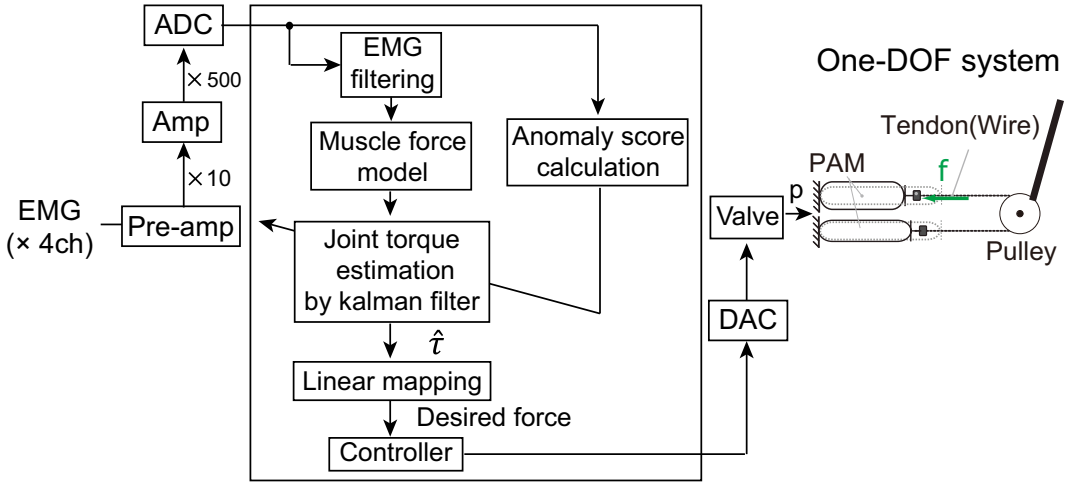

Figure 5.15: Online EMG-based control system.

5.2.3 Experiment with Unsupervised learning framework

I also evaluated my proposed fault tolerant estimation method in unsupervised learning with two different sensor fault situations: an EMG electrode Sensor is DisConnected from the amplifier (SDC), and one side of an EMG electrode Sensor is DeTached from skin surface (SDT) (see also Fig.5.8). In the SDC fault situation, measured signal by the disconnected channel became close to zero. On the other hand, in the SDT fault situation, measured signal by the detached channel was busted. Since I use identical measurement system for other channels, I will have the same results if we select other channels as the fault channel.

In this experiment with fault tolerant estimation model of unsupervised learning, the probabilistic model of the reference data $\bar{\mathscr{D}}$ is derived from the four-channel EMG measurements for 20 sec with no sensor fault. On the other hand, the time varying probabilistic model of the newly observed data $\mathscr{D}$ is derived from the measurements with 40 msec sliding time window to compute the anomaly score as introduced in Section 3.3.2.

Fig.5.15 shows schematic diagram of the online robot control experiment using the one-DOF system. The one-DOF system is controlled based on the estimated subject's elbow joint torque when the subject generate elbow movements on the sagittal plane. The anomaly scores and joint torque are computed simultaneously. According to the current anomaly score, the joint torque is estimated with the Kalman filter. Then, the estimated joint torque is converted to the air pressure command to drive the one-DOF robot.

In this experiment, I compare our proposed method with a standard EMG-based control approach in which all the sensor channels are always used. As suggested in previous studies [35] [101], I use a linear conversion model by which EMG signals are converted to joint torques. I consider two different control approaches for two different sensor fault situations:

- Standard controller with the SDC and SDT sensor fault situations .

- Proposed controller with the SDC and SDT sensor fault situations.

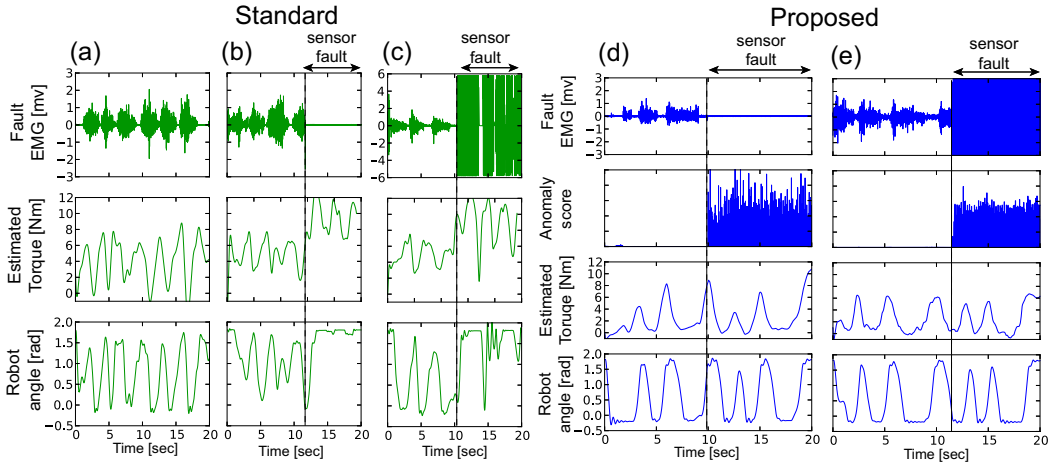

Figure 5.16: (a), (b), (c) Standard approach: (Top) Raw EMG signal of the fault sensor channel. (Middle) Estimated elbow joint torque. (Bottom) Joint angle of one-DOF robot. (d), (e) Proposed approach: (Top) Raw EMG signal of fault sensor channel. (2nd Middle) Anomaly score of fault sensor channel. (3rd Middle) Estimated elbow joint torque (Bottom) Joint angle of one-DOF robot. (a) No sensor fault condition. (b) Standard controller with the SDC sensor fault situation. (c) Standard controller with the SDT sensor fault situation. (c) Proposed controller with the SDC sensor fault situation. (d) Proposed controller with the SDT sensor fault situation.

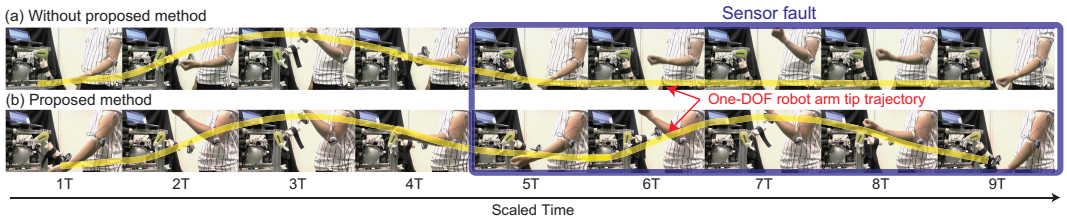

Figure 5.17: Control performances of one-DOF robot. (a) Without proposed method. (b) With proposed method.

5.2.4 Experimental Results with Unsupervised learning

In this experiment, I show the online control performances of the one-DOF robot system by comparing the proposed controller with a standard controller. Finally, I show the joint torque estimation performance with the two different sensor fault situations and compare the proposed method with a standard torque estimation method and also with a method using a conventional sensor fault detection algorithm [77]. I evaluated whether the measured data followed the normal distribution using the Anderson-Darling test and found that the distribution of the measured data was not significantly different from the normal distribution with a 5% significance level ($p > 0.05$).

Online EMG-based robot control

Figs. 5.16 (a), (b), and (c) shows the raw EMG signals, estimated elbow joint torques, and joint angle of one-DOF robot. Column (a) in Fig.5.16 shows the no sensor fault condition. From this column, the one-DOF robot was controlled normally based on the estimated

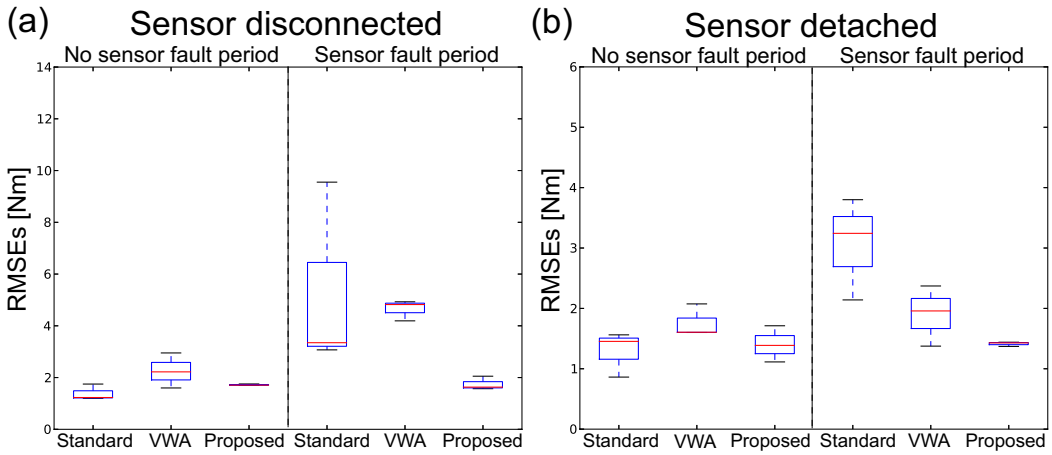

Figure 5.18: Root Mean Squared Error (RMSE) of estimated elbow joint torques with using the three different methods with five subject in the the no sensor failure period and the sensor failure period.

joint torque from EMG with no sensor fault. Columns (b) and (c) in Fig.5.16 show the results of the SDC and SDT sensor failure situations respectively with the standard control method. Figs 5.16 (d) and (e) shows the raw EMG signals, anomaly score of fault EMG channel, estimated elbow joint torque, and joint angle of one-DOF robot. Columns (d) and (e) in Fig. 5.16 show the results of the SDC and SDT sensor failure situations respectively with the proposed control method. As presented in Figs.5.16 (b), (c) and (d), (e), the standard method was not able to cope with the sensor failures. On the other hand, the proposed method was able to deal with the sensor failures, and the estimated joint torques was successfully used to control the one-DOF robot (see also Fig. 5.17.).

Estimated joint torque performances

In this section, we show the joint torque estimation performance of our proposed method by comparing with the standard method and the conventional approach (Variance Weighted Average: VWA) [77].

Fig. 5.18 (a) and (b) show the RMSEs between the actual and estimated joint torques with five subjects using the three different methods: the standard method, VWA, and the proposed method during the no sensor failure period and the sensor failure period. The RMSE of standard method was large in the two situation of sensor fault period. If I do not use any sensor fault detection, the estimated torque was not able to follow the actual torque profile. Even when I used the conventional method which explicitly take the existence of the sensor failure into account (VWA), the RMSE of estimated joint torque was large with the SDC sensor fault situation while the RMSE in the SDT sensor fault situation was smaller than the standard method. One of the reason can be that, as other previously proposed methods, the conventional method (VWA) relies on the variance of EMG signals to detect the sensor failure. Therefore, the conventional method were not able to precisely detect the sensor failure when the measured signal became close to zero as plotted in Fig.5.8 (a). On the other hand, the RMSEs of proposed method in the two sensor fault situations were smaller than other two approaches and similar to the one that in the no sensor failure period. These results clearly show the advantage of our proposed approach for the EMG-based robot control.

5.2.5 Discussion

In this experiment, I proposed novel fault tolerant strategy for a bio-signal based robot control in supervised and unsupervised learning framework.

In supervised learning framework, to cope with sudden sensor fault, I constructed a group of classifiers to detect each fault state and used the detected normal/fault state information to select an appropriate torque estimation model. I showed that the elbow-joint torques of five participants were properly estimated even when sensor faults occurred. Then the estimated torque profiles were used to control the one-DOF robot. The results show that the estimated torque was useful to control the real robot system. By selecting an appropriate movement estimation model using fault information, I showed that we can construct a fault tolerant biosignal-based robot control framework. In particular, I proposed that using a supervised learning approach to detect the fault sensor channel is a suitable for a measurement system that does not have too many sensors since we do not need to carefully design the threshold.

In unsupervised learning framework, I consider the EMG signals as the observation variables and I try to estimate user's intended movement from the observation. By considering the EMG-based control problem as an estimation problem of user's movement intention from observed EMG signals, we can easily treat the sensor noise problem and sensor failure situations. I showed that my proposed approach was able to control the one-DOF exoskeleton robot even under the EMG sensor failure situations while the standard method could not. Then, I also showed the estimated joint torque performance with five subjects by comparing the proposed method with the standard method and with a previously proposed method [77] which explicitly take the existence of the sensor failure into account and can be applicable to online robot control. The results show that the usefulness of proposed method even when the two different sensor failure situations were occurred.

In the experiment, I considered two different sensor fault situations: 1) an EMG electrode was disconnected from the amplifier, and 2) an EMG electrode was detached from the skin surface. Other kinds of sensor faults, such as noise contamination caused by other electrical devices or by sweat, are also interesting target situations. However, in these fault situations, all the channels can simultaneously observe the gradually collapsed signals. Therefore, these sensor faults, which are beyond the scope of our proposed method, suggest an interesting future direction to develop a method to cope with them. In addition, I will consider extending these approach to deal with wider variety of movements while the parameters of the estimation model are derived from the data acquired from other people by using transfer learning approaches proposed in our previous studies [118] [119]. If the number of sensor channels increases, the real-time computation of the correlation matrix for real-time robot control becomes difficult. To control multi-DOF robots that might require many EMG channels, we need to consider a parallel computation method for fast correlation matrix computation.

Using a multi-channel biosignal sensor system is useful to precisely extract user movement intentions. On the other hand, using multiple electrodes might increase the probability of sensor failure occurrences. In this study, I pointed out that multi-channel information can be used to extract sudden sensor faults.

5.3 Force Control Coordinated in Assistive Interaction

In this experiment, I first describe about experimental setup to test feasibility of the proposed controller under assistive interaction. Fig. 5.19 shows the block diagram of overview of the implementation of One-DoF system. Fig. 5.20 shows experimental setup. The subject (healthy adult) wears the One-DoF system with 2 EMG is attached to his arm. The two PAMs (PAM1 and PAM2) generates antagonistic force with pressure corresponding to the gravity compensation torque, and as the conscience, the arm holds weight.

Fig. 5.21 shows the EMG electrode locations on the subject's skin surface, corresponding to measuring the EMG mainly from Biceps Brachii and Triceps Brachii.

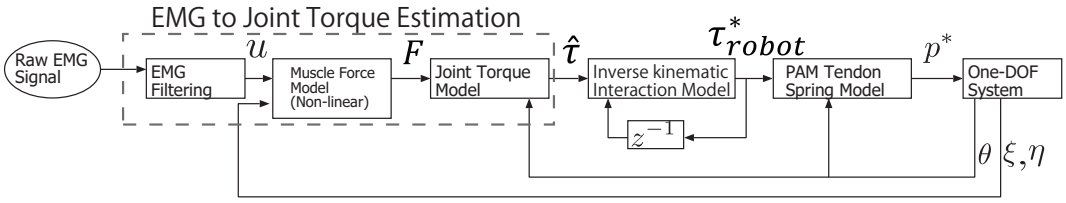

Figure 5.19: Feedback process considering Human-robot interaction

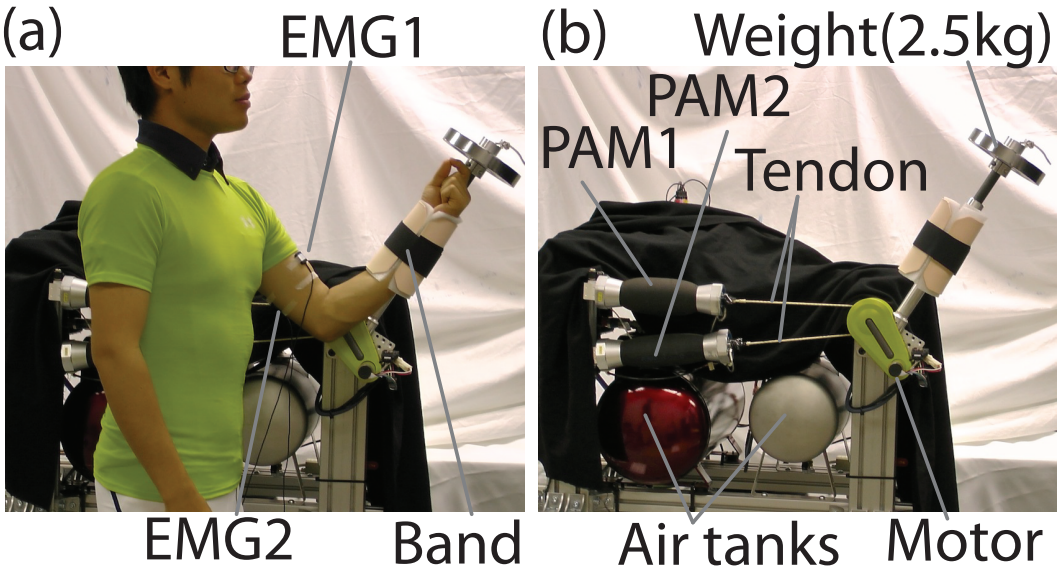

Figure 5.20: One-DoF assist experiment setup

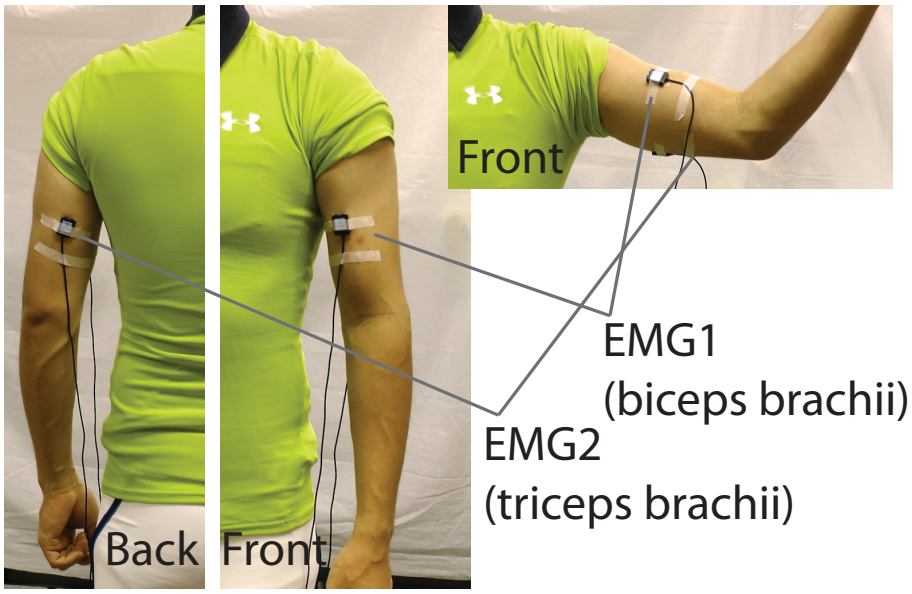

Figure 5.21: Measurement points of EMG

5.3.1 Experimental Results and Discussion

Fig. 5.22 (a) and (b) show the plots of two torque (estimated human torque τ_{human} and measured torque τ_{robot} from load-cells) transitions respectively. Fig. 5.22 (a) is the result of $(\alpha_1, \alpha_2) = (0.9, 0)$, and Fig. 5.22 (b) is the results of $(\alpha_1, \alpha_2) = (0.45, 0.45)$.

The figure 5.22 (a) is 2 times more large feedback and acquired similar amount of the assist at first several second, but the system response got very unstable in the middle of the experiment. Thus, the Figure (b) shows the smooth and stabilized because of the coordinated torque. α_1 and α_2 is trade of between instant torque and stability of interaction. Increasing α_1 improves response and increasing α_2 resulted in increasing time-constant of leaky filter effect.

In this experiment, we proposed the method to install the coordinated torque feedback term in the controller. The experiment results shows stabilized EMG-based torque controller under existing the human-robot interaction. This term is still the feed-forward term and didn't include any of the sensor. In the future, we are going to construct interaction sensing system and feedback into the torque controller.

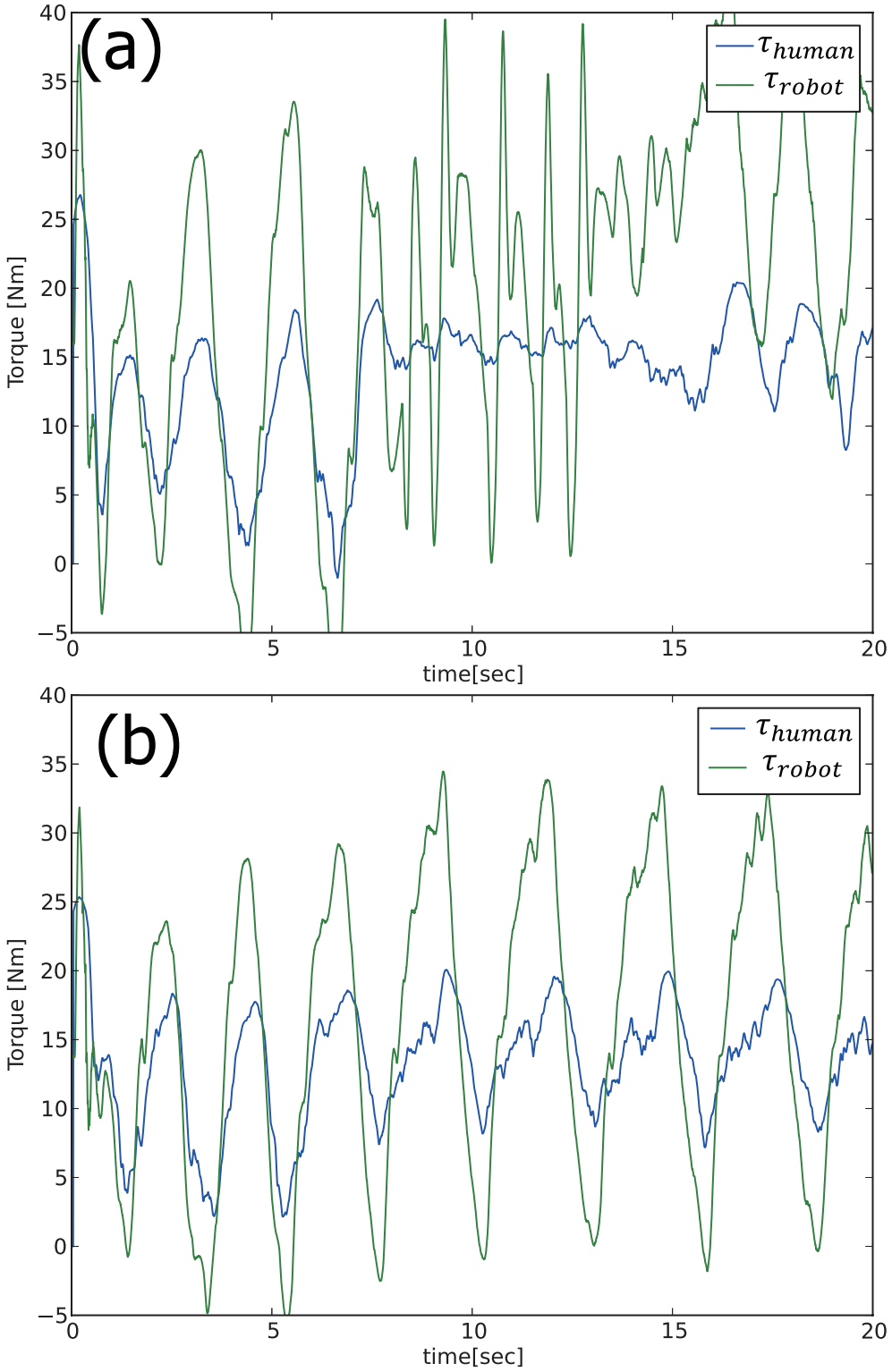

Figure 5.22: Results of feedback with conventional method

5.4 Four DoF upper-limb exoskeleton assistive robot control

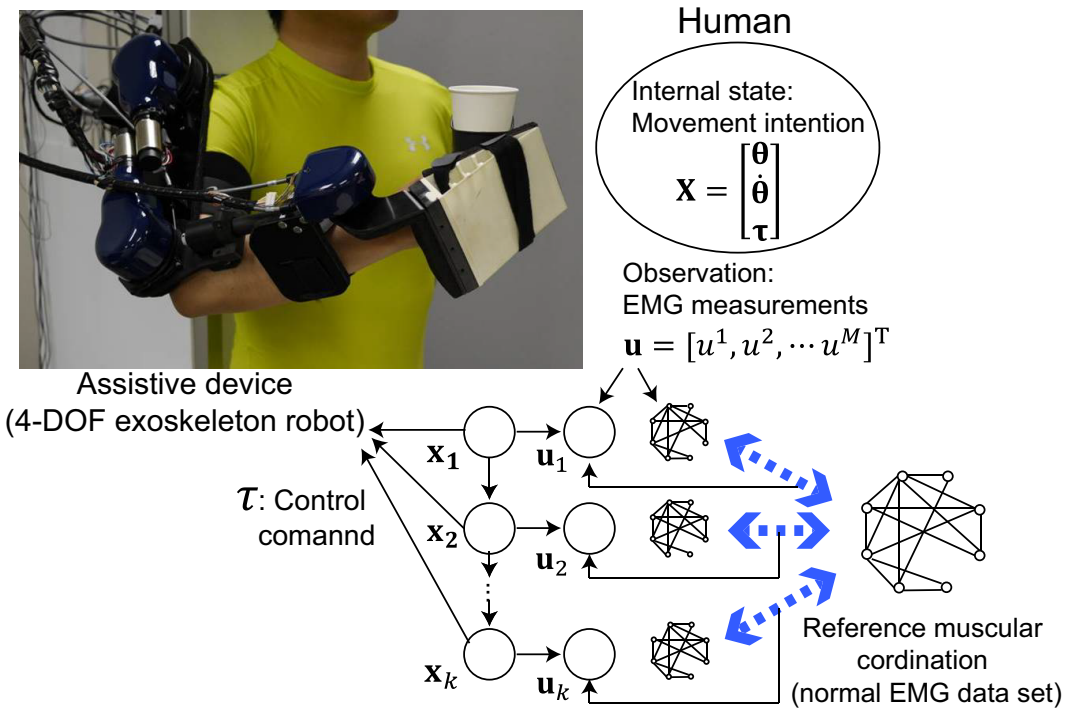

Figure 5.23: Schematic diagram of proposed human movement model that explicitly considers possibility of EMG-sensor failure occurrence. Estimated joint torques (τ) represented in the internal state ($\mathbf{x}$) of human movement model are used to control a torque-control-based assistive robot while EMG signals ($\mathbf{u}$) are observed. Deviation of the measured correlation among all EMG sensor channels from proper muscular coordination are used to detect anomalies in EMG sensor channels.

Here I introduce my experimental setups to evaluate our proposed approaches. First, I introduce our four-DOF upper-limb exoskeleton robot. Second, model parameter identification procedure is explained. Then, in the last two subsections, experimental designs are presented. As a target task to evaluate our proposed method, we considered a drinking movement as one of the daily life movements. I evaluated my proposed methods with five healthy male subjects (aged 24-32) who gave informed consent.

The estimated joint torques are used to control our four-DOF upper-limb exoskeleton robot actuated by pneumatic-electric (P-E) hybrid actuators [110]. As depicted in Fig. 4.3, the upper-limb exoskeleton robot has four degrees of freedom: Shoulder Flexion/Extension (SFE), Shoulder Abduction/Adduction (SAA), Elbow Flexion/Extension (EFE), and Wrist Flexion/Extension (WFE) joints. Each joint torque τ_{PAM} is mainly generated by a Pneumatic Artificial Muscle (PAM), and the SFE and EFE joints are also actuated by electric motor output τ_{Motor}. The PAM unit used in this study has about 80ms to 100ms latency to generate the joint torques. This slow response can be covered by the hybrid driven of electric motor. Details of the mechanical design and the torque-based control method are presented in [110]. On the other hand, the latency of the joint with PAM unit alone can be covered by the EMG-based control because the EMG signals activated 60ms to 100ms before generating the actual muscle tension [100].

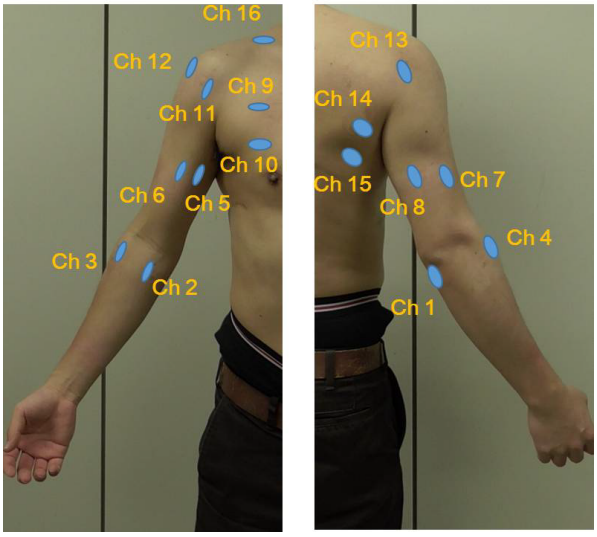

Ch1: Flexor carpi ulnaris
Ch2: Flexor carpi radialis
Ch3: Brachioradialis
Ch4: Extensor carpi radialis longus
Ch5: Biceps brachii short head
Ch6: Biceps brachii long head
Ch7: Triceps brachii lateral head
Ch8: Triceps brachii long head
Ch9: Upper pectoralis major
Ch10: Lower pectoralis major
Ch11: Deltoid front part
Ch12: Deltoid middle part
Ch13: Deltoid back part
Ch14: Latissmus dorsi
Ch15: Teram major
Ch16: Trapezius

Figure 5.24: EMG channel location. We used 16 channels to estimate four-DOF joint movements.

5.4.1 Model parameter identification

EMG signals are measured from the right arms of the subjects when they generate a drinking motion while wearing the four-DOF exoskeleton robot. These pre-recorded drinking motion data for parameter identification was used to find parameters of joint torque generator **A** and **B** in (3.18). Furthermore, we used 16 bipolar surface EMG electrodes and measured the EMG signals from 16 muscles (Fig.5.24). Simultaneously, the shoulder flexion, extension (SFE), the shoulder abduction, adduction (SAA), the elbow flexion, extension (EFE), and wrist flexion, extension (WFE) angle trajectories were recorded using the encoder of the four-DOF exoskeleton robot system. The sampled EMG signals are low-pass filtered with a cutoff frequency of 2.6 Hz, as suggested in previous work [120]. Then the processed EMG signals are used to calibrate the observation model parameters **C** in Eq. (3.19). These model parameters are identified individually for each subject.

5.4.2 Sensor anomaly situations during joint torque estimation

In this experiment, we consider three types of sensor anomaly conditions during the estimation of joint movements in drinking motion. In particular, we artificially made two types of sensor fault conditions simultaneously when the subjects generated the drinking motion, SDC and SDT (see Fig. 5.25 (a) and (b)). In addition, we also intentionally misplace the two EMG electrodes connection in 16-channel, and we named this anomaly condition: SEM (see Fig. 5.25 (c)). For the validation of our proposed method in SEM condition, we tested all possible anomaly combinations (${}_{16}C_2 = 120$). In the SDC fault condition, the measured EMG signal became close to zero. In the SDT fault condition, the measured signal was bust. In the SEM anomaly condition, the measured signal was seemingly-normal while the sensor information is interchanged.

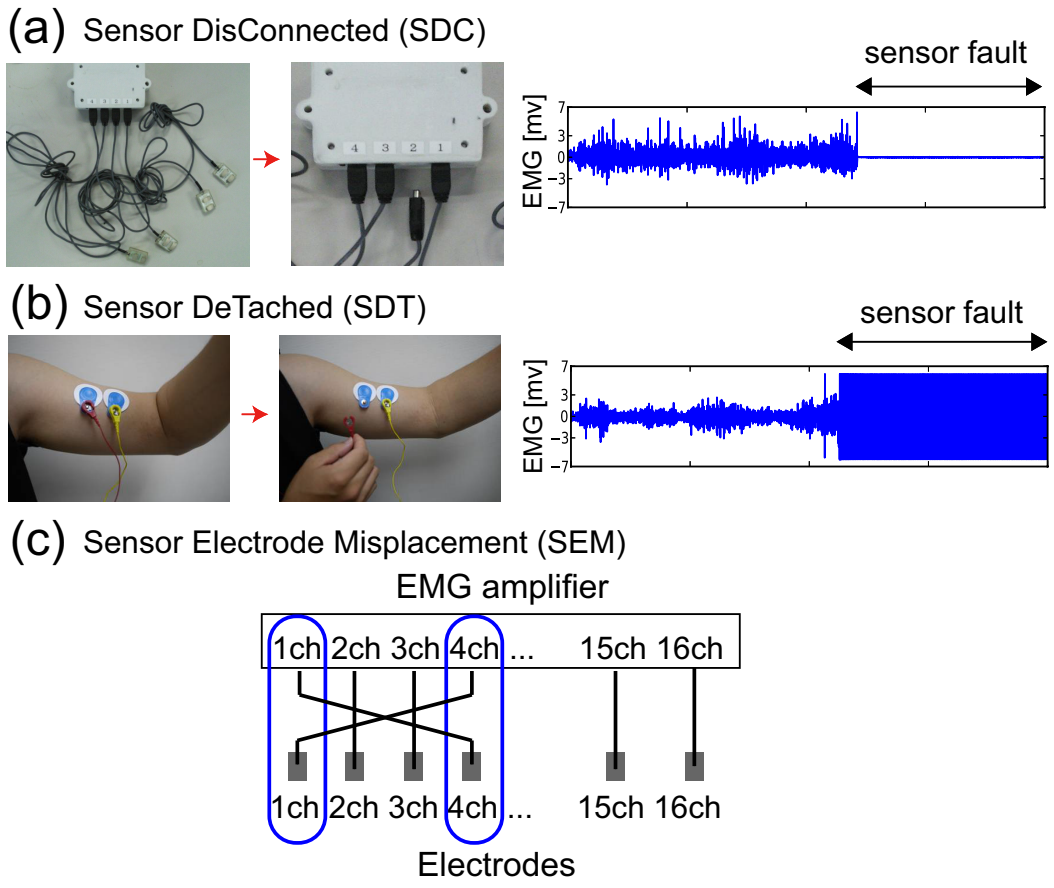

Figure 5.25: Three types of sensor failure situations and the raw EMG signals. (a) an EMG electrode sensor is disconnected from amplifier. (b) one side of an EMG electrode sensor is detached from skin surface. (c) Two EMG electrodes in 16 channels are misplaced.

5.4.3 Online EMG-based assist control

Figure 5.26 shows a schematic diagram of online upper-limb exoskeleton control system. The exoskeleton robot is controlled based on the estimated subjects' SFE, SAA, EFE, and WFE joint torques when generating a drinking motion. The joint torques are simultaneously estimated from measured EMG signals by using our proposed method in which the anomaly scores were monitored. Then the estimated joint torques are converted to air pressure and electric current commands to drive the upper-limb exoskeleton robot.

In the on-line robot control experiment, as an example, we chose the 6-th and 11-th EMG channels as simultaneous faults of SDC and SDT, where these mainly contributed to estimate shoulder and elbow joint movements.

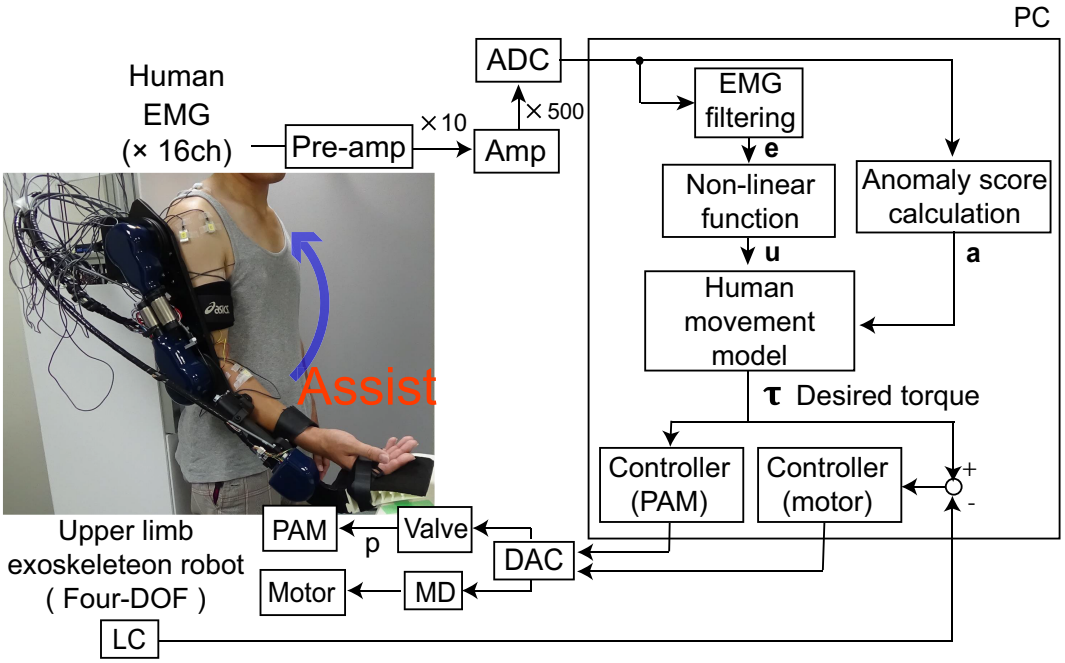

Figure 5.26: Online EMG-based upper limb exoskeleton robot control

5.4.4 Results

In this subsection, we first show the anomaly detection performance comparing our proposed method with logistic regression method [121] and well-tuned baseline method (threshold) against two simultaneous sensor fault conditions (SDC and SDT). To find the fault signal with baseline method, the minimum threshold was tuned by the minimum voluntary contraction and rest state of EMG signal. On the other hand, the maximum threshold was tuned by the maximum voluntary contraction of EMG signal. Then, we define the range from minimum and maximum threshold is normal state of EMG signal. The thresholds were tuned for each channel of EMG and each subject. Second, we show the estimation performance comparing our proposed method with threshold method against SEM anomaly situation. Then, we show the on-line assist control performance of the upper-limb exoskeleton robot by comparing the joint torque estimation performance and the angle trajectory generated from our proposed method with the standard method which has no sensor fault tolerability to see whether the subjects can properly perform their drinking motions even under sensor fault situations.

Anomaly detection and joint torque estimation performance

In order to show the anomaly detection accuracy, we use the ROC (Receiver Operating Characteristic) curve, which represents the averaged relationship between the detection rate (how many truly faulty variables are picked up) and the data coverage (how many variables are picked up). Figure. 5.27 shows the AUC (Area Under Curve) with five subjects to compare the goodness of different ROC curve of our proposed method, logistic regression method, and well-tuned threshold method against simultaneous SDC and SDT sensor fault condition. The maximum AUC = 1 means that the detection test is perfect. The minimum AUC should be considered a chance level, AUC = 0.5. We also applied Welch's *t*-test adjusted by Bonferroni correction to the AUC of logistic regression and threshold method with reference to our proposed method. We found a significant difference between pro-

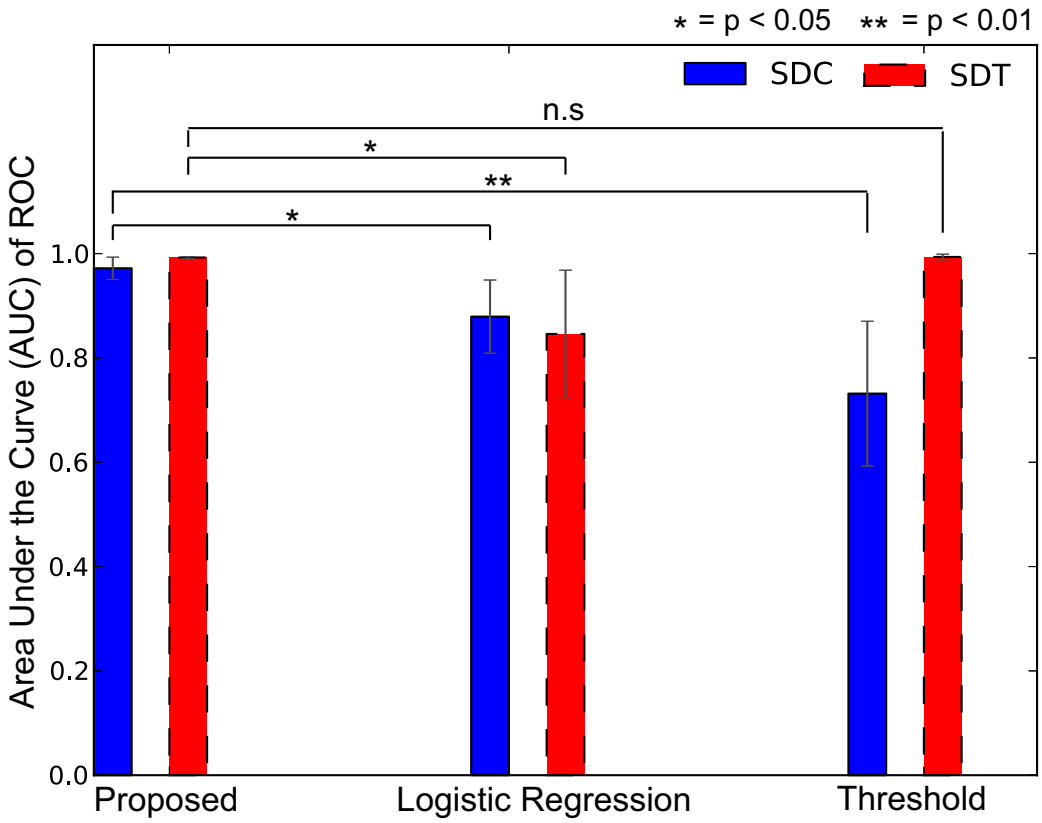

Figure 5.27: AUC (Area Under Curve) with five subjects to compare the goodness of different ROC curve of our proposed method, logistic regression method, and well-tuned threshold method against simultaneous SDC and SDT sensor fault condition.The maximum AUC = 1 means that the detection test is perfect and the minimum AUC should be considered a chance level, AUC= 0.5.

posed method and the logistic regression method ($p < 0.05$ for SDC and SDT), and the threshold method ($p < 0.01$ for SDC) except for the threshold method against SDT (no significant). The anomaly detection accuracy of the logistic regression method looks slightly worse. This is because the logistic regression method used in our previous works assumed that the sensor fault occurs only on one electrode at one time while the sensor fault occurs on two electrodes simultaneously in this experiment; one is SDC and the other is SDT. Therefore, using logistic regression method is not effective to estimate joint torques in the case assuming that more than one failure is occurred at a time. In addition, since the logistic regression need prior knowledge of all possible anomaly state to prepare the classifier and the estimation model to cope with the anomaly situation, the scalability is limited for on-line robot control also in terms of computing burden. On the other hand, the threshold method is more suitable than the classification method from the point of view of computational cost. However, the detection accuracy of the threshold against SDC fault condition also looks worse while the SDC fault is apparently easy to detect. This is because there is a case where the fault signal of SDC is presented in the normal state range without closing to zero by picking up noise. This result show the effectiveness of our proposed method to detect simultaneous sensor faults.

We also validate our proposed method of joint torque estimation performance in the SEM anomaly situation. In the SEM situation, we consider all possible anomaly state

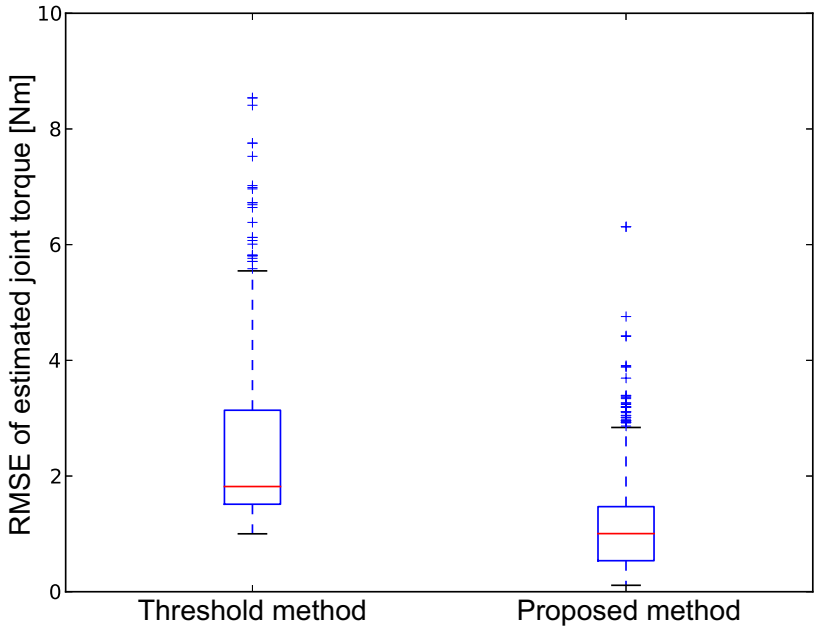

Figure 5.28: Root mean squared errors (RMSE) between actual and estimated joint torques combining of all joints (SFE, SAA ,EFE, and WFE) using threshold method and our proposed method with five subjects against SEM sensor anomaly condition. The SEM sensor anomaly situations are tested all possible combinations (${}_{16}C_2 = 120$ patterns) for each subject. Therefore, each boxplot include 600 sample data. Mann Whitney test was applied and there is a significant difference between them ($p < 0.01$)

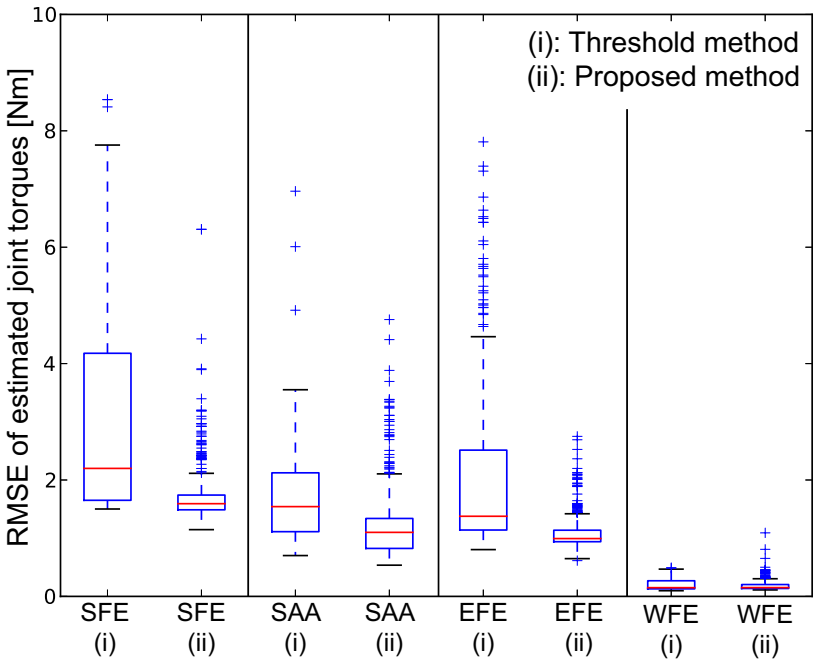

Figure 5.29: Root mean squared errors (RMSE) between actual and estimated joint torques of each joints (SFE, SAA ,EFE, and WFE) using threshold method and our proposed method with five subjects against SEM sensor anomaly condition.

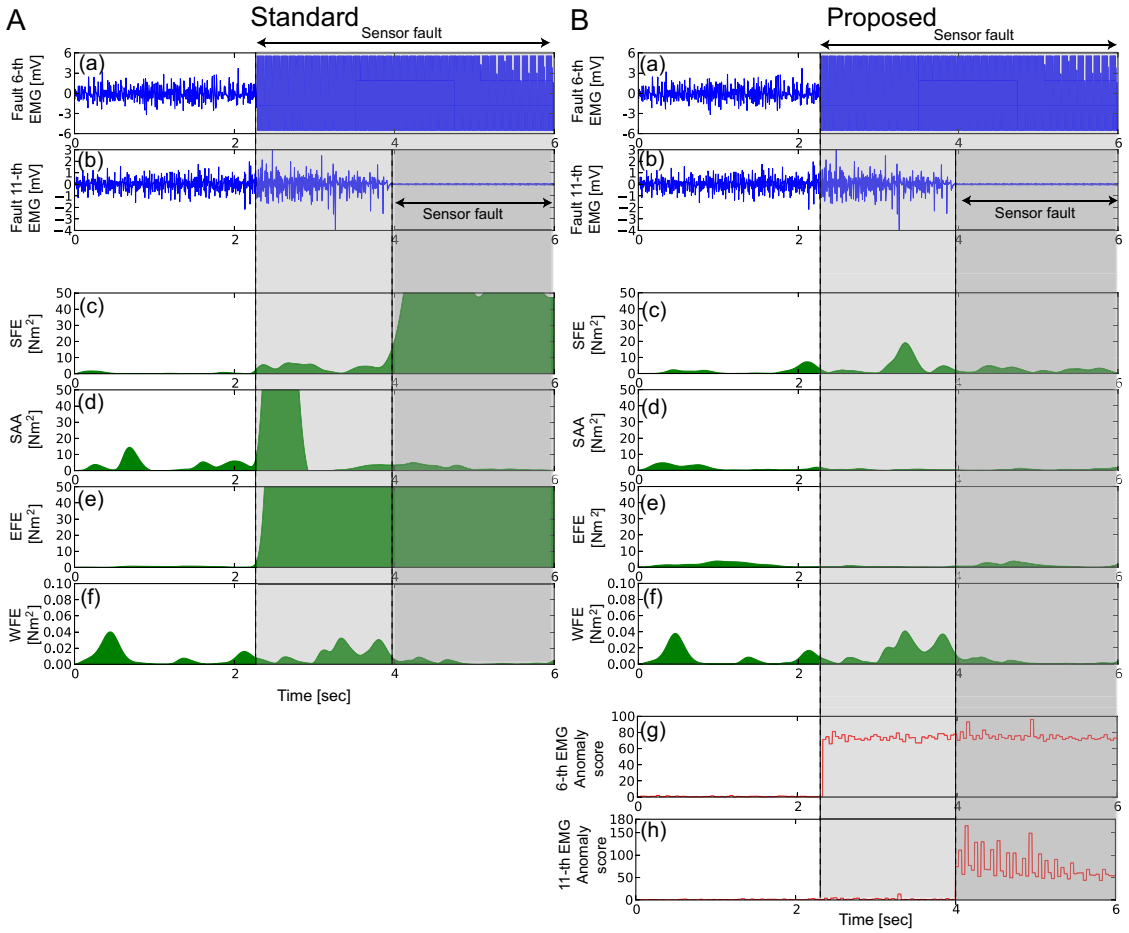

Figure 5.30: Estimated joint torque performance of standard and proposed methods. A-(a), A-(b), B-(a), and B-(b) show the raw fault EMG signals. A-(c) to A-(f) and B-(c) to B-(f) show squared errors between estimated and actual joint torques: SFE, SAA, EFE, and WFE. B-(g) and B-(h) show anomaly scores of fault EMG signals B-(a) and B-(b).

combinations in 16-channels ($_{16}C_2 = 120$ patterns) for each five subject. Since it is difficult to use logistic regression method in this case from the above reason, we compare our proposed method with threshold method. Figure. 5.28 shows the Root Mean Squared error (RMSE) between the actual and estimated joint torque combining all joints (SFE, SAA, EFE, and WFE) using proposed method and threshold method against SEM sensor anomaly situations. From this figure, the RMSE of our proposed method is lower than the threshold method. We applied Mann Whitney test to the two RMSEs and we found significant difference between them ($p < 0.01$). We also show each joint estimation performance is shown in Figure. 5.29. These results clearly show the advantage of our proposed method for anomaly detection and joint torque estimation.

Online EMG-based assist control

In this online EMG-based robot control experiment, we compared our proposed method with a standard method without fault tolerability that always use all the EMG sensor channels to derive the joint torques. Concretely, we used a linear conversion model in which the EMG signals are converted to joint torques, as suggested in a previous study [35] [68]

Table 5.3: Root Mean Square Error (RMSE) of estimated torque for each joint

Subject	**Joint**	**RMS**			
		Normal condition		**Fault condition**	
		Standard	Proposed	Standard	Proposed
A	SFE	1.32	1.36	**5.04**	**1.58**
	SAA	0.658	0.795	2.45	1.00
	EFE	0.625	0.793	$>$ **10**	**2.83**
	WFE	0.135	0.121	0.178	0.128
B	SFE	1.35	1.13	**2.06**	**1.79**
	SAA	1.54	1.43	1.44	1.35
	EFE	1.15	0.930	**2.23**	**0.951**
	WFE	0.129	0.128	0.151	0.135
C	SFE	1.18	1.19	$>$ **10**	**1.21**
	SAA	1.34	1.03	1.88	0.995
	EFE	0.674	0.918	**1.81**	**0.951**
	WFE	0.120	0.148	0.149	0.136
D	SFE	1.07	0.748	$>>$ **10**	**0.771**
	SAA	0.767	0.671	0.792	0.660
	EFE	0.794	0.751	**1.18**	**1.09**
	WFE	0.138	0.110	0.131	0.127
E	SFE	0.926	0.741	$>>$ **10**	**5.67**
	SAA	0.534	0.492	1.00	0.567
	EFE	0.728	0.697	**1.40**	**0.792**
	WFE	0.223	0.237	0.251	0.235

[101]:

$$\tau(k) = \mathbf{K}\mathbf{u}(k), \tag{5.5}$$

where $\mathbf{u}(k)$ is the processed EMG signals. The parameter $\mathbf{K}$ is derived from the training data used in Subsection 5.4.1.

As the experimental conditions with the sensor failure situations, we considered two different control approaches for two different sensor fault situations:

- standard controller with SDC and SDT sensor fault situations.
- proposed controller with SDC and SDT sensor fault situations.

Figure 5.30 shows the estimated joint torque performances of the standard and proposed methods for one of the five subjects. A-(a), A-(b), B-(a), and B-(b) show the raw EMG signal profiles include the two types of sensor fault situations, SDT and SDC. A-(c) to A-(f) show the squared errors between each estimated joint torque with the standard method and the actual joint torques, where the actual joint torques were derived from the inverse

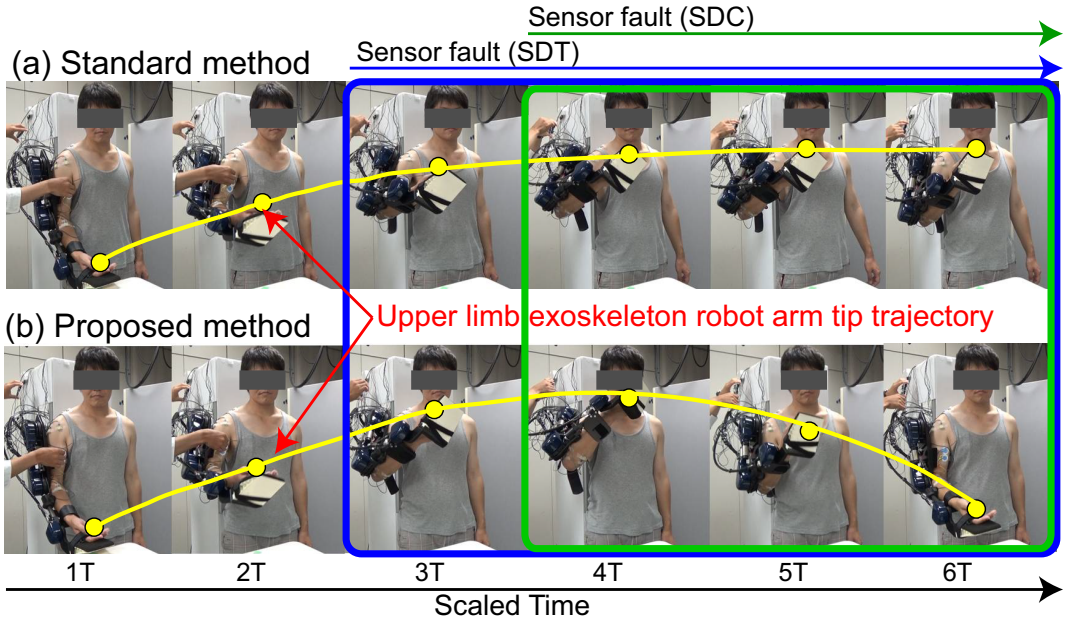

Figure 5.31: Control performance of upper limb exoskeleton: (a) Standard method. The robot movement almost stopped after the sensor failure occurrence. (b) Proposed method. The drinking motions were successfully generated with our proposed method even during the sensor faults period.

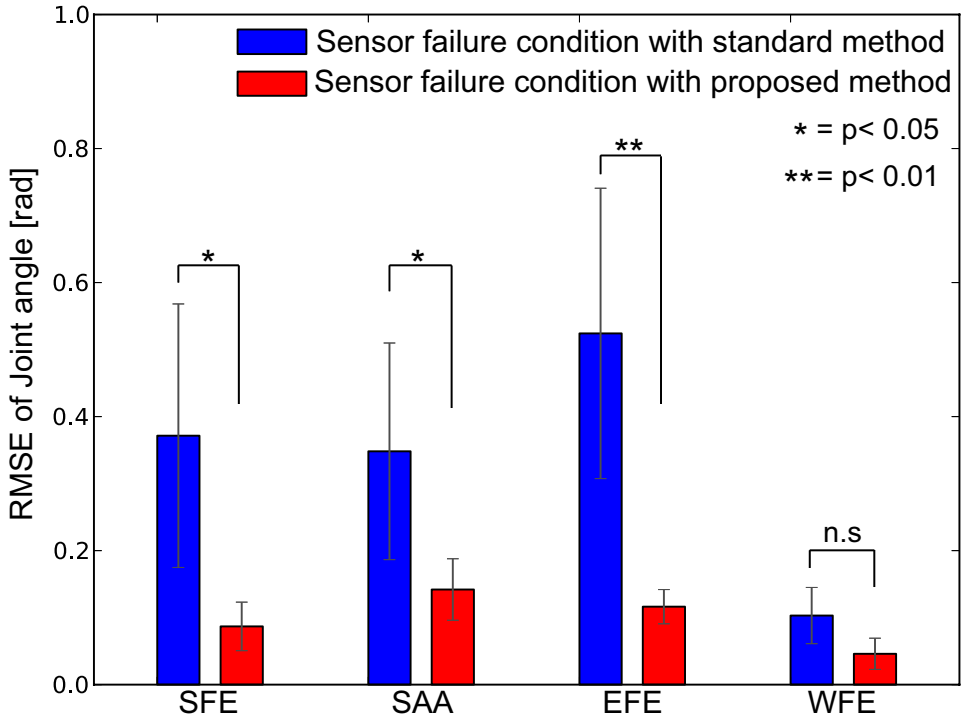

Figure 5.32: RMSEs between generated movements with exoskeleton assist control where all sensors are normal and joint angle trajectories generated with the exoskeleton assist control where the sensors are condition across all five subjects. The errors of our proposed method with the sensor failure was smaller than that of the standard method.

dynamics of a subject and the robot arms with the actual joint trajectories. B-(c) to B-(f) show the squared errors between each estimated joint torque with our proposed method and the actual joint torques. B-(g) and B-(h) show the anomaly scores of the fault EMG channels. B-(a) corresponds to SDT and B-(b) corresponds to SDC.

As presented in Figs. 5.30 A-(c) to A-(f), the errors of the standard method were large during the sensor fault condition and degraded the estimation performances. On the other hand, from B-(c) to B-(f) in Fig. 5.30, the error of our proposed method was much smaller than the standard method and successfully estimated the joint torques even after sensor faults occurred.

Table 5.3 shows the Root Mean Squared Error (RMSE) between the actual and estimated torques for each joint with all the five subjects using two different methods: the standard method and our proposed method during the normal condition and during the trial period which includes sensor fault conditions. From Table 5.3, the RMSEs of the standard method were always larger than that of the proposed method if the trials include the sensor failure periods. In the normal condition, the RMSEs of the standard method were similar to that of the proposed method. However, still, in thirteen out of twenty cases, the proposed method showed better estimation performances even in the normal condition. Since we selected the 6-th and 11-th EMG channels that contributed to estimate the SFE and EFE joint movements, large differences in the estimation performances between the standard and the proposed methods can be observed in SFE and EFE joints. On the other hand, the estimation performance of SFE joint in subject E is slightly worse than other subjects. This was because that the anomaly score of the fault electrode could not completely work for the estimation due to the smallest value than other subjects.

Figure 5.31 shows the control performance of our upper-limb exoskeleton robot. When we used the standard method, the robot movement almost stopped after the sensor failure occurrence. On the other hand, The drinking motions were successfully generated with our proposed method even during the sensor faults period.

Fig. 5.32 shows the RMSEs between generated movements with exoskeleton assist control where all sensors are normal and joint angle trajectories generated with the exoskeleton robot assist control where the two sensors are fault condition across all five subjects. We compared the control performance of the proposed method with that of the standard method. Concretely, we compared the proposed and standard methods in movement trials that include the sensor failure conditions. We also applied Welch's t-test to the RMSE of each joint and we found significant difference; SFE ($p < 0.05$), SAA ($p < 0.05$), EFE ($p < 0.01$). On the other hand, we found no significant difference in WFE joint. This can be considered that fault channel selected in this online experiment had low contribution for the WFE torque estimation.

From these results, the errors of the standard method were large if the movement trial periods include the sensor faults. On the other hand, the control performances of our proposed method with the sensor failure periods were much better than that of the standard method. Note that some amount of errors remained even when we used our proposed method partially due to the variations of subjects' intended drinking movements (see Figure. 5.33). These results clearly show the advantage of using the human movement model for EMG-based assist robot control.

5.4.5 Discussion

In this experiment, I proposed a human movement model both for EMG-based assistive control and for biosignal-sensor-failure detection. The sensor anomaly detection and joint movement estimations were combined by exploiting the human muscular coordination pat-

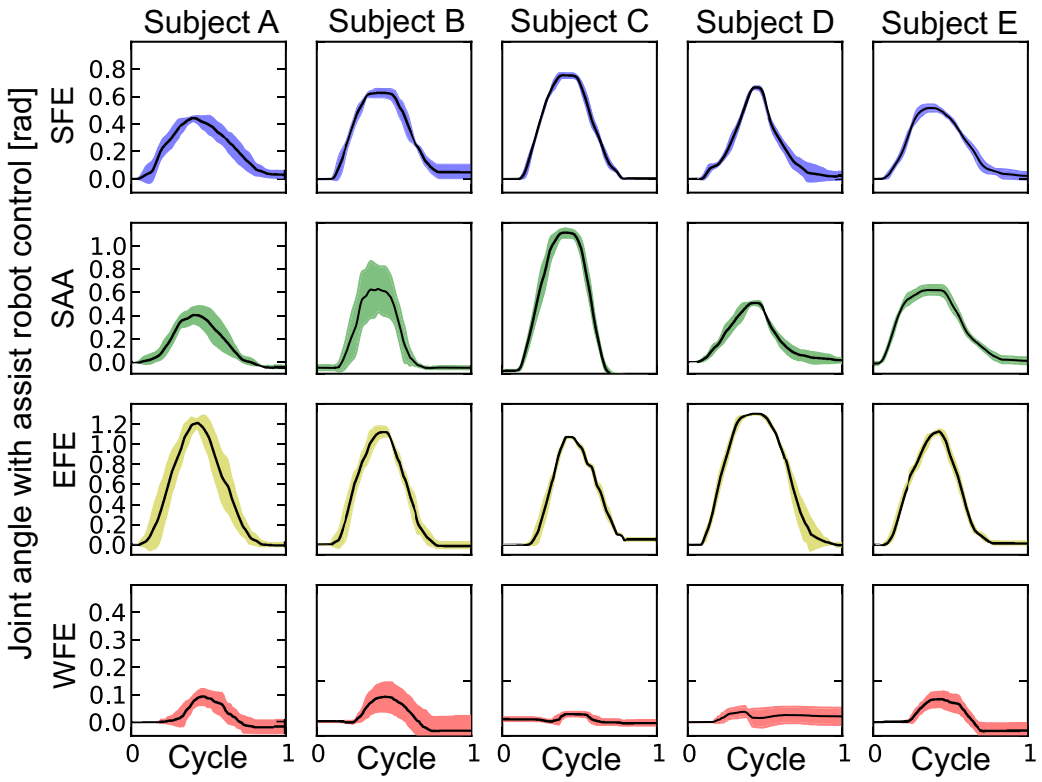

Figure 5.33: The mean and standard deviation of joint angles generated from each subject without exoskeleton assist control during drinking motion.

terns measured from multiple EMG electrodes. My proposed model considers EMG signals to be observation variables that take uncertain observations into account and estimates the intended movements of users from observations. To validate our proposed method, I used 16 EMG channels and a four-DOF upper limb exoskeleton robot driven by estimated joint movements with five healthy subjects who performed a drinking motion. In this experiment, we considered three types anomaly situations; An EMG electrode was disconnected from the amplifier (SDC) in which the sensor signal became close to zero, an EMG channel was detached from the skin surface (SDT) in which the sensor signal was bust, and two EMG electrodes connection in 16-channel were misplaced (SEM) in which the sensor signal seemingly-normal. During our experiment, I artificially created two types of sensor faults (SDC and SDT) simultaneously, and intentionally misplace the two EMG electrodes connection in which all possible anomaly state combinations were tested.

Our proposed model more successfully detected the anomaly sensors and estimated the joint movements of the users than other conventional anomaly detection methods. In addition, by using our proposed method, five healthy subjects successfully controlled the four-DOF upper-limb exoskeleton robot to generate drinking motions even under two EMG sensor simultaneous faults conditions. With respect to the subject E, the SFE joint torque estimation performance was slightly worse than other subjects. This was because that the anomaly score of disconnection fault EMG channel contributed to SFE joint was the smallest in all subjects and did not completely work for the estimation. However, the estimation performance with our proposed method was better than the estimation performance with standard method. My results show the usefulness of using the human movement model for EMG-based assistive robot control using multiple electrodes.

Chapter 6

EEG-based Assistive Robot Control

Since many counties are facing the aging population problem, development of an exoskeleton robot which can be used to assist user movements is becoming important research topic [122] [23]. In particular, these exoskeleton robot can be used as prosthetic devices for patients such as stroke patients and spinal cord injury patients in rehabilitation programs [14] [15] [18].

In recent years, it has been found that using brain activity to control robotic assistive system can be useful for stroke patients to enhance recovery of motor function [47]. Therefore, there would be also a possibility to enhance recovery of lower limb motor functions if an exoskeleton robot to assist power body can be controlled by brain activities. This rehabilitation approach is called Brain-Machine Interface (BMI) rehabilitation [123].

For BMI rehabilitation, we develop a Electroencephalogram (EEG)-Exoskeleton robot system, where the exoskeleton robot is connected to the EEG system so that the users can control the exoskeleton robot by using their brain activities (see Fig.6.1). We use a classification method which considers covariance matrices of measured EEG signals as input to decode brain activities. The decoded brain activities are used to control exoskeleton movements. In this study, we consider assisting the stand-up movement which is one of the most frequently appeared movements in daily life activities and also a standard task movement as a rehabilitation training. To assist the stand-up movement, we use our developed exoskeleton robot (see Fig. 4.2). To test the EEG-robot system, we also use one-DOF exoskeleton robot (see Fig. 4.1).

I show that a user was able to control the EEG-oneDoF system using subject's brain activities. Furthermore, the results show that the exoskeleton robot successfully assisted the stand-up movements, where the assist system was controlled by the decoded brain activities.

6.1 Deoding Brain Activities

To decode brain activities, we use classification method proposed by [124] [125] because the method classification matrices with spectral l_1-norm regularization which can lead to good generalization performance. In addition, the decoder can be efficiently derived by solving a convex optimization problem [124].

As suggested in [124], we use the covariance matrices of the measured EEG signals $\mathbf{C}$ as the input variables. In this classification method, the output probabilities of the two-class

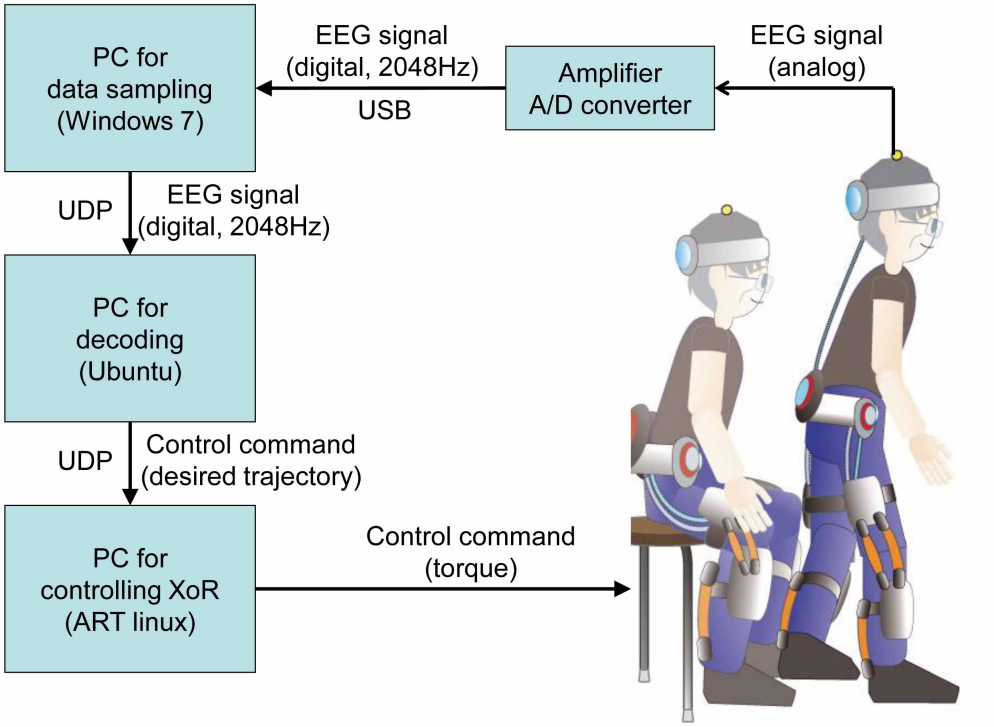

Figure 6.1: EEG-Exoskeleton System. EEG signals are detected by active electrodes (BIOSEMI) and the detected brain activities are amplified and converted to digital signals with 2048 Hz sampling rate. The sampled data are transmitted to computers and the received data are decoded to generate control command for the exoskeleton robot. The generated command is sent to the control system of the exoskeleton robot. According to the control command, the exoskeleton robot activates the assist control system.

classification problem are represented as:

$$P(q_t = +1|\mathbf{C}_t) = \frac{1}{1+\exp(-a_t)}, \tag{6.1}$$

$$P(q_t = -1|\mathbf{C}_t) = \frac{\exp(-a_t)}{1+\exp(-a_t)}, \tag{6.2}$$

where q_t denotes the class label. The log odds or logit [126] is modeled as a liner function of the input $\mathbf{C}$:

$$a_t = \ln \frac{P(y=+1|\mathbf{X})}{P(y=-1|\mathbf{X})} = tr\left[\mathbf{W}^\top \mathbf{C}_t\right] + b \tag{6.3}$$

Here $\mathbf{W}$ is a parameter matrix and b is a bias.

6.1.1 Learning Classifier

To construct the classifier, we consider minimizing a objective function:

$$\min \sum_{t=1}^{n} l(z_t) + \lambda ||\mathbf{W}||_1, \tag{6.4}$$

$$z_t = q_t a_t, \tag{6.5}$$

where λ is the regularization constant and each term of the objective function is represented as:

$$l(z_t) = \ln(1 + \exp(-z_t)) \tag{6.6}$$

$$||\mathbf{W}||_1 = \sum_{i=1}^{r} \sigma_i[\mathbf{W}], \tag{6.7}$$

where $\sigma_i[\mathbf{W}](i = 1, \ldots, r)$ is the i-th singular value of a matrix $\mathbf{W}$ and r is the rank of $\mathbf{W}$. This optimization problem can be efficiently solved by considering an equivalent linear matrix inequality (LMI) problem [124].

6.1.2 Online Decoding

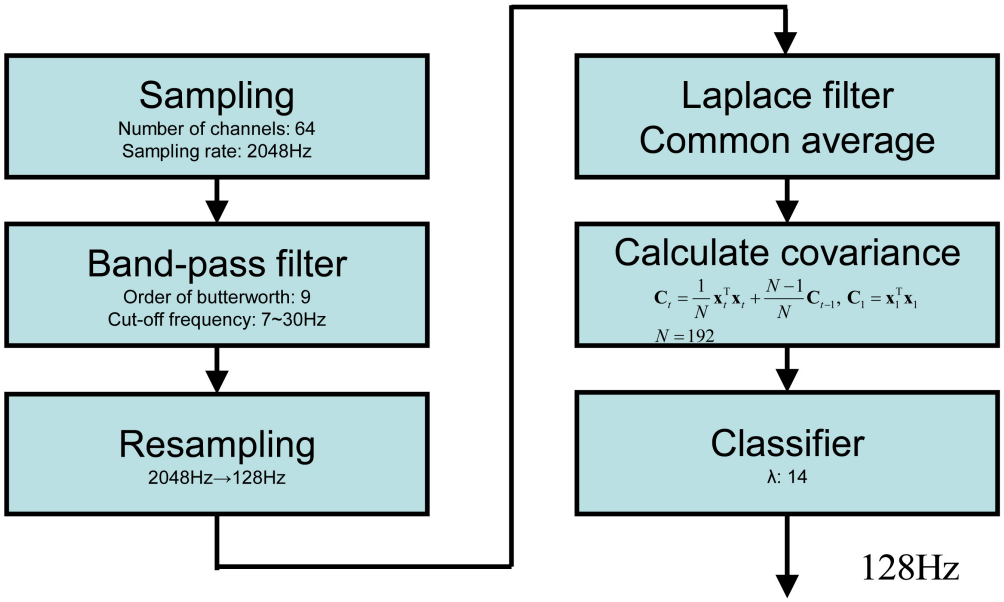

Figure 6.2: EEG signal processing procedure: A band-pass filter with the frequency 7-30 Hz are applied to the measured EEG signals. The filtered signals are down-sampled with 128 Hz. Laplace filter and common average subtraction are applied for removing bias voltage on electrodes. The covariance matrix of the processed data is used as the input variable for the classifier. We used the classifier with the selected regularization parameter $\lambda = 14$.

We decode brain activities by using the classification method introduced above after preprocessing measured EEG data. Figure 6.2 shows the processing procedure. A band-pass filter with the the frequency $7 - 30$ Hz are applied to the measured EEG signals.

The filtered signals are down-sampled with 128 Hz. Laplace filter and common average subtraction are applied for removing voltage bias. The covariance matrix of the processed data is used as the input variable for the classifier. we update a covariance matrix $\mathbf{C}_t$ of filtered EEG signal at every time step ($t = 1, 2, \cdots$):

$$\mathbf{C}_t = \begin{cases} \mathbf{x}_t^\top \mathbf{x}_t & (t = 1) \\ \frac{1}{N}\mathbf{x}_t^\top \mathbf{x}_t + \frac{N-1}{N}\mathbf{C}_{t-1} & (t \geq 2) \end{cases} . \tag{6.8}$$

Here, $\mathbf{x}_t \in \Re^{1\times D}$ is a filtered EEG signal at time t ($D = 64$). By using estimated weight matrix $\mathbf{W} \in \Re^{D\times D}$ and bias constant $b \in \Re$, we estimate a probability $P(q_t = +1|\mathbf{C}_t)$ and $P(q_t = -1|\mathbf{C}_t)$ as in Eqs. (6.1) and (6.2).

Next, we explain how to select a control command $g_t = \{up, \quad down\}$ which is given to the robot. Since input variables are based on measured EEG signals, the output of the classifier can be fluctuated. Therefore, we employed following hysteresis:

$$g_t = \begin{cases} up & (P(q_t = +1|\mathbf{C}_t) > P_{threshold}) \\ down & (P(q_t = -1|\mathbf{C}_t) > P_{threshold}) \\ g_{t-1} & otherwise \end{cases} , \tag{6.9}$$

where up denotes upward state of the oneDOF system or stand-up state of the exoskeleton robot, and $down$ denotes downward state of the oneDOF system or sit-down state of the exoskeleton robot. We set the threshold as $P_{threshold} = 0.7$.

According to the output of the classification, upward/stand-up or downward/sit-down movements on the oneDOF system or the exoskeleton robot, respectively, are generated by using the torque control method introduced in the device chapter 4.

6.2 Results

Here I show the results of the developed EEG-robot systems.

6.2.1 EEG-oneDoF system

Fig. 6.3 shows the experimental setup. A subject watched the display during all the experiment to recognize classifier output (EEG decoder output) in real-time. Fig. 6.4 and 6.5 show the control performance of the EEG-oneDoF system. The subject does not wear the one-DoF system to follow the up/down direction indicated on the display by motor imagery. The white/gray region in figure 6.5 shows the up/down target direction respectively.

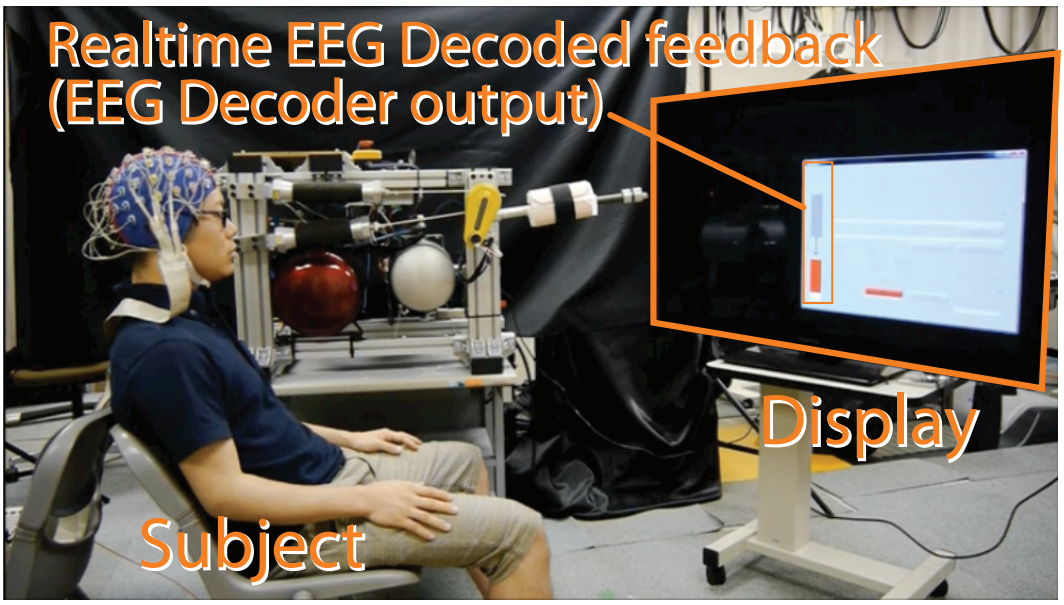

Figure 6.3: EEG realtime visual feedback; The subject watches the display during experiment to get visual EEG decoded feedback. The visual feed back is displayed as the red bar (upper/lower) in the picture as probability of EEG decoder output($P(q_t = +1|\mathbf{C}_t)$ and $P(q_t = -1|\mathbf{C}_t)$ respectively). The direction queue is displayed at the middle of the bars. The subject task is motor imagery of left arm movement and right arm movement, corresponding to up/down direction.

Fig. 6.5 and 6.6 show, again, control performance of the EEG-oneDoF system. However, in this case, the subject wears the oneDoF system. The subject tries to control one-DoF system to follow the up/down direction indicated on the display by motor imagery. The white/gray region in Fig. 6.6 shows the up/down target direction respectively.

In both cases, i.e., 1) the case in which the subject does not wear the robot and 2) the case in which the subject wears the robot, the indicated robot movements are correctly generated in most cases.

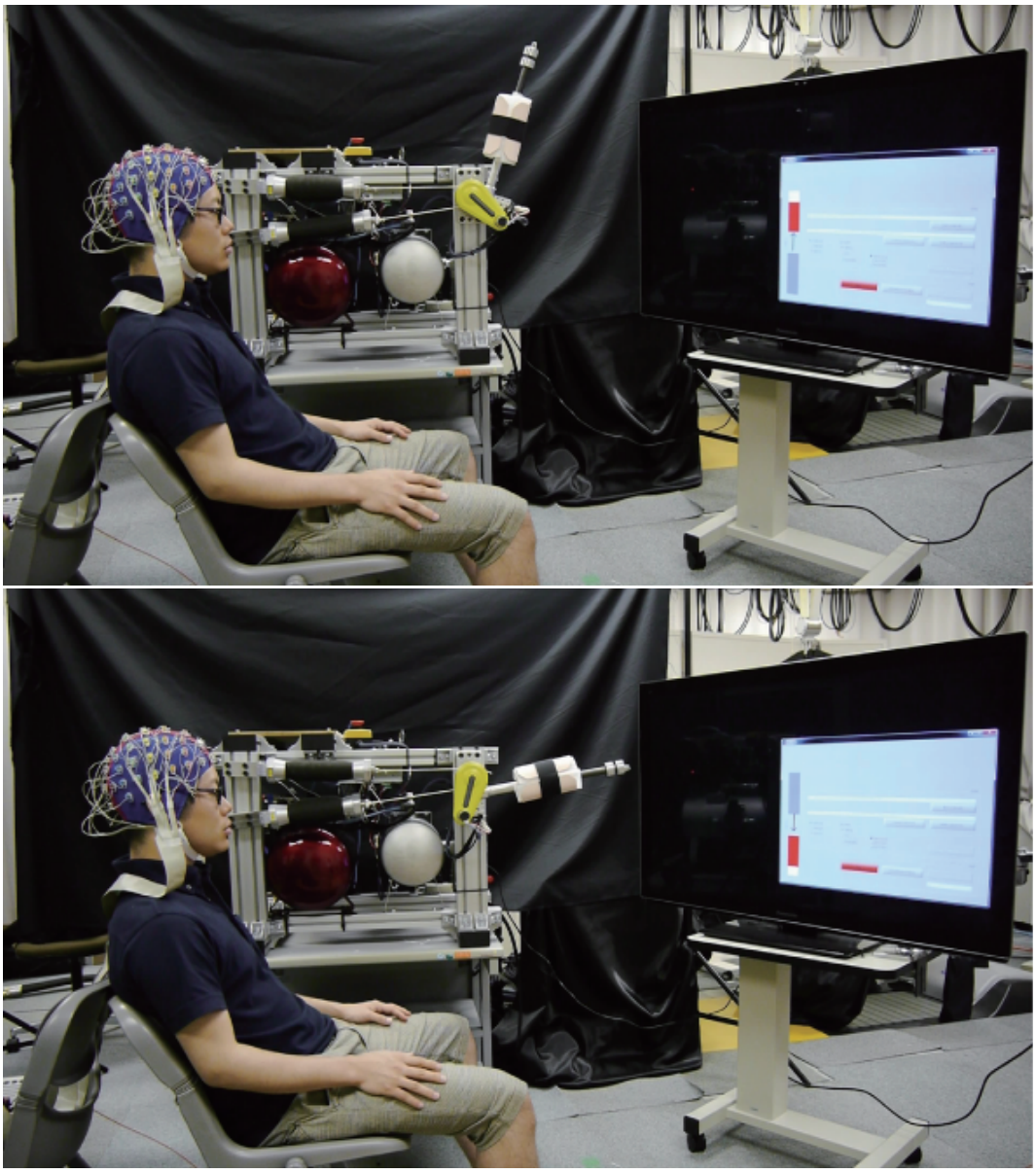

Figure 6.4: EEG-oneDOF experiment; The subject does not wear the oneDOF system in this example. The subject tries to control oneDOF system to follow the up/down direction indicated on the display the subject by using motor imagery. (Top) Up state. (Bottom) Down state

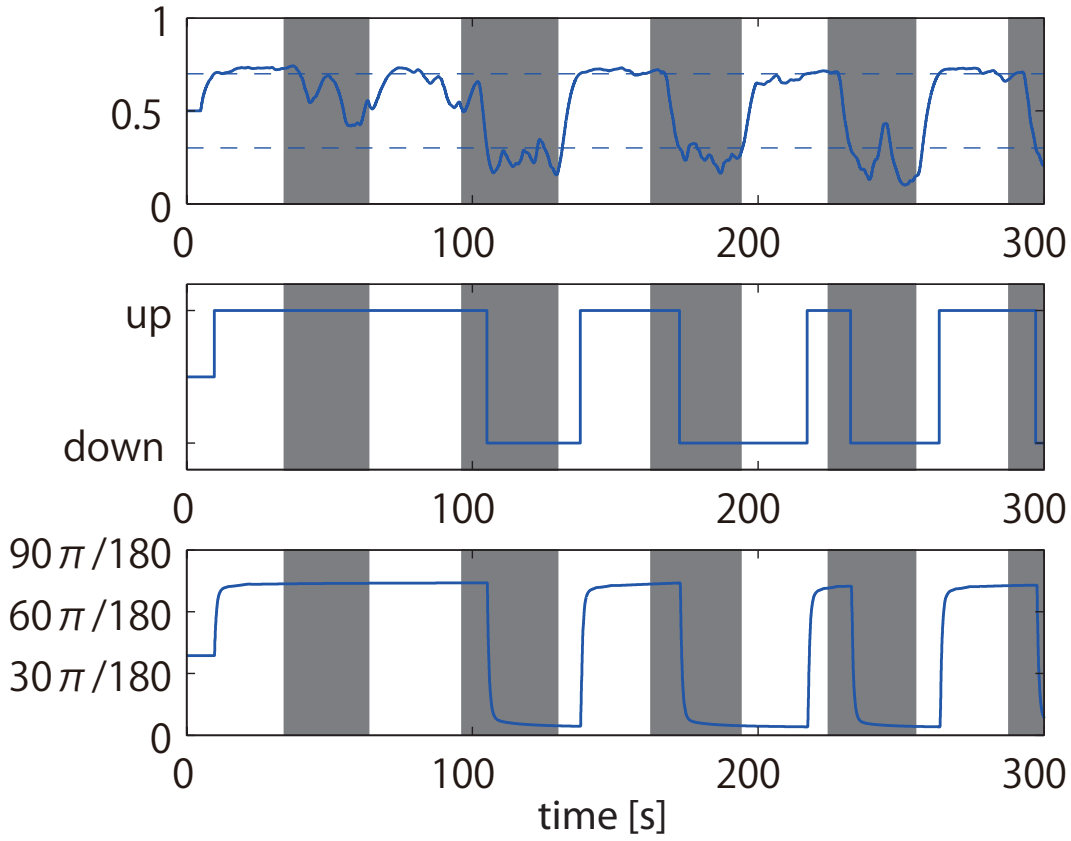

Figure 6.5: Control performance of the EEG-oneDOF system. The wite/grey region shows the up/down target direction respectively. The performance (0.5 thresholded correct rate) was 0.8113 in the last half of the session from 150 sec to 300 sec. (Top) Decoded brain activities. (Middle) Control command generated from the decoded brain activities. (Bottom) Joint angle trajectory of the oneDOF robot.

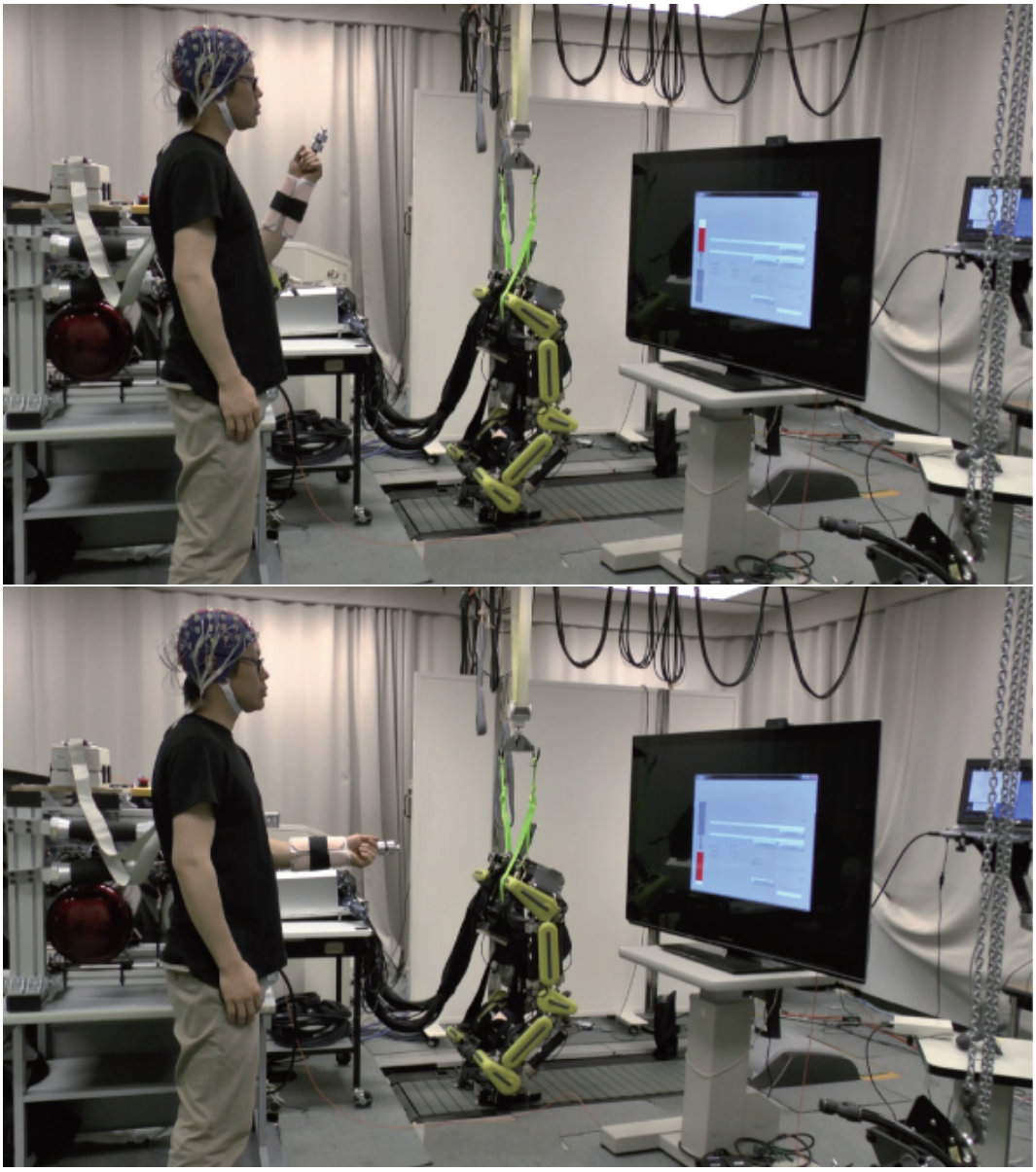

Figure 6.6: EEG-oneDOF experiment; The subject wears the oneDOF system in this example. The subject tries to control oneDOF system to follow the up/down direction indicated on the display by using motor imagery. The performance (0.5 threshold correct rate) was 0.7188 in the last half of the session from 150 sec to 300 sec. (Top) Up state. (Bottom) Down state

6.2.2 EEG-Exoskeleton system

Fig. 6.7 and 6.8 show control performance of the EEG-Exoskeleton system. The subject tries to control EEG-Exoskeleton system to follow the stand-up/sit-down direction indicated on the display by motor imagery. The white/gray region in fig. 6.8 shows the stand-up/sit-down target direction respectively. The user was successfully controlled the exoskeleton robot by his brain activities.

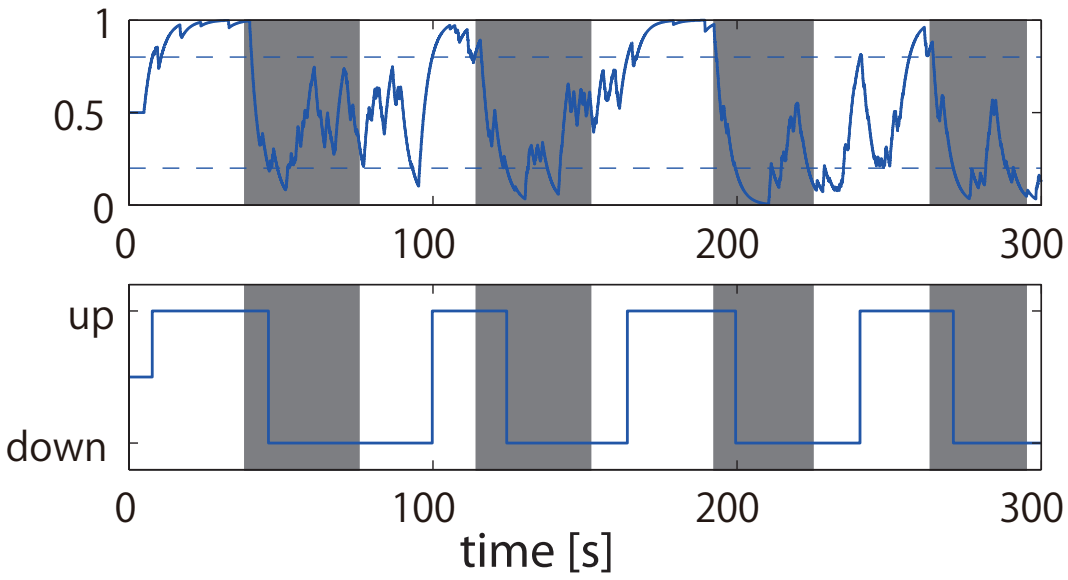

Figure 6.7: Control performance of the EEG-oneDOF system. The subject wears the one-DOF system. (Top) Decoded brain activities. (Bottom) Control command generated from the decoded brain activities.

6.3 Discussion

In this study, we developed the EEG-Exoskeleton system in which the exoskeleton robot were controlled by using decoded EEG signals. Brain activities of the users are decoded by using a classification method which can consider covariance matrix of the observed EEG signals as input variables. Then, we connected the EEG system to our one DoF test system. The subject tried to control the robot with two different situations: 1) the subject did not wear the robot and 2) the subject wore the robot. We showed that EEG-oneDoF system was successfully controlled by using the decoded brain activities in the two different situations. Finally, we connected the EEG system to the exoskeleton robot. We showed that even when the EEG system was used with the exoskeleton robot, the user was able to decode the brain activities and control the exoskeleton robot. This our developed EEG-based exoskeleton robot can be used in rehabilitation application such as stand-up from bedside and wheel chair.

One of the problem in this system was the difference of performance between subjects. The difference comes from the accuracy of motor imagery decoding, e.g., some subject can easily be detected the image but others can not. So, there is a possibility that all of subject can not control the robot by using only EEG data. However, it can be considered that this problem is able to alleviate by combining fMRI, NIRS, or MEG data as a prior distribution because these data are high spatial or temporal resolution.

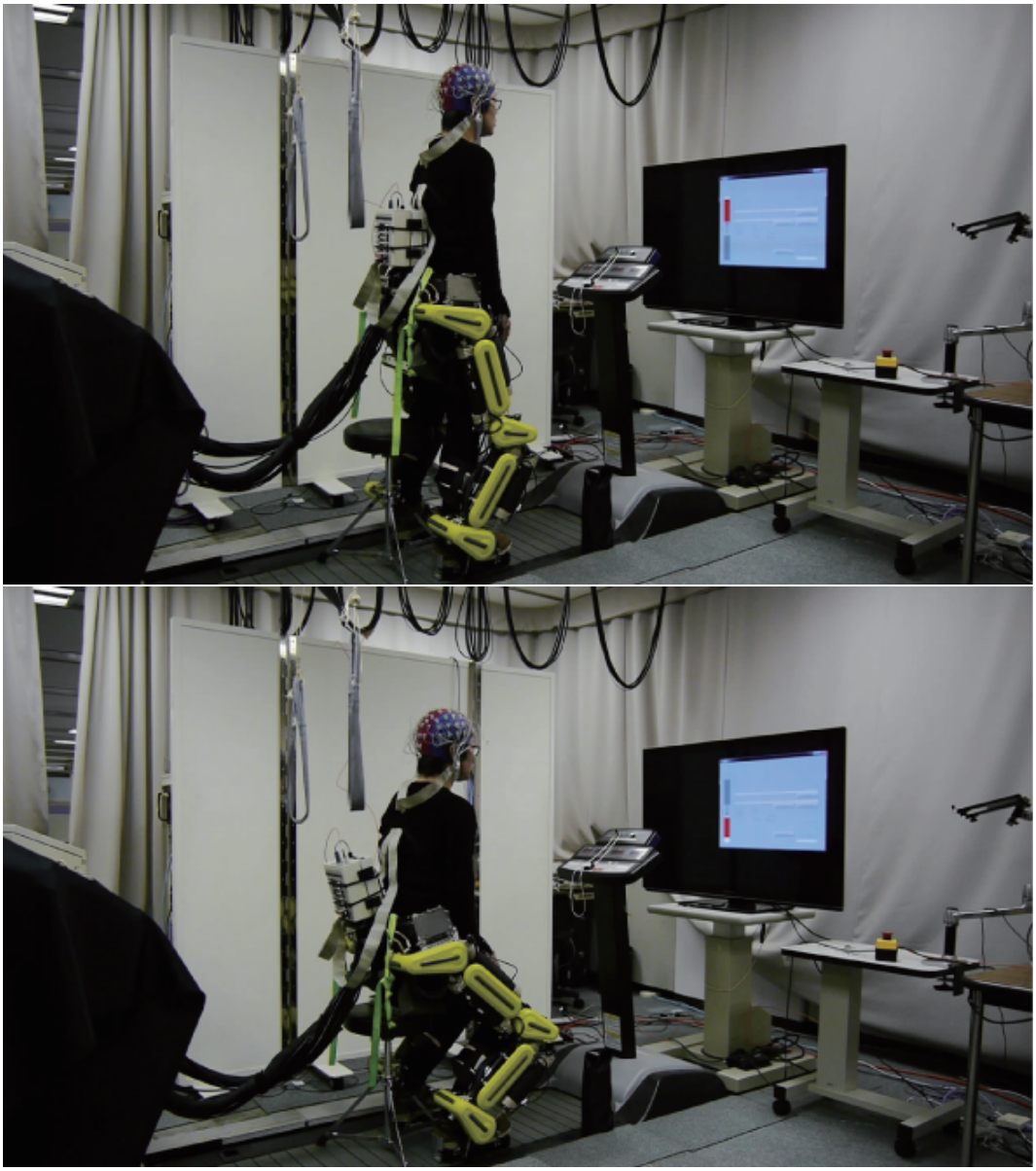

Figure 6.8: EEG-Exoskeleton experiment; The subject tries to control EEG-Exoskeleton system to follow the stand-up/sit-down direction indicated on the display by using motor imagery. The gravity compensation of lower limb model (total weight of XoR and human lower limbs) was activated when the EEG decoding is ”up”. The PAM torque controller was implemented with tendon-spring equilibrium model. When this system used in rehabilitation, self-balancing torque controller and another safety systems can be also installed. The performance (0.5 threshold correct rate) was 0.7146 in the last half of the session from 60 sec to 120 sec. (Top) Sit-down state. (Bottom) Stand-up state.

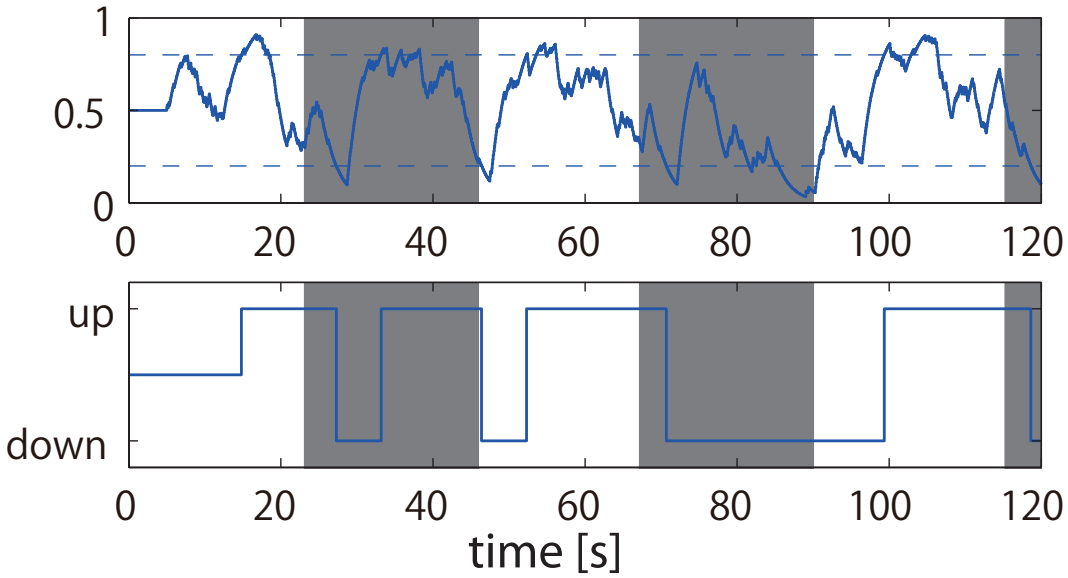

Figure 6.9: Control performance of the EEG-Exoskeleton system. The white/gray region shows that the target direction is stand-up/sit-down respectively. (Top) Decoded brain activities. (Bottom) Control command generated from the decoded brain activities.

Furthermore, we have to consider the human-robot interaction. Because the assist itself is realized by physical interaction between human and robot, and human get the physical feedback. In order to deal with this, we first need to investigate the effect of passive assist during decoding. The, we have to construct a decoder considering the interaction effect. In addition, we also need to make these EEG-based control more robust against sensor anomaly, because the EEG has also usually multi-channel. But, in the classification based control we also can use the robust estimation method as shown in subsection 3.3.1.

Chapter 7

Conclusion

7.1 Summary

Bio-signal based assistive robot have been widely studied, but they have yet to low feasibility despite high efficiency. One of this reason is the instability and vulnerability of bio-signal. In this study, I proposed human-robot interface to control assistive robots based on human motor intention which was robustly estimated from multi-channel bio-signals, and developed hardware and software to realize the system. In order to assist human movement with high affinity, developed devices in this study were force controllable.

For the EMG-based assistive robot control, I estimated joint torques based on the human motor control model in which humans activate their muscles by the command calculated inverse dynamics in the brain. To make estimation model, I proposed measurement technique during human dynamic motion due to the difference of human motor control criteria between static and dynamic motion. I acquired the joint torques and EMG data set for the model calibration using inverse dynamics. Then, the muscle activities were converted to muscle forces considering the non-linearity based on bio-mechanical knowledge. From these data set, I can make tendon-pulley linear estimation model by low calibration cost. In order to evaluate the estimated joint torques during dynamic motion, I used my newly developed EMG-driven weight support system which has a wider operational range and can adaptively change the amount of support. The weight support system was driven by vertical forces of knee and ankle joint torques estimated from simple linear estimation model. As a results, the subjects were able to one-leg squat by the assist with weight support system. Healthy subjects took part in this experiment, but as an application, this system can possibly be used for partial weight bearing therapies. Concretely, compensating the disabled side of the body for the early stage of therapies. Then, the vertical component force can be gradually decreased as the patient recovers lower body motor functions.

In order to robustly estimate human movement from multi-channel EMG signals, I proposed fault tolerant estimation method. Although using multiple sensor channel is a promising approach to estimate multi-degree of freedom of human movement and motor intention in detail, it is difficult to use multi-sensors because of its vulnerability. The sensor anomaly was detected by correlation structure of muscle activity, and the robustness of estimation was achieved by the informational redundancy of multi-channel bio-signals. I proposed robust estimation method both in supervised and unsupervised framework. In order to evaluate the method, I artificially created two kinds of sensor fault: an EMG electrode sensor is disconnected from the amplifier and one side of an EMG electrode sensor is detached from skin surface during on-line EMG-based robot control. The results showed that the robot was properly controlled based on the estimated joint torque using my

proposed method even when EMG electrodes have problems while standard method with no fault tolerability was unable to deal with these fault situations.

In addition, I also considered the effect of human-robot interaction into the controller when robot assist human limbs although almost conventional studies did not take into account. The proposed controller was evaluated experimentally with one-DOF exoskeleton robot assist, and I showed that the EMG-based feedback system with proposed method was more stable compared to conventional controller.

Finally, I combined these method, and proposed a human movement model both for EMG-based assistive control and for biosignal-sensor failure detection. In this experiment, we also considered sensor anomaly situation; the two EMG sensor electrodes connection in 16-channel were misplaced (SEM) in addition to SDC and SDT anomaly situations. For the SEM validation, we tested all possible anomaly combinations. As a results, our proposed method could deal with all sensor anomaly situations (SDC, SDT and SEM anomaly situations) and subjects were able to successfully controlled the four-DoF upper-limb exoskeleton robot to generate drinking motions, and assisted stably even under two types simultaneous sensor fault conditions.

The exoskeleton robot can be used as prosthetic devices for patients such as stroke and spinal cord injury patients in rehabilitation, and it has been found that using brain activity to control assistive robot is useful for such patients. Therefore, there would be possibility to enhance recovery of motor functions if an exoskeleton robot to assist human body can be controlled by their brain activities. For the purpose of brain activity based assistive robot, portable measurement system such as EEG is suitable to control assistive robot. However, the portability lead to signal vulnerability, and it is difficult to estimate human motor intention. Moreover, we have difficulty in estimating human motor intention in detail from EEG to control assistive device. In this study, we combined the EEG-decoding technique into exoskeleton robot that has autonomous technologies and was able to control big forces precisely by PE-Hybrid actuation system. This system enable us to control the exoskeleton robot based on brain signals. The human motor intention was estimated by classification using covariance matrix of EEG data as an input. Then, the exoskeleton robot was controlled by user's motor imagery. As a results, the EEG-based robot system was able to control robustly by brain signals even in the presence of human-robot interaction.

From this study, I found that we can control the multi-DoF assistive robot system robustly taking advantage of the redundancy of high dimensional bio-signals.

7.2 Future Direction

In this study, I proposed multi-channel bio-signal based robust human-robot interface to control assistive robot. This study may be useful to our society where sensor technology is more and more developing to yield practical application of assistive devices such as not only exoskeleton robot but also general purpose type of humanoid robot. In the future, I will extend this proposed approach to deal with wider variety of movements with multiple sensor channels. Some conventional studies have used non-linear model such as neural network to control multi-DoF robot from bio-signals [69]. However, this kind model have generalization problem against new motion which was excluded from calibration data, and also new subject. In order to generally estimate wider variety motion, basic feature of human motor intention need to be investigated. The proposed multi-channel bio-signal based human movement model in this study focused on connectivity among bio-signals to estimate human motor intention and cope with sensor anomaly. This connectivity of muscle or brain activation has possibility to explain the basic motor element, because the evi-

dence that neural connection between certain muscles coordinately controls some muscles is physiologically supported [127] [128].

If we can deal with basic features of motor, we have possibility to control the feature inversely. In fact, recent neuro science study found that repetitive inductions of particular activation pattern in human early visual areas lead to visual performance improvement to a specific visual feature using decoded fMRI neurofeedback techniques [129]. Thanks to recent large scale integrated technologies, multi-channel bio-signals also have the potential to capture the feature of motor skills. High dimensional bio-signal based wider variety robot control technologies will be able to use to change the feature of human motor by physical interaction, and advance the existing assist robot framework to motor skill transfer framework. This new robot control frame work will be more helpful for the rehabilitation application of unhealthy people, training system of healthy people, and also motor learning research.

Bibliography

[1] F Rosenblatt. *Principles of neurodynamics; perceptrons and the theory of brain mechanisms*. Spartan, 1962.

[2] John H. Holland. *Adaptation in natural and artificial systems*. University of Michigan Press, 1975.

[3] A.D. Ames. Human-inspired control of bipedal walking robots. *IEEE Transactions on Automatic Control*, 59(5):1115–1130, May 2014.

[4] E.W. Hawkes, D.L. Christensen, A.K. Han, H. Jiang, and M.R. Cutkosky. Grasping without squeezing: Shear adhesion gripper with fibrillar thin film. In *IEEE International Conference on Robotics and Automation (ICRA2015)*, pages 2305–2312, May 2015.

[5] T.E.A. de Oliveira, A.-M. Cretu, V.P. da Fonseca, and E.M. Petriu. Touch sensing for humanoid robots. *IEEE Instrumentation Measurement Magazine*, 18(5):13–19, October 2015.

[6] W. Huo, S. Mohammed, J.C. Moreno, and Y. Amirat. Lower limb wearable robots for assistance and rehabilitation: A state of the art. *IEEE Systems Journal*, PP(99):1–14, 2014.

[7] T. Shimizu, R. Saegusa, S. Ikemoto, H. Ishiguro, and G. Metta. Robust sensorimotor representation to physical interaction changes in humanoid motion learning. *IEEE Transactions on Neural Networks and Learning Systems*, 26(5):1035–1047, May 2015.

[8] Weihua Sheng, A. Thobbi, and Ye Gu. An integrated framework for human-robot collaborative manipulation. *IEEE Transactions on Cybernetics*, 45(10):2030–2041, Oct 2015.

[9] Tadashi Isa, Masaharu Kinoshita, and Yukio Nishimura. Role of Direct vs. Indirect Pathways from the Motor Cortex to Spinal Motoneurons in the Control of Hand Dexterity. *Front Neurol*, 4:191, 2013.

[10] Latash ML, Scholz JP, and Schoner G. Toward a new theory of motor synergies. *Motor Control*, 11(3):276–308, 2007.

[11] S. Uda, T. H. Saito, T. Kudo, T. Kokaji, T. Tsuchiya, H. Kubota, Y. Komori, Y. Ozaki, and S. Kuroda. Robustness and compensation of information transmission of signaling pathways. *Science*, 341(6145):558–561, Aug 2013.

[12] A.M Dollar and H Herr. Lower extremity exoskeletons and active orthoses: Challenges and state-of-the-art. *Robotics, IEEE Transactions on*, 24(1):144–158, 2008.

[13] A. Fougner, O. Stavdahl, P.J. Kyberd, Y.G. Losier, and P.A. Parker. Control of upper limb prostheses: Terminology and proportional myoelectric control–a review. *IEEE Transactions on Neural Systems and Rehabilitation Engineering*, 20(5):663–677, 2012.

[14] K Suzuki, G Mito, H Kawamoto, Y Hasegawa, and Y Sankai. Intention-based walking support for paraplegia patients with robot suit hal. *Advanced Robotics*, 21(12):1441–1469, 2007.

[15] S. K. Au, P. Dilworth, and H. Herr. An ankle-foot emulation system for the study of human walking biomechanics. In *IEEE International Conference on Robotics and Automation*, pages 2939–2945, 2006.

[16] H. Kobayashi, A. Takamitsu, and T. Hashimoto. Muscle Suit Development and Factory Application. *International Journal of Automation Technology*, 3(6):709–715, 2009.

[17] G. Yamamoto and S. Toyama. Development of Wearable-Agri-Robot- Mechanism for Agricultural Work. In *IEEE/RSJ International Conference on Intelligent Robots and System*, pages 5801–5806, 2009.

[18] T. Kagawa and Y. Uno. Gait pattern generation for a power-assist device of paraplegic gait. *The 18 th IEEE International Symposium on Robot and Human Interactive Communication*, pages 633–638, 2009.

[19] R Osu, Y Otaka, J Ushiba, S Sakata, T Yamauchi, T Fujiwara, K Kondo, and M Liu. A pilot study of contralateral hononymous muscle activity simulated electrical stimulation in chronic hemiplegia. *Brain Inj*, (26):1105–1112, 2012.

[20] S.K Banala, S.H Kim, S.K Agrawal, and J.P Scholz. Robot assisted gait training with active leg exoskeleton (alex). *Neural Systems and Rehabilitation Engineering, IEEE Transactions on*, 17(1):2–8, 2009.

[21] H Kazerooni, R Steger, and L Huang. Hybrid control of the berkeley lower extremity exoskeleton (bleex). *The International Journal of Robotics Research*, 25(5-6):561–573, 2006.

[22] Adam B. Zoss, H. Kazerooni, and Andrew Chu. Biomechanical design of the berkeley lower extremity exoskeleton(bleex). *IEEE/ASME Trans. Mechatronics*, 11(2):128–138, 2006.

[23] H. Kazerooni and A. Chu nad R. Steger. That Which Does Not Stabilize, Will Only Make Us Stronger. *International Journal of Robotics Research*, 26(1):75–89, 2007.

[24] C. J. Walsh, K. Pasch, and H. Herr. An autonomous, underactuated exoskeleton for load-carrying augumentation. *In Proc. IEEE/RSJ Int. Conf. Intell. Robot Syst. (IROS), Beijing, China*, pages 1410–1415, 2006.

[25] C. J. Walsh, D. Paluska, k. Pasch, W. Grand, A. Valiente, and H. Herr. Development of a lightweight, underactuated exoskeleton for load-carryng augmentation. *in Proc. IEEE Int. Conf. Robot*, pages 3485–3491, 2006.

[26] R Banz, M Bolliger, S Muller, C Santelli, and R Riener. A method of estimating the degree of active participation during stepping in a driven gait orthosis based on actuator force profile matching. *Neural Systems and Rehabilitation Engineering, IEEE Transactions on*, 17(1):15–22, 2009.

[27] J Rosen, M Fuchs, and M Arcan. Performances of hill-type and neural network muscle models–toward a myosignal-based exoskeleton. *Computers and Biomedical Research*, Jan 1999.

[28] J. Rosen, M. Brand, M.B. Fuchs, and M. Arcan. A myosignal-based powered exoskeleton system. *IEEE Transactions on Systems, Man and Cybernetics, Part A: Systems and Humans*, 31(3):210–222, 2001.

[29] K Kiguchi, S Kariya, K Watanabe, K Izumi, and T Fukuda. An exoskeletal robot for human elbow motion support-sensor fusion, adaptation, and control. *IEEE Transactions on Systems, Man, and Cybernetics, Part B: Cybernetics*, 31(3):353–361, 2001.

[30] K Kiguchi, T Tanaka, and T Fukuda. Neuro-fuzzy control of a robotic exoskeleton with emg signals. *IEEE Transactions on Fuzzy Systems*, 12(4):481–490, 2004.

[31] K Kiguchi. A study on emg-based human motion prediction for power assist exoskeletons. *International Symposium on Computational Intelligence in Robotics and Automation, 2007. CIRA 2007.*, pages 190–195, 2007.

[32] S Lee and Y Sankai. Power assist control for walking aid with hal-3 based on emg and impedance adjustment around knee joint. *Intelligent Robots and Systems, 2002. IEEE/RSJ International Conference on*, 2:1499–1504 vol. 2, 2002.

[33] T Hayashi, H Kawamoto, and Y Sankai. Control method of robot suit hal working as operator's muscle using biological and dynamical information. *Intelligent Robots and Systems, 2005.(IROS 2005). 2005 IEEE/RSJ International Conference on*, pages 3063–3068, 2005.

[34] A Tsukahara, Y Hasegawa, and Y Sankai. Standing-up motion support for paraplegic patient with robot suit hal. *Rehabilitation Robotics, 2009. ICORR 2009. IEEE International Conference on*, pages 211–217, 2009.

[35] C Fleischer, , and G Hommel. A human-exoskeleton interface utilizing electromyography. *IEEE TRANSACTION ON ROBOTICS*, 24(4):872–882, August 2008.

[36] Jongsang Son, Sungjae Hwang, and Youngho Kim. An emg-based muscle force monitoring system. *J Mech Sci Technol*, 24(10):2099–2105, Oct 2010.

[37] K.E Gordon and D.P Ferris. Learning to walk with a robotic ankle exoskeleton. *Journal of Biomechanics*, 40(12):2636–2644, 2007.

[38] C.R Kinnaird and D.P Ferris. Medial gastrocnemius myoelectric control of a robotic ankle exoskeleton. *IEEE Transactions on Neural Systems and Rehabilitation Engineering*, 17(1):31–37, 2009.

[39] K. Nagata and K. Magatani. Basic study on combined motion estimation using multichannel surface EMG signals. In *Engineering in Medicine and Biology Society, EMBC, 2011 Annual International Conference of the IEEE*, pages 7865–7868, 2011.

[40] A. Holobar, M.A. Minetto, A. Botter, F. Negro, and D. Farina. Experimental Analysis of Accuracy in the Identification of Motor Unit Spike Trains From High-Density Surface EMG. *IEEE Transactions on Neural Systems and Rehabilitation Engineering*, 18(3):221–229, June 2010.

[41] M. Kawato. Computational schemes and neural networks models for formation and control of multijoint arm trajectory. *In Miller. T, Sutton. R S, Werbos. P J, Neural Networks for Control. MIT Press, Cambridge, Massachusetts*, pages 197–228, 1990.

[42] P. D. Cheney and E. E. Fetz. Functional classes of primate corticomotoneuronal cells and their relation to active force. *Journal of Neurophysiology*, (44):773–791, 1980.

[43] D. J. Bannet. Time-varying stiffness of human elbow joint during cyclic voluntary movement. *Experimental Brain Research*, (88):433–442, 1992.

[44] David J.Bannet. Torques generated at the human elbow joint in response to constant position errors imposed during voluntary movements. *Experimental Brain Research*, (95):488–498, 1993.

[45] H. Gomi, Y. Koike, and M. Kawato. Human hand stiffness during discrete point-to-point multi-joint movement. *Proceedings of IEEE Engineering in Medicine and Biology Society*, pages 1628–1629, 1992.

[46] H. Gomi and M. Kawato. Equilibrium-point control hypothesis examined by measured arm-stiffness during multi-joint movement. *Science*, (272):117–120, 1996.

[47] K. Shindo, K. Kawashima, J. Ushiba, N. Ota, M. Ito, T. Ota, A. Kimura, and M. Liu. Effects of neurofeedback training with an electroencephalogram-based brain-computer interface for hand paralysis in patients with chronic stroke: a preliminary case series study. *J. Rehabil. Med.*, 43:951–957, 2011.

[48] T. Matsubara, A. Uchikata, and J. Morimoto. Full-body exoskeleton robot control for walking assistance by style-phase adaptive pattern generation. *IEEE/RSJ IROS 2012*, 2012.

[49] E. Bizzi, A. Polit, and P. Marasso. Mechanism underlying achievement of final head position. *Journal of Neurophysiology*, (39):435–444, 1976.

[50] E. Bizzi, N. Accornero, W. Chapple, and N. Hogan. Posture control and trajectory formation during arm movement. *The Journal of Neuroscience*, 89(4):2738–2744, 1984.

[51] N. Hogan. Impedance control: an approach to manipulation: Part 1. theory. asme. *Jounal of Dynamic System, Measurement and Control*, (107):1–7, 1985.

[52] N. Hogan. Impedance control: an approach to manipulation: Part 2. theory. asme. *Jounal of Dynamic System, Measurement and Control*, (107):8–16, 1985.

[53] N. Hogan. Impedance control: an approach to manipulation: Part 3. theory. asme. *Jounal of Dynamic System, Measurement and Control*, (107):17–24, 1985.

[54] M Katayama and M Kawato. Virtual trajectory and stiffness ellipse during force-trajectory control using a parallel-hierarchical neural network model. In *Advanced Robotics, 1991. 'Robots in Unstructured Environments', 91 ICAR., Fifth International Conference on*, 2013.

[55] M.Katayama and M.Kawato. Virtual trajectory and stiffness ellipse during multijoint arm movement predicted by neural inverse models. *Biological Cybernetics*, 69(5):353–362, 1993.

[56] AV Hill. The heat of shortening and the dynamic constants of muscle. *Proceedings of the Royal Society of London. Series B, Biological Sciences*, 126(843):136–195, 1938.

[57] H Hatze. A myocybernetic control model of skeletal muscle. *Biological Cybernetics*, 25(2):103–119, 1977.

[58] S Stroeve. Learning combined feedback and feedforward control of a musculoskeletal system. *Biological Cybernetics*, 75(1):73–83, 1996.

[59] Claudio Castellini, Angelo Emanuele Fiorilla, and Giulio Sandini. Multi-subject / daily-life activity EMG-based control of mechanical hands. *Journal of NeuroEngineering and Rehabilitation*, 6:41, 2009.

[60] C K Battye, A Nightingale, and J Whillis. The use of myo-electric currents in the operation of prostheses. *Journal of Bone & Joint Surgery, British Volume*, 37-B(3):506–510, 1955.

[61] Neville Hogan and Robert W Mann. Myoelectric signal processing: Optimal estimation applied to electromyography-part II: experimental demonstration of optimal myoprocessor performance. *IEEE Transactions on Biomedical Engineering*, 27(7):396–410, 1980.

[62] Necille Hogan and Robert W Mann. Myoelectric signal processing: Optimal estimation applied to electromyography-part I: Derivation of the optimal myoprocessor. *IEEE Transactions on Biomedical Engineering*, 27(7):396–410, 1980.

[63] K.H. Ha, H.A. Varol, and M. Goldfarb. Volitional control of a prosthetic knee using surface electromyography. *IEEE Transactions on Biomedical Engineering*, 58(1):144–151, 2011.

[64] L.J Hargrove, H. Huang, A.E. Schultz, B.A. Lock, R. Lipschutz, and T.A. Kuiken. Toward the development of a neural interface for lower limb prosthesis control. *Conf Proc IEEE Eng Med Biol Soc*, 2009:2111–2114, 2009.

[65] M DiCicco, L Lucas, and Y Matsuoka. Comparison of control strategies for an EMG controlled orthotic exoskeleton for the hand. In *ICRA 2004 IEEE International Conference on*, volume 2, pages 1622–1627, 2004.

[66] J. Ngeo, T. Tamei, T. Shibata, M.F.F. Orlando, L. Behera, A. Saxena, and A. Dutta. Control of an optimal finger exoskeleton based on continuous joint angle estimation from emg signals. In *35th Annual International Conference of the IEEE Engineering in Medicine and Biology Society (EMBC)*, pages 338–341, July 2013.

[67] Y. Hasegawa, Y. Mikami, K. Watanabe, Z. Firouzimehr, and Y. Sankai. Wearable handling support system for paralyzed patient. In *IROS 2008. IEEE/RSJ International Conference on*, pages 741–746, Sept 2008.

[68] T. Lenzi, S.M.M. De Rossi, N. Vitiello, and M.C. Carrozza. Intention-Based EMG Control for Powered Exoskeletons. *IEEE Transactions on Biomedical Engineering*, 59(8):2180–2190, 2012.

[69] K. Kiguchi and Y. Hayashi. An EMG-Based Control for an Upper-Limb Power-Assist Exoskeleton Robot. *IEEE Transactions on Systems, Man, and Cybernetics, Part B: Cybernetics*, 42(4):1064–1071, Aug 2012.

[70] Y.H. Yin, Y.J. Fan, and L.D. Xu. EMG and EPP-Integrated Human-Machine Interface Between the Paralyzed and Rehabilitation Exoskeleton. *IEEE Transactions on Information Technology in Biomedicine*, 16(4):542–549, 2012.

[71] G.S. Sawicki and D.P. Ferris. A pneumatically powered knee-ankle-foot orthosis (KAFO) with myoelectric activation and inhibition. *Journal of Neuro Engineering and Rehabilitation*, 6:23, 2009.

[72] C. Fleischer and G. Hommel. Calibration of an emg-based body model with six muscles to control a leg exoskeleton. *Robotics and Automation, 2007 IEEE International Conference on*, 2007.

[73] M.A. Ahad, A. Al Zaman, M. Ferdjalllah, and G.F. Harris. Multichannel grid electrode interface for EMG mapping. In *Circuits and Systems, 2005. 48th Midwest Symposium on*, volume 2, Aug 2005.

[74] D. Staudenmann, I. Kingma, A. Daffertshofer, Dick F. Stegeman, and J.H. van Dieen. Improving EMG-based muscle force estimation by using a high-density EMG grid and principal component analysis. *IEEE Transactions on Biomedical Engineering*, 53(4):712–719, April 2006.

[75] P.K. Artemiads and K.J. Kyriakopoulos. An EMG-Based Robot Control Scheme Robust to Time-Varying EMG Signal Features. *IEEE Transactions on Information Technology in Biomedicine*, 14(3):582–588, 2010.

[76] N.A. Dimitrova and G.V. Dimitrov. Interpretation of EMG changes with fatigue: facts, pitfalls, and fallacies. *Journal of Electromyography and Kinesiology*, 13:13–16, 2003.

[77] N.M. Lopez, F. di Sciascio, C.M. Soria, and M.E. Valentinuzzi. Robust EMG sensing system based on data fusion for myoelectric control of a robotic arm. *BioMedical Engineering Online*, 8:5, 2009.

[78] R. Halabi, M.O. Diab, B. Moslem, M. Khalil, and C. Marque. Detecting missing signals in multichannel recordings by using higher order statistics. *34th Annual International Conference of the IEEE EMBS*, pages 3110–3113, 2012.

[79] Y. Liu, F. Zhang, Y. Sun, and H. Huang. Trust sensor interface for improving reliability of EMG-based user intent recognition. In *Engineering in Medicine and Biology Society, EMBC, Annual International Conference of the IEEE*, pages 7516–7520, 2011.

[80] X.Zhang, Y.Liu, F.Zhang, J.Ren, Y.L.Sun, Q.Yang, and H.Huang. On Design and Implementation of Neural-Machine Interface for Artificial Leds. *IEEE Transactions on Industrial Informatics*, 7(5):418–429, 2012.

[81] He Huang, Fan Zhang, Yan L Sun, and Haibo He. Design of a robust EMG sensing interface for pattern classification. *Journal of Neural Engineering*, 7(5):056005, 2010.

[82] L. Hochberg, D. Bacher, B. Jarosiewicz, N. Masse, J. Simeral, J. Vogel, S. Haddadin, J. Liu, S. Cash, P. van der Smagt, and P. Jhon. Reach and grasp by people with tetraplegia using a neurally controlled robotic arm. *Nature*, 485(7398):372–375, 2012.

[83] J. H. Lee, J. Ryu, F. A. Jolesz, Z. H. Cho, and S. S. Yoo. Brain-machine interface via real-time fMRI: preliminary study on thought-controlled robotic arm. *Neurosci. Lett.*, 450(1):1–6, Jan 2009.

[84] N. Naseer, M. J. Hong, and K. S. Hong. Online binary decision decoding using functional near-infrared spectroscopy for the development of brain-computer interface. *Exp Brain Res*, 232(2):555–564, Feb 2014.

[85] J. Mellinger, G. Schalk, C. Braun, H. Preissl, W. Rosenstiel, N. Birbaumer, and A. Kubler. An MEG-based brain-computer interface (BCI). *Neuroimage*, 36(3):581–593, Jul 2007.

[86] Yongwook Chae, Jaeseung Jeong, and Sungho Jo. Toward brain-actuated humanoid robots: Asynchronous direct control using an eeg-based bci. *IEEE Transactions on Robotics*, 28(5):1131–1144, Oct 2012.

[87] C. Neuper, G.R. Muller, A. Kubler, N. Birbaumer, and G. Pfurtscheller. Clinical application of an eeg-based brain-computer interface: A case study in a patient with sever motor impairment. *Clin. Neuro physiol*, 114:399–409, 2003.

[88] G. Pfurtscheller, G.R. Muller-Putz, R. Scherer, and C. Neuper. Rehabilitation with brain-computer interface systems. *IEEE Computer Mag*, 41(10):58–65, Oct 2008.

[89] P. Horki, T. Solis-Escalante, C. Neuper, and G. Muller-Putz. Combined motor imagery and SSVEP based BCI control of a 2 DoF artificial upper limb. *Med Biol Eng Comput*, 49(5):567–577, May 2011.

[90] Yan Song, Yihao Du, Xiaoguang Wu, Xiaoling Chen, and Ping Xie. A synchronous and multi-domain feature extraction method of eeg and semg in power-assist rehabilitation robot. In *2014 IEEE International Conference on Robotics and Automation (ICRA)*, pages 4940–4945, May 2014.

[91] J.L. Contreras-Vidal and R.G. Grossman. Neurorex: A clinical neural interface roadmap for eeg-based brain machine interfaces to a lower body robotic exoskeleton. In *Engineering in Medicine and Biology Society (EMBC), 2013 35th Annual International Conference of the IEEE*, pages 1579–1582, July 2013.

[92] David G Lloyd and Thor F Besier. An emg-driven musculoskeletal model to estimate muscle forces and knee joint moments in vivo. *Journal of Biomechenics*, 36:765–776, 2003.

[93] M Mistry, J Buchli, and S Schaal. Inverse dynamics control of floating base systems using orthogonal decomposition. *Robotics and Automation (ICRA), 2010 IEEE International Conference on*, pages 3406–3412, 2010.

[94] Lev P. Latash and Mark L. Latash. A new book by n. a. bernstein: ”on dexterity and its development ”. *Journal of Motor Behavior*, 26(1):56–62, 1994.

[95] K. M. Steele, M. C. Tresch, and E. J. Perreault. The number and choice of muscles impact the results of muscle synergy analyses. *Front Comput Neurosci*, 7:105, 2013.

[96] J. Roh, W. Z. Rymer, and R. F. Beer. Robustness of muscle synergies underlying three-dimensional force generation at the hand in healthy humans. *J. Neurophysiol.*, 107(8):2123–2142, 2012.

[97] G. Torres-Oviedo, J. M. Macpherson, and L. H. Ting. Muscle synergy organization is robust across a variety of postural perturbations. *J. Neurophysiol.*, 96(3):1530–1546, Sep 2006.

[98] Tomoyuki Noda, Junichiro Furukawa, Tatsuya Teramae, and Jun Morimoto. An Electromyogram based Force Control Coordinated in Assistive Interaction. In *Robotics and Automation (ICRA), 2013 IEEE International Conference on*, pages 2657–2662, May 2013.

[99] J.R. Potvin, R.W. Norman, and S.M. McGill. Mechanically corrected EMG for the continuous estimation of erector spinae muscle loading during repetitive lifting. *European Journal of Applied Physiology and Occupational Physiology*, 74(1-2), 1996.

[100] Yasuharu Koike and Mitsuo Kawato. Estimation of dynamic joint torques and trajectory formation from surface electromyography signals using a neural network model. *Biological Cybernetics*, 73(4):291–300, 1995.

[101] Junichiro Furukawa, Tomoyuki Noda, Tatsuya Teramae, and Jun Morimoto. An EMG-Driven Weight Support System With Pneumatic Artificial Muscles. *IEEE Systems Journal*, 2014, in press.

[102] *Convex optimization techniques for fitting sparse Gaussian graphical models*, 2006.

[103] J. Friedman, T. Hastie, H. Hofling, and R. Tibshirani. Path wise coordinate optimization. *Annals of Applied Atatistics*, pages 302–332, 2007.

[104] *Proximity-Based Anomaly Detection using Sparse Structure Learning*, 2009.

[105] Wei Wu, Yun Gao, Elie Bienenstock, John P. Donoghue, and Michael J. Black. Bayesian population decoding of motor cortical activity using a kalman filter. *Neural Comput.*, 18(1):80–118, January 2006.

[106] Frank L. Lewis. *Optimal Estimation: With an Introduction to Stochastic Control Theory*. Wiley-Interscience, 1986.

[107] I. Sardellitti, J. Park, D. Shin, and O. Khatib. Air muscle controller design in the distributed macro-mini (DM2) actuation approach. In *IEEE/RSJ International Conference on Intelligent Robots and Systems*, pages 1822–1827, 2007.

[108] K. Inoue. Rubbertuators and applications for robots. In *Proceedings of the 4th international symposium on Robotics Research*, pages 57–63. MIT Press, 1988.

[109] D.G. Caldwell, A. Razak, and MJ Goodwin. Braided pneumatic muscle actuators. In *Proceedings of the IFAC Conference on Intelligent Autonomous Vehicles*, pages 507–512, 1993.

[110] T. Noda, T. Teramae, B. Ugurlu, and J. Morimoto. Development of an upper limb exoskeleton powered via pneumatic electric hybrid actuators with bowden cable. In *Intelligent Robots and Systems (IROS 2014), 2014 IEEE/RSJ International Conference on*, pages 3573–3578, Sept 2014.

[111] Sang-H Hyon, Jun Morimoto, Takamitsu Matsubara, Tomoyuki Noda, and Mitsuo Kawato. Xor: Hybrid drive exoskeleton robot that can balance. pages 2715–2722, San Francisco, USA, Sep25-30 2011.

[112] Tomoyuki Noda, Norikazu Sugimoto, Junichiro Furukawa, Masaaki Sato, Sang Ho Hyon, and Jun Morimoto. Brain-controlled exoskeleton robot for bmi rehabilitaion. In *IEEE/RAS International Conference on Humanoid Robotics (Humanoids2012), Osaka*, pages 21–27, 2012.

[113] A Hildebrandt, O Sawodny, R Neumann, and A Hartmann. Cascaded control concept of a robot with two degrees of freedom driven by four artificial pneumatic muscle actuators. pages 680–685, 2005.

[114] S. Maeda, N. Tsujiuchi, T. Koizumi, M. Sugiura, and H. Kojima. Development and control of pneumatic robot arm for industrial fields. In *IECON 2011 - 37th Annual Conference on IEEE Industrial Electronics Society*, pages 86–91, Nov 2011.

[115] J. Ueda, Ding Ming, V. Krishnamoorthy, M. Shinohara, and T. Ogasawara. Individual muscle control using an exoskeleton robot for muscle function testing. *Neural Systems and Rehabilitation Engineering, IEEE Transactions on*, 18(4):339–350, Aug 2010.

[116] H. Kobayashi. Development on wearable robot for human power support. In *IECON 02 [Industrial Electronics Society, IEEE 2002 28th Annual Conference of the]*, volume 4, pages 3091–3096 vol.4, Nov 2002.

[117] T. W. Anderson and D. A. Darling. Asymptotic Theory of Certain "Goodness of Fit" Criteria Based on Stochastic Processes. *The Annals of Mathematical Statistics*, 23(2):193–212, 1952.

[118] Takamitsu Matsubara and Jun Morimoto. Bilinear modeling of emg signals to extract user-independent features for multiuser myoelectric interface. *IEEE Transactions on Biomedical Engineering*, 60(8):2205–2213, 2013.

[119] Takamitsu, Sang-Ho Hyon, and Jun Morimoto. Real-time stylistic prediction for whole-body human motions. *Neural Networks*, 25:191–199, 2012.

[120] M. Yoshida and M. Terao. Suitable cutoff frequency of low-pass filter for estimating muscle force by surface electromyogram. In *Proceedings of the 25th Annual International Conference of the IEEE Engineering in Medicine and Biology Society*, volume 2, pages 1709–1711 Vol.2, Sept 2003.

[121] Junichiro Furukawa, Tomoyuki Noda, Tatsuya Teramae, and Jun Morimoto. Fault tolerant approach for biosignal-based robot control. *Advanced Robotics*, 29(7):505–514, 2015.

[122] S. Jacobsen. On the Development of XOS, a Powerful Exoskeletal Robot. In *2007 IEEE/RSJ International Conference on Intelligent Robots and Systems, Plenary Talk*, 2007.

[123] D. Kamatani, J. Fujiwara, J. Ushiba, K. Shindo, A. Kimura, and L. Meigen. Study for evaluation method of effect of bmi rehabilitation by using near infrared spectoscopy. In *in Neuro2010*, pages p2–f16, 2010.

[124] Ryota Tomioka and Kazuyuki Aihara. Classifying matrices with a spectral regularization. In *Proceedings of the 24th international conference on Machine learning (ICML'07)*, pages 895–902. ACM Press, 2007.

[125] R. Tomioka and K. R. Müller. A regularized discriminative framework for EEG analysis with application to brain-computer interface. *NeuroImage*, 49:415–432, 2010.

[126] Christopher M. Bishop. *Pattern Recognition and Machine Learning*. Springer, NY, USA, 2006.

[127] Y. Shinoda, J. Yokota, and T. Futami. Divergent projection of individual corticospinal axons to motoneurons of multiple muscles in the monkey. *Neuroscience Letters*, 23(1):7–12, 1981.

[128] Y. Shinoda, T. Yamaguchi, and T. Futami. Multiple axon collaterals of single corticospinal axons in the cat spinal cord. *Journal of Neurophysiology*, 55(3):425–448, 1986.

[129] K. Shibata, T. Watanabe, Y. Sasaki, and M. Kawato. Perceptual learning incepted by decoded fMRI neurofeedback without stimulus presentation. *Science*, 334(6061):1413–1415, Dec 2011.

Acknowledgements

I would like to express my respect and gratitude to Prof. Toshio Yanagida of Graduate School of Frontier Biosciences Osaka University whose enormous support and insightful comments were invaluable during the course of my study.

I am deeply grateful to Director Mitsuo Kawato of ATR Computational Neuroscience Labs and Head of Department Jun Morimoto of Dept. of Brain Robot Interface ATR Computational Neuroscience Labs who gives me constructive comments and warm encouragement.

I would like appreciate Dr. Tomoyuki Noda and Dr. Tatsuya Teramae of Dept. of Brain Robot Interface ATR Computational Neuroscience Labs. They have collaborated on the researches in this thesis and give me a significant advice and encouragement.

I would like to thank Mr. Akihide Inano and Mr. Nao Nakano Research Engineers of Dept. of Brain Robot Interface ATR Computational Neuroscience Labs. They help me to develop the devices and maintenance.

I would also like to thank Ms. Kazuko Devis who gives me grateful helps.

For providing a good environment for my works, I would like to thank all the staff of Graduate School of Frontier Bioscience Labs and ATR computational Neuroscience Labs.

Finally, I would like to express the deepest appreciation to my parents and family. I received generous support from them.

Research Achievement

1. Refereed International Journal Papers

1. **Jun-ichiro Furukawa**, Tomoyuki Noda, Tatsuya Teramae, and Jun Morimoto, "Human movment modeling to detect bio-signal sensor failure for myoelectric assistive robot control", *IEEE Transactions on Robotics*, 2016, submitted (under the revision).

2. **Jun-ichiro Furukawa**, Tomoyuki Noda, Tatsuya Teramae, and Jun Morimoto, "Fault tolerant approach for biosignal-based robot control", *Advanced Robotics*, Vol. 29, No.7, pp. 505–514, 2015.

3. **Jun-ichiro Furukawa**, Tomoyuki Noda, Tatsuya Teramae, and Jun Morimoto, "An EMG-driven Weight Support System with Pneumatic Artificial Muscles", *IEEE Systems Journal*, 2014, in press

4. Karim Bouyarmane, Joris Vaillant, Norikazu Sugimoto, Francois Keith, **Jun-ichiro Furukawa**, and Jun Morimoto, "Brain-Machine Interface Control of Whole-Body Humanoid Motion", *Frontiers in System Neuroscience*, Vol.8, no.00138, 2014.

2. Refereed International Conference (Proceedings)

1. **Jun-ichiro Furukawa**, Tomoyuki Noda, Tatsuya Teramae, and Jun Morimoto, "Estimating Joint Movements from Observed EMG signals with Multiple Electrodes under Sensor Failure Situations toward Safe Assistive Robot Control", *IEEE International Conference on Robotics and Automation (ICRA2015)*, pp. 4985–4991, Seattle, Washington, May, 26th-30th, 2015.

2. Tomoyuki Noda, **Jun-ichiro Furukawa**, Tatsuya Teramae, and Jun Morimoto, "An Electromyogram based Forced Control Coordinated in Assistive Interaction", *IEEE International Conference on Robotics and Automation (ICRA2013)*, pp.2657–2662, Karlsruhe, Germany, May, 5th-10th, 2013.

3. Tomoyuki Noda, Norikazu Sugimoto, **Jun-ichiro Furukawa**, Masa-aki Sato, Sang-Ho Hyon, and Jun Morimoto, "Brain-Controlled Exoskeleton Robot for BMI Rehabilitation" *IEEE/RAS International Conference on Humanoid Robotics (Humanoids2012)*, pp.21–27, Osaka, Nov 29th-Dec 1st, 2012.

4. Karim Bouyarmane, Joris Vaillant, Norikazu Sugimoto, Francois Keith, **Jun-ichiro Furukawa**, and Jun Morimoto, "BCI control of whole-body simulated humanoid by combining motor imagery detection and autonomous motion planning"*20th International conference on Neural information processing (ICONIP2013)*, pp.310–318, Korea, Nov 3rd-7th, 2013.

3. Refereed Domestic Conference (Proceedings)

1. **Jun-ichiro Furukawa**, Tomoyuki Noda, Tatsuya Teramae, and Jun Morimoto, “Joint torque estimation of human movement using EMG” in Japanese, *Robotics Symposia*, 5C3 pp. 510–515, Yamagata, Japan, March, 2013.

2. Tomoyuki Noda, **Jun-ichiro Furukawa**, Tatsuya Teramae, and Jun Morimoto, “Electromyogram based Force Control for Assistive Robot Coordiantion in Interaction” in Japanese, *Robotics Symposia*, 4C1 pp. 392–398, Yamagata, Japan, March, 2013.

4. Non-Refereed Domestic Conference

1. **Jun-ichiro Furukawa**, Tomoyuki Noda, and Jun Morimoto, “Robust torque estimation utilizing of surface Electromyogram”, *The 30-th Annual Conference of the RSJ*, 3F1-05, Tokyo, September, 2013.

2. **Jun-ichiro Furukawa**, Tomoyuki Noda, and Jun Morimoto, “Controlling biped model using EMG data and joint angles observed from human movement”, *The 30-th Annual Conference of the RSJ*, RSJ2012AC2K1-6, Hokkaido, September, 2012.

3. **Jun-ichiro Furukawa**, and Jun Morimoto “Torque estimation from EMG signals considering inverse dynamics of human for exoskeleton robot”, *21st Machine Learning Summer School (MLSS2012)*, Kyoto, September, 2012.

5. Patent

1. Tomoyuki Noda, **Jun-ichiro Furukawa**, Jun Morimoto, ”CONTROL SIGNAL GENERATION DEVICE, AND POWER ASSIST APPARATUS”, Japanese Unexamined Patent Application Publication (JPA) 2015-47404.

2. Tomoyuki Noda, Tatsuya Teramae, **Jun-ichiro Furukawa**, Jun Morimoto, ”POWER ASSIST ROBOT”, JPA2014-155998.

3. Tomoyuki Noda, Tatsuya Teramae, **Jun-ichiro Furukawa**, Jun Morimoto, ”POWER ASSIST DEVICE AND REHABILITATION SUPPORT DEVICE USING THE SAME”, JPA2014-155653.

4. Jun Morimoto, Tomoyuki Noda, Tatsuya Teramae, **Jun-ichiro Furukawa**, ”EXTERNAL SKELETON ROBOT, AND REHABILITATION DEVICE”, JPA2014-104549.

6. Award, etc.

1. IEEE Kansai Section Student Paper Awards, 2015.

2. IEEE-Humanoids2012 Award for best paper Nomination finalist, 2012.

3. Research fund, Tateishi Science and Technology Foundation, 2015.